11-30-2015

Simulation Guided Synthesis and Processing of Polymer Dielectrics

Rui Ma
University of Connecticut - Storrs, rachel.ma27@gmail.com

Simulation Guided Synthesis and Processing of Polymer Dielectrics

Rui Ma, PhD

University of Connecticut, 2015

Electrical energy storage devices are indispensable components in modern electronics. It is always important but challenging, to explore new materials to fulfil the demand of their continuous miniaturization and improved functionality. Among these devices, which include batteries, supercapacitors, fuel cells, etc., parallel plate capacitors offer high power density but low energy density. Therefore, it is essential to improve their performance by designing new dielectric materials with high capacitive energy density. To maximize the energy density, a desirable dielectric should exhibit high dielectric constant (K), high breakdown strength, and low loss during charge-discharge cycles. The current state-of-the-art polymer dielectric film, biaxially oriented polypropylene (BOPP) has a breakdown strength of 730 MV/m and low dielectric loss ($\tan\delta \sim 0.0002$ at 1kHz, r.t.), but suffers from a low dielectric constant of 2.2 and a reduced breakdown strength and cycle life at temperatures in excess of 85^{o}C. Many approaches have been taken to enhance energy density by increasing K and breakdown field through the use of materials such as polymer nanocomposites, modified ferroelectric crystalline polymers, and amorphous polar polymers with low loss. Rational strategies combining computational and experimental procedures accelerate the process of designing and predicting properties of new materials for a specific application. Here, this dissertation work will present a synergetic dielectric material design scheme, which consists of a simulation guided synthesis through hierarchical screening, an improved performance by incorporating polar functional groups and exploring chemical space (hybrid systems containing metal elements) and a scale up and optimization of processing. With the computational tool as guidance for experimental work, a wide range of polymer materials were investigated for capacitor dielectrics; organic polymers

polyimide, polyurea, polyurethane and polythiourea, organometallic polymers containing tin, cadmium and zinc, with a scope of developing more material of the same kind and in the same manner. With building a dataset combining experimental and computational data, we are attempting to establish structure-property relationship for polymer as dielectrics and to provide guidance in a way of relational database. Also, several interesting discoveries experimentally will be discussed in detail on systematic study of the effect of chemical functional group on dielectric properties, control of morphology to influence dielectric property through chemistry and processing.

Simulation Guided Synthesis and Processing of Polymer Dielectrics

Rui Ma

B.S., Shanghai Jiao Tong University, 2011

A Dissertation

Submitted in Partial Fulfillment of the

Requirements for the Degree of

Doctor of Philosophy

at the

University of Connecticut

2015

APPROVAL PAGE

Doctor of Philosophy Dissertation

Simulation Guided Synthesis and Processing of Polymer Dielectrics

Presented by

Rui Ma, B.S.

Major Advisor

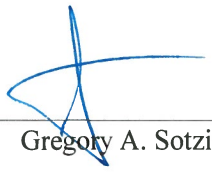

Gregory A. Sotzing

Associate Advisor

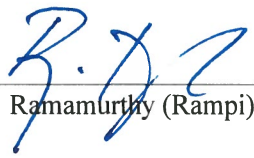

Ramamurthy (Rampi) Ramprasad

Associate Advisor

Yang Cao

Associate Advisor

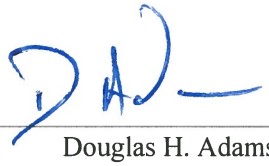

Douglas H. Adamson

University of Connecticut
2015

to my family

my dear mother Xia Ma and father Zhongguo Ma

ACKNOWLEDGEMENTS

First and foremost, I would like to express my utmost gratitude to my major advisor Professor Gregory A. Sotzing, for his insightful advice and sincere support. His unique way of guiding the path for my research and career really changed my way of thinking through my Ph.D. It built up my capability of independent thinking and efficient organize skills, which will continue to be helpful in the future.

I am really grateful that I can be part of the Multidisciplinary University Research initiative (MURI) project. It is a wonderful team. The rigorous scientific attitude and insightful ideas of all the professors in the team influence me deeply. The frequent discussion with professors and students facilitated the progress for my research and was really fruitful. Especially, I want to thank Prof. Rampi Ramprasadm Prof. Yang Can and Prof. Steven Boggs for their kind guidance and thoughtful academic suggestions. I also want to say thank you to their group members, Dr. Chenchen Wang, Dr. Vinit Sharm, Arun Kumar Mannodi Kanakkithodi, Dr. Huan Tran Lihua Chen, Dr. Ying Sun and Mattewos Tefferi for their great help in my research. I want to thank our collaborator Dr. Miko Cakmak and his student Ido Offenbach for their help and generous advice on polymer processing. The financial support of this work is from a Multi-University Research Initiative (MURI) grant of the Office of Naval Research.

Specifically, I want to say thank you to Dr. Aaron Baldwin for being my mentor and my great friend and big brother through my study. Without working with him, I would not achieve what I have now. Many thanks are owed to my current and past group members for their help and priceless friendship, Gregory Treich, Shamima Narseen, Dr.

Yumin Zhu, Mengfang Li and Xiaozheng Zhang. I also want to say thank you to Dr. Douglas Adamson or being my Associate Advisor and the Program Director during my study, and his student Zhenhua Cui for a collaborative work.

I also would like to acknowledge the help from all my friends in UConn, especially Yuan Ren, Hongwei Xia and Chen Diao for being there for me all the time.

I want to dedicate this dissertation to my family, my mother Xia Ma, and my father Zhongguo Ma for their unconditional love. I'll never forget the support they give whenever I fall. Their everlasting love is the motivation for me to overcome and to achieve.

TABLE OF CONTENTS

LIST OF FIGURES

LIST OF TABLES AND SCHEMES

Chapter 1

Introduction

1.1 Capacitor and dielectrics

As commercial, consumer and military requirements for more compact, efficient and reliable electrical power systems grow dramatically, development of higher energy density capacitor continues to be one of the major technology elements. For microsecond to fractional-second electrical energy storage, discharge, filtering and power conditioning, capacitor technology is required to meet a broad range of requirements. The US Navy is developing electromechanical devices with all-electric controls to move away from traditional hydraulic, pneumatic and mechanical devices, as a means of replacing many traditional weapon systems with directed energy and electric ones. For most of the new devices, a pulsed power supply system is required, since we require a system that can store energy stably for a long period of time and can also release the energy quickly. For example, high-energy laser systems need quick reaction and rapid fly-out, which requires a lot of energy to be released really quickly over a short period of time; For railguns, a projectile launch mass exceeding 20kg needs 100 MJ of energy to be provided by pulsed power systems; And radars need the highest power and less-frequent tracking mode, which requires the use of a pulsed power system to reach high electrical power quality. The necessary value for operation of these devices can be up to several gigajoules, and instantaneous power may exceed 20 gigawatts. [1-4]

A lot of the devices above use capacitor power supplies, because they are widely available and can be easily used and reconfigured according to different modes with characteristics in both power and frequency. It also can provide high energy with fast response. However, there are several issues to consider for improving capacitor performance. First, a larger capacitor bank will be required for higher energy storage. This brings a demand to develop materials with higher energy density to reduce the volume and weight of the capacitor. Second, thermal management is always considered for capacitor energy storage system. Dielectric materials are good electrical insulators, as well as good thermal insulators (with few exceptions). Therefore, a more thermally stable material is in demand. Third, efficiency is also significant for a lot of systems. From a ship integration point of view, methods to improve efficiency for capacitors are essential.

Capacitors are also widely used in commercial and consumer products. Within the last few years, designers have established a solid powertrain foundation for hybrid vehicles (HEVs) and electric vehicles (EVs). All major auto manufactures see the hybrid and electric vehicle market as one continuing to enjoy steady growth. One major driving factor to the projected increased growth is the significant technology advances taking place that directly impact the HEV and EV power electronic systems. At the heart of HEV and EV power electronic systems is the inverter (converting the DC battery energy into ac drive power), and at the heart of the inverter is the DC link capacitor. The capacitors used in these types of inverter applications will encounter a wide range of electrical loading through their lifetime as well as being required to meet the full range of mechanical and environmental specifications associated with automotive applications. As noted by the Department of Energy, the capacitors used in existing inverters occupy a

significant fraction of inverter volume (~35%), weight (~23%) and cost (~25%), so the more precisely the capacitor can be tailored to the application, the more efficient the inverter design can be.

Pulsed power capacitors are also used in numerous other applications where high power is required for a fraction of a second. For example, they are used in medical equipment such as defibrillators, surgical lasers, and X-ray equipment. In the commercial world they are used in cable fault detection equipment, food sterilization, and metal forming. In the national and international laboratories they are used for nuclear effects simulation, high-powered accelerators, and high intensity magnetic field experiments. Therefore, we need to design or discover a new material to improve the energy storage of the capacitors for these applications.

A capacitor generally consists of metallic conducting plates or foils separated by thin layers of an insulating medium, with the plates on the opposite sides charged by a voltage source and the electrical energy is stored in the polarized insulating medium. The basic configuration is shown in Figure 1.1. The capacitor is charged by a high-energy DC source and maintains the charge until used. The static capacitance is related to the applied voltage as $C = \frac{Q}{V}$, where Q is the charge density indicating the charge stored in the capacitor and V is the total voltage difference on plates. Geometrically, $= \varepsilon \frac{A}{d}$, where A is the area of the plate and d is the thickness of the insulating medium. In general, the metallic electrode plate area is determined by the dimensions the user requires, and the separation thickness is controlled almost totally by the lifetime the user specifies. The specific performance properties of the insulating medium/media will dominate all performance parameters of the capacitor, with the possible exception of peak current

limits in very high power applications. It is important to note that some insulating media have dielectric constants that are a function of the applied voltage, causing a nonlinear dependence of the capacitance upon applied voltage. We will discuss in detail for polymer materials in the following Section. This nonlinear dependence can increase internal power dissipation inside the capacitor as well as enhance electromechanical stress from repeated charging and discharging cycles.[2]

This energy is stored in the insulating media between the capacitor plates and can be released into the load. It is important to note that the discharge of this stored energy gives rise to mechanical forces inside the capacitor, which can cause material fracturing. In repetitive operation, the discharge can excite mechanical resonances in the capacitor structure, eventually resulting in destructive damage and electrical breakdown. The mechanisms of dielectric breakdown of polymer materials will be discussed in detail in Chapter 2.

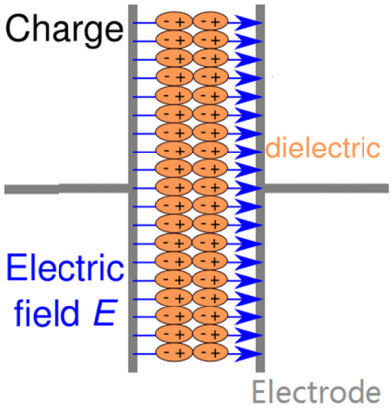

Figure 1.1 Structure of a Basic Capacitor

Capacitors available today are based on three basic technologies: electrolytics (Aluminum and Tantalum), Ceramic and film (polymer, mica and paper) capacitors.[3] The distinction between aluminum and tantalum electrolytics is the presence of a liquid aluminum versus dry impregnant tantalum. Electrolytic capacitor technology provides

moderate energy and power density, but has relatively high losses. Because the electrolytic capacitor is polarity dependent, it is therefore primarily used in dc circuits. Ceramic capacitors have similar energy density and are commonly used for blocking, buffering, bypass, coupling, low frequency filtering, tuning and timing for frequencies up to giga-hurtz. The third one, thin film technology provides a readily scalable capacitor technology, from nanojoules to hundreds of kilojoules per unit. It can be used for both dc and ac applications involving high power electronics pulse-duty circuits, high frequency filtering, continuous ac operation like lighting ballast and high frequency inverters, solid state switch snubbers, SCR commutation circuits, power factor correction, and fractional to large horsepower motor start and run capacitors.

The rapid expansion of high frequency electronics for various applications is putting dramatic pressure on the capacitor industry. There is a strong need for very low dissipation factor capacitors that are inherently reliable by their nature and gracefully fails. Graceful failure permits the capacitor to fail in a “soft” mode without shortening the whole device. Polymer film capacitors are presently the primary choice of materials for energy storage capacitors due to their relatively high electric breakdown field, low loss and fast speed. Most importantly, they are the only capacitor technology that can provide graceful failing or aging performance. Compared to ceramic capacitor technology, polymer films have lighter weight, which will improve the efficiency.

As we know, capacitors store energy electrostatically by the polarization of dielectric material. It is important to understand the material’s behavior under electric field. When sandwiched in between the two electrodes in capacitor, the material will respond to the applied electric field by redistributing its component charges to some extent, positive

charges being attracted towards the negative electrode and vice versa. Compared to the vacuum medium, where the charge:

$$Q = \varepsilon_0 E,$$

the polarization (***P***) of dielectric material increases the charge or the capacitance. The ratio of the increased capacitance to the vacuum capacitance is called the dielectric constant or relative permittivity of the material, expressed as:

$$\varepsilon = \frac{C}{C_0} = \frac{Q+P}{Q}.$$

Substituting Q in the equation, we can obtain the expression of polarization

$$\boldsymbol{P} = (\varepsilon - 1)\varepsilon_0 \boldsymbol{E}.$$

The quantity $\varepsilon_0 \varepsilon \boldsymbol{E}$ is called the electric displacement $\boldsymbol{D}$ in the material and can be expressed as

$$\boldsymbol{D} = \varepsilon_0 \varepsilon \boldsymbol{E} = \varepsilon \boldsymbol{E} + \boldsymbol{P}.$$

On the molecular level, the effect of the applied electric field is to induce an electric dipole $\boldsymbol{m}$ on each individual molecule. The magnitude depends on the local electric field $\boldsymbol{E_L}$ at the molecule, as in $\boldsymbol{m} = \alpha \boldsymbol{E}_L$. The constant α is called molecular polarizability.[4] The dielectric constant can relate to polarization via the Clausius-Mossotti relationship:

$$\frac{\varepsilon - 1}{\varepsilon + 2} \frac{M_W}{\rho} = \frac{N_A \alpha}{3\varepsilon_0},$$

where M_w is the molecular weight of the molecule, ρ is the density, and N_A is the Avogadro's number. However, this relationship above only works for the electronic and atomic polarization. When taking the orientation of molecules and inter-molecular interaction into consideration, it is complicated and difficult to predict the dielectric constant in terms of polarization. For polymers, the morphology highly affects the

dielectric properties, so one equation to calculate the dielectric constant based on the polarizability of each chemical bond is not sufficient in our study for material screening and design.

Orientation of molecular dipoles is a relatively slow process if compared to electronic transitions or molecular vibrations. Only when sufficient time is allowed after the application of an electric field for the orientation to attain equilibrium will the maximum polarization be achieved in the material. Therefore, under an alternating field: $\boldsymbol{E} = \boldsymbol{E_0}\cos\omega t$, one should observe a lag behind the applied field. It can be described by a phase lag in the electric displacement:

$$\boldsymbol{D} = \boldsymbol{D_0}\cos(\omega t - \delta).$$

It can be written as

$$\boldsymbol{D} = \boldsymbol{D_1}\cos\omega t + \boldsymbol{D_2}\sin\omega t,$$

where $\boldsymbol{D_1} = \boldsymbol{D_0}\cos\omega t$ and $\boldsymbol{D_2} = \boldsymbol{D_0}\sin\omega t$. This made it easy to define dielectric constant as a complex function:

$$\varepsilon^* = \varepsilon' - i\varepsilon'',$$

where the real part of dielectric constant $\varepsilon' = \frac{D_1}{\varepsilon_0 E_0}$ and imaginary part of dielectric constant $\varepsilon'' = \frac{D_2}{\varepsilon_0 E_0}$. The ratio of the two parts, $\varepsilon'/\varepsilon''$ is termed the dissipation factor, tan δ. The frequency dependence of the real and complex parts are describe with Debye's equations:

$$\varepsilon_r'(\omega) = n^2 + \frac{\varepsilon_s - n^2}{1 + \omega^2\tau^2}$$

$$\varepsilon_r''(\omega) = \frac{\varepsilon_s - n^2}{1 + \omega^2\tau^2}\omega\tau$$

where $n^2 = \varepsilon_\infty$ is the dielectric constant at very high frequency, ε_s is the static dielectric constant, and τ is called dielectric relaxation time.

The dielectric loss of the material is affected by many external factors: temperature, humidity, voltage and the frequency of the applied voltage. For polymers, as temperature is increased the forces between polymer chains is broken allowing for more susceptibility towards thermal motion. If there are polar groups within the material then they become easier to orient with the electric field. At very low temperature the segmental motion of the polar groups is frozen while so it is to disrupt the orientation. A major feature of the behavior of polymer materials is the glass transition (T_g). We can expect that at the onset of the molecular mobility above T_g, permanent dipoles attached rigidly to the polymer backbone become free to orient in an electric field, and this is accompanied by a major dielectric dispersion. There are usually several distinct dielectric relaxation processes present in solid polymer materials. They can be easily seen by scanning dielectric loss at constant frequency as a function of temperature (Figure 1.2). As the temperature is raised, molecular motilities of various types become energized and available for dipolar orientation. The relaxation peaks are labeled from the high temperature end to the low temperature end as α, β, γ and so on. Some polymers are completely amorphous and there is only one phase present in the solid material. In that case, there is always an α relaxation peak associated with the micro-Brownian motion of the entire polymer chain and at least one of the lower temperature subsidiary relaxation. Detailed examination of the relaxations requires isothermal scans of dielectric constant and loss as a function of frequency so that effective dipole moments and activation energies of relaxation times

can be obtained. The graphs like these are usually called dielectric spectra, and it will be discussed in detail in Chapter 2.

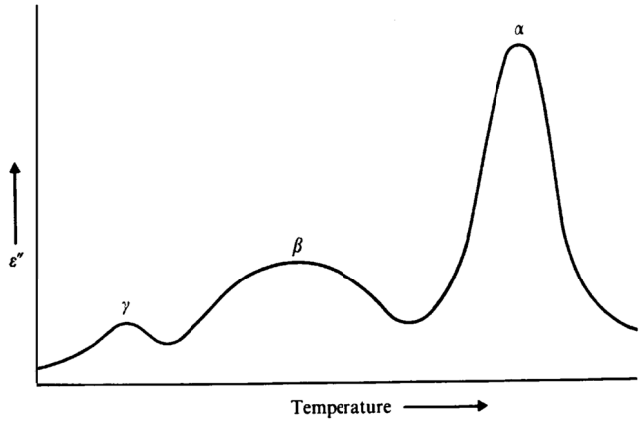

Figure 1.2 Dielectric relaxation peaks as a function of temperature

The polarization of dielectric material consists of five types: electronic, atomic (or vibrational), orientational (or dipolar), ionic and interfacial polarization.[5,6] Ionic polarization here refers to ion migration over a rather large distance, different from slight shifts of ions in the crystal lattice. Each polarization is associated with a dielectric loss at a specific frequency. These five types of polarizations can be divided into two regimes

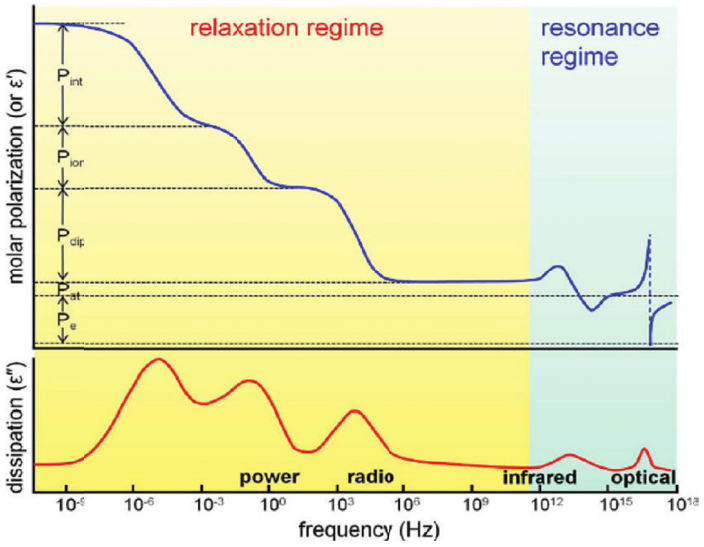

Figure 1.3 Different types of polarization as a function of frequency in polymers [Reprinted with permission from L. Zhu, J. Phys. Chem. Lett. 2014, 5, 3677. Copyright (2014) American Chemical Society]

(Figure 1.3),[7] resonance and relaxation regimes. For polymer dielectrics, the resonance regime includes electronic and atomic polarizations, since their losses are in the infrared and optical frequencies. The relaxation regime includes dipolar, ionic and interfacial polarizations. At the molecular level, we focus more on the first three types of polarization.

Electronic polarization is produced by the slight displacement of the electrons of any atom with respect to the positive nucleus under the electric field (Figure 1.4). The shift is quite small because the applied electric field is usually weak relatively to the intra-atomic field. Electronic polarization can respond to very high frequency and is responsible for the refraction of light. Atomic polarization is caused by distortion of the atomic nuclei in a molecule or a lattice (Figure 1.3). The movement of the nuclei is more sluggish than the electrons so that atomic polarization cannot occur at high frequency as electronic polarization. Since the force constants for bending or twisting of molecules are generally much lower than those for bond stretching, so one should expect bending modes to be making the major contribution to atomic polarization. The magnitude of atomic

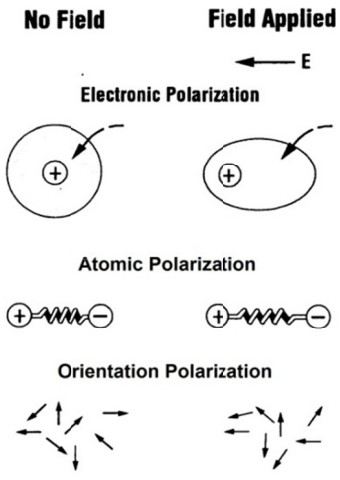

Figure 1.4 Schematic of molar polarization

polarization is usually quite small, often only one-tenth of that of electronic polarization.

If the molecules already possess permanent dipole moments, as always the case for polymer material, the dipoles will be aligned by the applied electric field to give a net polarization. This is the dipolar polarization. The orientation of molecular dipoles can make a rather large contribution to the total polarization, but it may be slow to develop and highly depends on the inter-molecular interactions. For polymers, dipolar relaxation usually takes place approximately between a fraction of 1 Hz and 100 MHz, depending on the nature of dipoles, phase transitions and temperature.[7,8] Ionic polarization discussed here involves physical transport of incorporated ions in polymers, typically happens between a second to hours. Ionic polarization is the fundamental mechanism for super-capacitors and batteries.[9,10] Maxwell-Wagner-Sillers interfacial polarization refers to charge carriers accumulated at interfaces in multicomponent polymer systems, and these real charges take hours to years to discharge.[7,8,11] The examples utilizing the interfacial polarization are copy machines, later printers, and high-efficiency air filters.[12,13] As we can see from Figure 1.2, the more types of polarization we utilize, the higher the polarization or dielectric constant we will achieve. However, the corresponding dielectric loss will also be generated.

1.2 Polymer dielectrics

Numerous polymer films have been studied for their application as a dielectric film in high energy density capacitors. Polymer film capacitors nearly replaced Kraft paper, a paper or paperboard produced from chemical pulp using the Kraft process, impregnated with dielectric fluids which were thermally limited and very inefficient. The first polymer that was developed called BOPP (biaxially oriented polypropylene). In 1963, G.E.

invented the MAGVAR® system which replaced most of the Kraft paper with BOPP film. Polypropylene was used because in the early 1960's, twenty-two different polymers were surveyed as to which one fit the following key requirements the best; 1) dissipation factor vs. frequency and temperature (thermal limitations), 2) dielectric strength (volume and cost), 3) dielectric constant (capacitance per unit area), 4) cost of monomer, 5) processability, 6) dielectric oil compatibility, 7) machinability, and 8) dielectric wear out and monomer purity. The operating temperature range was set at 100-110 ^{o}C. This operating temperature eliminated polyethylene and polyvinyldiene chloride as choices. The monomers used to produce the polysulfones and polyimides were too costly even though they had a higher dielectric constant. Polystyrene was used as a capacitor material but showed large variations in capacitance (>10 percent) over the operating temperature range. Polyethylene terephthalate and polycarbonate also cost more for the monomers and also possess critical property defects. Polyethylene terephthalate has a large dissipation increase in the operating temperature range (thermal runaway). Polycarbonate had good stability but a higher dissipation factor than polypropylene (0.25 vs. 0.1 percent). Therefore, polypropylene was the best choice to use as a dielectric insulator in capacitors. The biaxially oriented films showed an increase (about 2 fold) in dielectric strength versus unoriented films. The relation of improved dielectric strength versus orientation can be related to the improved mechanical properties of the oriented state.[14] Recent advances in the production of high energy density biaxially oriented polypropylene (BOPP) have increased the energy density from 0.5 J/cm^3 in the early 1990s to 5 J/cm^3 at breakdown as of today. BOPP possesses a low dielectric constant of ca. 2.2 with the best achievable dielectric constant being 2.5. Besides exhibiting

extremely low dissipation, BOPP also has an electronic polarizability breakdown of 720 MV/m for films that are ~10μm thick.[15,16] With the fact that BOPP suffers from a low dielectric constant of 2.2 and a reduced breakdown strength and cycle life at temperatures in excess of 85^{o}C, many approaches have been taken to enhance energy density by increasing K and breakdown field through the use of materials.

Polymer nanocomposite is one of the focused topics in this effort. Conventional dielectric materials are ceramics, as discussed above, with large dielectric constants as well as high stiffness and excellent thermal stability.[17-20] However, their applicability for practical high energy density capacitors is largely impeded by the low breakdown strength, high density, poor flexibility and challenging processing conditions. Polymer, on the other hand, have becomes an important choice for dielectric material as discussed above. However, most polymers still fall significantly short of the rising demands for high energy density capacitor because of their relatively low dielectric constants. The introduction of inorganic particles into polymer matrices for form dielectric composites has drawn plenty of attention. The idea is that the combination of high dielectric constant inorganic particles with polymers with high breakdown strength may result in a high energy density.

Previous investigations on dielectric composites concentrated mainly on the microsized particle, but their development is impaired due to the surface defects and stress cracking after a long-serving time.[21-24] The thickness of the microcomposite films is often limited by the size of the microparticles.[25,26] The way to improve is to prepare the nanocomposite polymer system. The advantages of that include low filler loading, nanometer sizes, and large internal surface area. Research in the past years concentrated

on the ferroelectric metal oxides particles such as TiO_2,[27-32] BaTiO3,[34-37], ZrO_2 [38-40] and so forth. However, as the particle shrinks from micrometer to nanometer scale, the physical properties of the particles change and some properties are sacrificed. Taking $BaTiO_3$ as an example, the dielectric constant decreases dramatically from 5000 to hundreds as the grain size is reduced from 1 μm to 30 nm.[41-44] Another concern is the special surface characteristics for the nanoparticle due to the large surface area to volume ratio. This leads to the primary issue associated with the physical dispersion of the nanoparticles.

The high surface energy of dielectric nanoparticles usually leads to agglomeration and phase separation from the polymer matrix, leading to poor quality films and weakened dielectric properties, such as high dielectric loss and low dielectric strength. There is another challenge associated with the fundamental weakness, the electric field intensification in the polymer matrix.[45,46] Since there is a large difference in dielectric constant between the two phases, the field intensifies on the polymer matrix. The nanoparticles with high dielectric constant act as electrical defect centers in filled polymers. And those centers effectively distort the distribution of the electric field, making the local electric field much higher than the average electric field. This effect results in an early breakdown of the polymer. For composites with the same shape, size and distribution of the filler, the larger dielectric constant difference, the higher the local electric field distortion it will create. As compared to the smaller particle size, a larger size of filler tends to induce a higher degree of field intensification.

In order to achieve a high dielectric constant and a corresponding high energy density, the content of nanofiller needs to be high but below the percolation threshold, which was

predicted by computational work to be ~30-35 vol% for spherical fillers.[47] An obvious increase of apparent dielectric constant and energy density is only observed until percolation is reached. Achieving a uniform dispersion of such a high content of nanofiller into the polymer matrix is not a trivial problem considering any defects and agglomerations would exist as weak points under electric field and would lower breakdown strength. It has been predicted by computational study that through changing the shape of nanofillers into the ones with higher aspect ratio, one can decrease the percolation threshold and circumvent the high loading of nanofiller. With the aspect ratio of 3, the percolation threshold of spheroidal particle decreases to 18 vol%.[48] Recently, $Ba_{0.2}Sr_{0.8}TiO_3$ nanorods were used in compliance with PVDF to achieve a dielectric constant of 17 with a loading of only 7.5 vol%.[49] Given that, a nonspherical nanofiller with high aspect ratio should be considered. Recently, a method to prepare a sandwiched structure of a boron nitride/polymer composite was reported to show improved dielectric behavior.[50]

Another focus for recent research is poly (vinylidene fluoride) (PVDF) and their copolymers, in attempt to modify their ferroelectric behavior. Polar crystalline polymers can usually be divided into three categories: normal ferroelectric, paraelectric and novel ferroelectric. PVDF and copolymers are famous examples for ferroelectric polymers. Large hysteresis loops are commonly observed for normal ferroelectric crystalline polymers, and they are originated from high spontaneous polarization (inside the ferroelectric domain) and high compensation polarization or interdomain coupling (outside the ferroelectric domain).[51-53] PVDF and its random copolymers were studied based on the effects of crystal orientation, polymorphism, crystallite size (or domain size),

and crystallinity on the ferroelectric behaviour and whether it can be used for high energy density application. In a recent study,[54] P(VDF-co-hexafluoropropylene) [P(VDF−HFP) 96/4 (mol/mol)] films with chain axes parallel and perpendicular to the film normal direction are obtained by solution-casting and hot-pressing and stretching, respectively. It is known that the dielectric properties of PVDF are anisotropic: the dielectric constants perpendicular and parallel to the chain axes are different. People found that in P(VDF−HFP) system, the hot-pressed and stretched film with a parallel crystal orientation is a better candidate than solution casted film with a perpendicular crystal orientation, because the α relaxation peak of the hot-pressed and stretched film can be shifted out of the power frequency range with increasing the temperature. However, it undergoes irreversible phase transformation under repeated poling, which causes high values of unreleased percent of energy. The effects of crystallite size[55-56] and crystallinity were also studied using this system. It seems the small crystallites favour narrower hysteresis loops for high energy density and low loss dielectrics. By adding more HFP comonomer, the crystallinity of the system decreases, and the hysteresis loops become continuously slimmer. However, the maximum electric displacement also decreases due to the suppressed intercrystal coupling.

Due to the large unreleased energy percentage (40-60%) in these ferroelectric polymer systems, they are not suitable for high energy density applications. And the truly reversible paraelectric crystalline polymers are so limited that a long time poling will often result in normal ferroelectric behaviour. Therefore, people also studied novel ferroelectric polymers for this application. For example, relaxor ferroelectric is one of them, which belongs to a class of disordered crystals with compositional nanodomains.

The relaxor ferroelectric behaviour is first reported for electron-beam-irradiated P(VDF-TrFE) system.[57] Since then, there have been several other methods to achieve this behaviour and the target is to introduce defects in the crystalline lattice. Many efforts have been using chemistry way to deliberately introduce crystal defects by using bulky comonomers such as chlorofluoroethylene (CFE), chlorodifluoroethylene (CDFE) and chlorotrifluoroethylene (CTFE) into P(VDF−TrFE) to form defect modified terpolymers.[58,59] For a specific P(VDF-TrFE-CFE) terpolymer, the discharged energy density reaches ~10 J/cc at 400MV/m, with the unreleased percent of energy to be ~20%. Even though the system has a really high dielectric constant (~50), the improvement of released energy density compared to BOPP is not substantial. Compared to relaxor ferroelectrics, antiferroelectric polymers appear to be a better choice due to a small hysteresis. However, no genuine antiferroelectric crystalline phase has been identified for polymer so far. The way to achieve the antiferroelectric behaviour in ferroelectric polymers is to decrease the polarizatbility of the amorphous phase at the amorphous/crystal interface. For example, decreasing the temperature to below the glass transition temperature can reduce the polarizatbility of the amorphous phase. As a result double hysteresis loops can be observed for β-PVDF at temperatures below -60^{o}C.[60] To utilize this method, polystyrene side chains were grafted onto a P(VDF-TrFE-CFE) terpolymer using ATRP to confine the ferroelectric PVDF crystals. The best system with 34% of polystyrene released energy density of ~10 J cm^{-3} at 600 MV m^{-1}, a fairly low dielectric loss (tan δ = 0.006 at 1 kHz), and a low ferroelectric/conduction loss (unreleased% =17.6% at 550 MV/m).

Recently, the approach on developing amorphous polar polymers, such as polyimides,[61-63] polyurethanes, polyureas[64] and polythioureas[65] took over the thought of utilizing dipolar orientational polarization for high K,[66] as well as minimizing nonlinear behaviour originating from highly oriented polar polymer chains. Our team explored chemical space to incorporate tin covalently into polymer chain and achieved increased dielectric constant and band gap.[67]

In order to "shoot for the right target", and make the material design process more efficient, we need to establish the criteria for polymer dielectric design. Chapter 2 will discuss the screening criteria we chose in this dissertation work.

Another unique side of this dissertation work is that we combined computational tools with the experiments to establish a complete design strategy, as shown in Figure 1.5. In order to facilitate the material screening process, in Chapter 3, the author will introduce a hierarchical search process using Density Functional Theory (DFT) based on recent works of her fellow scientists.

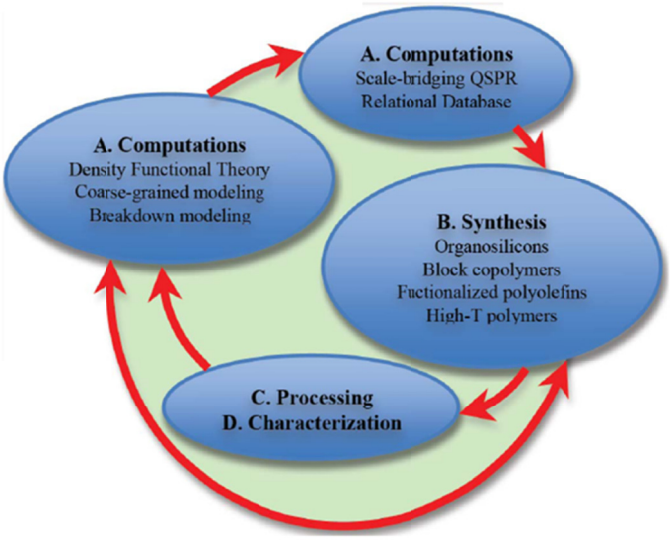

Figure 1.5 A complete loop of design strategy

From Chapter 4 to Chapter 7, the author will discuss in detail of the design of organic polymer and organometallic polymers used as dielectric material. Based on rational design from computational guidance, systematic synthesis and characterization and processing optimization, major conclusion for each type of material will be summarized at the end of each chapter. Chapter 4 will focus on polyimide as a dielectric material where different chain segments were designed to study the effect of polar groups as well as conjugated structures on dielectric properties. One promising candidate was developed with the capability of melt processed and stretched into thin film for capacitor assembling. Chapter 5 similarly is based on polythiourea as we switched the functional group and category from polyimide to polythiourea to investigate the difference. With the idea of mapping the period table for our searching, organometallic polymers were introduced to be applied as dielectric materials. Tin, Zinc and Cadmium as three candidates were discussed in full detail here and the effect of metal-oxygen complex on dielectric performance were investigated. Efforts were also invested on improving film quality of organometallic polymers through blending, copolymerization as well as processing conditions.

In Chapter 8, we will gather all the materials and their properties to establish structure-property relationships and to the provide directions for further work. The author also introduce the concepts of reverse design with computational and experimental combined database.

Reference

1. F. C. Beach, and I. R. McNabe, *IEEE Conference on Pulsed Power*, Monterey, CA, 2005, 1.

2. H. E. Duckworth, *Electricity and Magnetism*, Holt, Rinehardt, and Winston, New York, 1961.
3. H. S. Nalwa, *Handbook of Low and High Dielectric Constant Materials and Their Applications. Volume 1: Materials and Processing. Volume 2: Phenomena, Properties and Applications*, Academic Press, New York 1999
4. C. Ku, R. Liepins, *Electrical Properties of Polymers*, Hanser Publishers, 1987.
5. A. R. Blythe and D. Bloor, *Electrical Properties of Polymers*, 2nd ed.; Cambridge University Press: Cambridge; New York, 2005.
6. K.-C. Kao, *Dielectric Phenomena in Solids: with Emphasis on Physical Concepts of Electronic Processes;* Elsevier Academic Press: Boston, MA, 2004.
7. L. Zhu, *J. Phys. Chem. Lett.* 2014, **5**, 3677.
8. F. Kremer and A. Schönhals, *Broadband Dielectric Spectroscopy*; Springer: New York, 2003.
9. P. Simon and Y. Gogotsi, *Nat. Mater.* 2008, **7**, 845.
10. K. Xu, *Chem. Rev.* 2004, **104**, 4303.
11. G. H. Sessler and R. Gerhard-Multhaupt, *Electrets,* 3rd ed.; Laplacian Press: Morgan Hill, CA, 1998.
12. J. H. Dessauer and H. E. Clark, *Xerography and Related Processes*; Focal Press: London, 1965.
13. R. Thakur, D. Das and A. Das, *Sep. Purif. Rev.* 2013, **42**, 87.
14. J. L. Nash, *J. Polym. Eng. Sci.* 1988, **28**, 862.
15. E.J. Barshaw, J. White, M.J. Chait, J.B. Cornette, J. Bustamante, F. Folli, D. Biltchick, G. Borelli, G. Picci, M. Rabuffi, *IEEE Transactions on Magnetics* 2007, **43**, 223.
16. E.W. Anderson and D.W. McCall, *J. Polym. Sci. Part A: Polym. Chem.* 1958, **31**, 241.

17. P. Barber , S. Balasubramanian , Y. Anguchamy , S. Gong , A. Wibowo , H. Gao , H. J. Ploehn and H.C. Zur Loye , *Materials* 2009 , **2** , 1697.

18. J. Ihlefeld, B. Laughlin, A. Hunt-Lowery, W. Borland, A. Kingon, J. P. Maria, *J. Electroceram.* 2005, **14**, 95.

19. S. H. Yao, J. K. Yuan, P. Gonon, J. Bai, S. Pairis, A. Sylvestre, *J. Appl. Phys*. 2012, **111**, 104109 .

20. J. B. Wu, C. W. Nan, Y. H. Lin, Y. Deng, *Phys. Rev. Lett.* 2002, **89**, 21760 .

21. E. Tuncer, I. Sauers, D. R. James, A. R. Ellis, M. P. Paranthaman, A. Goyal and K. L. More, *Nanotechnology* 2007, **18**, 325704 .

22. J. K. Nelson and Y. Hu , *J. Phys. D: Appl. Phys.* 2005, **38**, 213.

23. R. W. Coppard, J. Bowman, L. A. Dissado, S. M. Rowland and R. T. Rakowski, *J. Phys. D: Appl. Phys.* 1990, **23**, 1554.

24. Y. Y. Sun, Z. Q. Zhang and C. P. Wong, Polymer 2005, **46**, 2297.

25. Z. M. Dang, H. P. Xu and H. Y. Wang, *Appl. Phys. Lett.* 2007, **90**, 012901.

26. S. Ramesh, B. A. Shutzberg, C. Huang, J. Gao and E. P. Giannelis, *IEEE Trans. Adv. Packaging* 2003, **26**, 17.

27. T. I. Yang and P. Kofi nas, *Polymer* 2007, **48**, 791.

28. B. Balasubramanian, K. L. Kraemer, N. A. Reding, R. Skomski, S. Ducharme, D. J. Sellmyer, *ACS Nano* 2010, **4**, 1893.

29. D. L. Ma, T. A. Hugener, R. W. Siegel, A. Christerson, E. Martensson, C. Onneby, L. S. Schadler, *Nanotechnology* 2005,**16**, 724.

30. S. Lin, X. Kuang, F. Wang, H. Zhu, *Phys. Status Solidi*, 2012, **6**, 352.

31. G. Ouyang, K. Wang, X. Y. Chen and J. Micromech. Microeng. 2012, **22**, 074002 .

32. Z. M. Dang, Y. J. Xia, J. W. Zha, J. K. Yuan, J. Bai, *Mater. Lett.* 201, **65**, 3430 .

33. B. H. Fan, J. W. Zha, D. Wang, J. Zhao and Z. M. Dang, *Appl. Phys. Lett.* 2012, **100**, 012903.

34. J. Li, J. Claude, L. E. Norena-Franco, S. Il Seok, Q. Wang, *Chem. Mater.* 2008, **20**, 6304 .

35. P. Kim, N. M. Doss, J. P. Tillotson, P. J. Hotchkiss, M. J. Pan, S. R. Marder, J. Li, J. P. Calame and J. W. Perry, *ACS Nano* 2009, **3**, 2581 .

36. P. Kim, S. C. Jones, P. J. Hotchkiss, J. N. Haddock, B. Kippelen, S. R. Marder, J. W. Perry, *Adv. Mater* 2007, **19**, 1001.

37. Z. Li, L. A. Fredin, P. Tewari, S. A. DiBenedetto, M. T. Lanagan, M. A. Ratner, T. J. Marks, *Chem. Mater.* 2010, **22**, 5154.

38. C. Zou, D. Kushner, S. Zhang, *Appl. Phys. Lett.* 2011, **98**, 082905.

39. J. Li, P. Khanchaitit, K. Han and Q. Wang, *Chem. Mater.* 2010, **22**, 5350.

40. N. Guo, S. A. DiBenedetto, P. Tewari, M. T. Lanagan, M. A. Ratner, T. J. Marks, *Chem. Mater.* 2010, **22**, 1567.

41. B. H. Fan, J. W. Zha, D. Wang, J. Zhao and Z. M. Dang, *Appl. Phys. Lett.* 2012, **100**, 012903.

42. G. Arlt, D. Hennings and G. Dewith, *J. Appl. Phys.* 1985, **58**, 1619.

43. K. Uchino, E. Sadanaga and T. Hirose, *J. Am. Ceram. Soc.* 1989, 72, 1555.

44. U. Y. Hwang, H. S. Park, Y. R. Kim andK. K. Koo, *Ind. Eng. Chem. Res.* 2004, **43**, 3141.

45. J. Y. Li, C. Huang and Q. M. Zhang, *A ppl. Phys. Lett.* 2004, **84**, 3124.

46. Y. Cheng, X. Chen, K. Wu, S. Wu, Y. Chen and Y. Meng, *J. Appl. Phys.* 2008, **103**, 034111.

47. A. L. An and S. A. Boggs, *Proceedings of the 2006 IEEE International Symposium on Electrical Insulation*, Toronto, June 2006.

48. L. An, S. A. Boggs and J. P. Callame, *IEEE Electr. Insul. Mag.* 2008, **24**, 5.

49. H. Tang and H. A. Sodano, *Nano Lett.* 2013, **13**, 1373.

50. Z. Cui, Z. Cao, R. Ma, A. V. Dobrynin and D. H. Adamson, *ACS Appl. Mater. Interfaces*, 2015, **7 (31),** 16913.

51. G. A. Samara, *J. Phys.: Condens. Matter* 2003, **15**, R367.

52. Y. Zhou, F. G. Shin, *J. Appl. Phys.* 2006, **100**, 024101.

53. V. A. Stephanovich, I. A. Luk'yanchuk, M. G. Karkut, *Phys. Rev. Lett.* 2005, **94**, 047601.

54. F. Guan, J. Pan, J. Wang, Q. Wang and L. Zhu, *Macromolecules* 2010, **43**, 384.

55. F. Guan, J. Wang, J. Pan, Q. Wang and L. Zhu, *Macromolecules*, 2010, **43**, 6739.

56. F. Guan, J. Wang, J. Pan, Q. Wang and L. Zhu, *IEEE Dielectr. Electr. Insul.* 2011, **18**, 1293.

57. Q. M. Zhang, V. Bharti, X. Zhao, *Science* 1998, **280**, 2101.

58. T. C. Chung, A. Petchsuk, *Ferroelectr. Lett. Sect.* 2001, **28**, 135.

59. T. C. Chung and A. Petchsuk, *Macromolecules* 2002, **35**, 7678.

60. T. Furukawa, M. Date and E. J. Fukada, *Appl. Phys.* 1980, 1135.

61. J. Li, J. Claude, L. E. Norena-Franco, S. I. Seok, Q. Wang, *Chem. Mater.* 2008, **20**, 6304.

62. N. Guo, S. A. DiBenedetto, P. Tewari, M. T. Lanagan, M. A. Ratner, T. Marks, *J. Chem. Mater*. 2010, **22**, 1567.

63. J. P. Calame, *J. Appl. Phys.* 2006, **99**, 084101.

64. A. L. An and S. A. Boggs, *Proceedings of the 2006 IEEE International Symposium on Electrical Insulation*, Toronto, June 2006.

65. B. Chu, X. Zhou, K. Ren, B. Neese, M. Lin, Q. Wang, F. Bauer and Q. M. Zhang, *Science*, 2006, **313**, 334.

66. F. Guan, J. Pan, J. Wang, Q. Wan, and L. Zhu, *Macromolecules,* 2010, **43**, 384.

67. W. Li, L. Jiang, X. Zhang, Y. Shenb and C. W. Nan, *J. Mater. Chem. A,* 2014, *2*, 15803.

Chapter 2

Criteria for New Polymer Dielectric Design

Over the years, the materials design process has undergone major evolution. From manually testing materials one-by-one to determine their performance, to capturing the key characteristics and criteria for material screening before any testing is done, the progress has been quite a leap. The area of designing polymer dielectrics has been a topic of interest to materials scientists and polymer chemists working on high energy storage, transistors, photovoltaics and insulators. As discussed in Chapter 1, polymers have emerged as attractive dielectric material options due to their easy processability, flexibility, high resistance to external chemicals and graceful failure. Many organic polymers such as polyvinylidene fluoride (PVDF), polypropylene (PP), polyethylene terephthalate (PET) and polyethylene (PE) have been used as dielectrics in a variety of energy and electronic applications. The current standard material BOPP with its high breakdown field and low cost, still suffers from low dielectric constant and operating temperature. PVDF and copolymers, nanocomposite dielectrics and many other efforts have been focused to address these issues, however without a systematic and rational approach. In this particular dissertation work, we combined the advanced computational tools to help polymer dielectric design. In order to efficiently and successfully establish a hierarchical screening strategy, it's essential to clarify the criteria for polymer dielectric material screening.

For this capacitor energy storage application, we are designing polymer material for high energy density and low loss. Generally, the energy density of a dielectric material is illustrated as an integral:

$$U_e = \int_{D_{max}}^{0} E \, dD$$

where E is the electric field and D_{max} is the electric displacement at the highest field. For a linear dielectric material, this equation becomes:

$$U_e = \frac{1}{2} DE = \frac{1}{2} \varepsilon_r \varepsilon_0 E^2$$

So it is clear that in order to improve the energy density, we need to increase the dielectric constant as well as the breakdown strength. To also achieve a high efficiency for energy storage, a low dielectric loss, including relaxation loss as well as conduction loss is required. The mechanical, thermal and chemical stability and durability for polymer materials are important effects on the final performance. In the area of

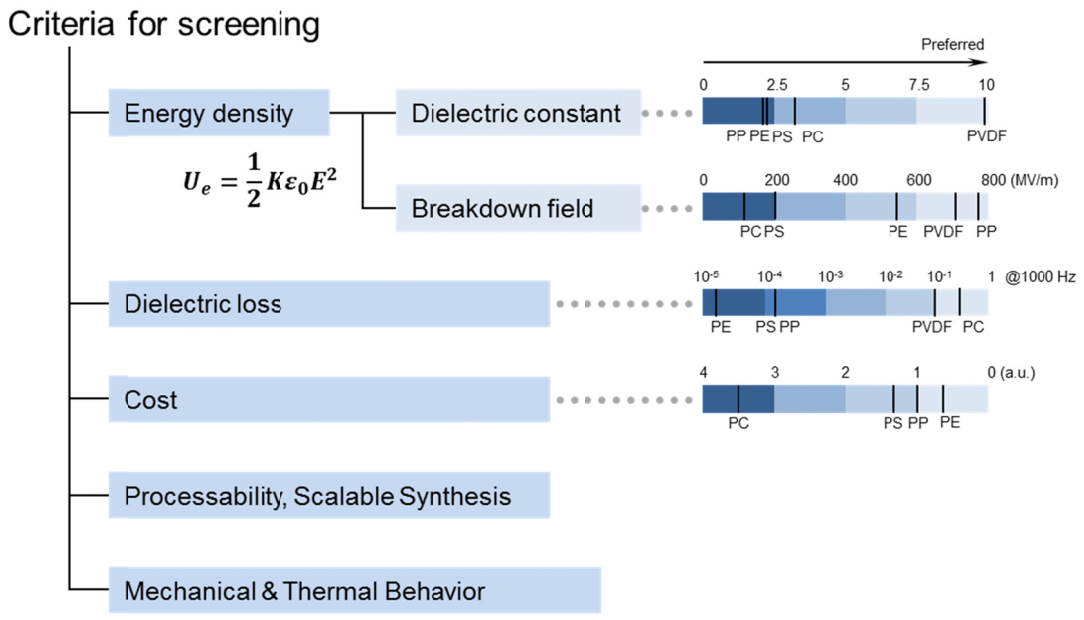

Figure 1.5 A complete loop of design strategy

dielectrics, thermal properties determines the dielectric relaxation behavior, breakdown mechanism at high voltage, as well as the aging and degradation, which is related to long time scale performance. At last, for a new material development, one always needs to consider a facile method of material synthesis and preparation, which can be eligible for large scale production and performance consistency. We here summarized the criteria for dielectric screening as the chart in Figure 2.1, with detailed discussion following.

2.1 Dielectric constant, polarization and corresponding relaxation loss

As discussed in Chapter 1, the ability of dielectric material to store energy electrostatically comes from the polarization of the material, and the polarization consists of five types: electronic, atomic (or vibrational), dipolar (or orientational), ionic and interfacial polarization. The more types of polarization we utilize, the higher the dielectric constant that we can achieve. And it's important to investigate each type of polarization and determine whether it can be efficiently utilized to bring a high dielectric constant as well as an acceptable dielectric loss.

From the lower end of the frequency spectrum, interfacial polarization takes the longest time to complete. And because of this reason, it is not desirable to use it for capacitor energy storage and pulsed power applications. However, it does exist in all multicomponent dielectric systems, and even in a semicrystalline polymer the crystal/amorphous interfaces may cause interfacial polarization. As discussed in detail in Chapter 1, nanocomposite polymer dielectric utilizes interfacial polarization to achieve high dielectric constant. However, this approach is facing both the processing and theoretical difficulties. Another utilization of interfacial polarization on interfacial polarization is the multilayer polymer films. Using multilayer coextrusion technology,[1]

alternating layers of a high breakdown dielectric polymer [e.g., polycarbonate (PC) or polysulfone] and a high energy density ferroelectric polymer (e.g., PVDF or its random copolymers) have been fabricated. Because all interfaces are perpendicular to the electric field direction, space charges (i.e., electrons and/or holes) as well as impurity ions can be accumulated at the multilayer interfaces upon electric poling, again owing to contrasts in both dielectric constant ($\varepsilon_{r,PVDF}$ = 10−12 and $\varepsilon_{r,PC}$ = 2.8) and bulk conductivity (σ_{PVDF} = 10−13 S/m and σ_{PC} = 10−16 S/m). These interfacial charges form effective traps for injected electrons from the metal electrode.[2] Intriguingly, instead of a decrease, an enhanced electric breakdown strength is observed for multilayer films as compared to the linear average of PC and PVDF controls.[3-5] However, there are lack of prove how much the interfacial charges are playing a role in enhancing the performance. Ionic polarization has been used in polymer electrolytes to enhance the capacitance of gate dielectrics for organic field effect transistors. However, as discussed in Chapter 1, the transport of ions will result in high dielectric loss. This is often observed for impurity ion –containing polar polymers such as PVDF and nylons, even though the impurity concentration is only at or below the ppm level.[6,7] This leads to another criteria for screening, which is a synthesis method that requires no or completely movable catalyst, and produce no or completely movable byproduct.

Since interfacial and ionic polarizations cannot be directly utilized to achieve high dielectric constant and low loss polymer dielectrics, what have left for consideration are electronic, atomic and bipolar polarizations. The three types of polarizations are commonly coexist for polymer systems. Since electronic and atomic polarization have no relaxation losses in the power and radio frequency range, can they be further enhanced

for polymer dielectrics? On the basis of polarization mechanisms for organic polymers, electrons need to be further delocalized in order to increase electronic polarization, and atoms need to change from carbon to other elements such as Si in order to enhance the mobility and then increase the atomic polarization. However, as we all know, delocalization of electrons will generally decrease the band gap, for example, in conjugated polymers. Therefore, it is important to study the relationship between electronic and atomic polarization with band gap and establish the upper limit boundary where we can improve to the most.

Dipolar polarization can be used to increase the dielectric constant efficiently, and a famous example would be ferroelectric polymer PVDF. How to push this dielectric behavior to another extreme and achieve linear dielectric behavior is the challenge. As mentioned in Chapter 1, isolated dipoles are favored compared to ferroelectric crystal domains, since they have weak interactions between each other and can also freely move. Under electric field, a slim D-E loop can be obtained. Therefore, polar amorphous polymers have been another focus in recent studies.[8-10] These studies show that addition of permanent dipoles help to increase the dielectric constant in the amorphous polymers within some extent, since the mobility of dipoles are hindered by either their glass state or their neighboring chains. Methods to design the molecular structure instead of adding side chains or groups needs to be investigated to further improve the dipole mobility, as well as push the dipole relaxation towards higher frequency range.

In addition to the relaxation loss mechanisms mentioned above, electronic conduction is another source of loss for polymer dielectrics, especially at elevated temperatures. Borrowing from semiconductor theories, major modes for electronic conduction include

both electrode-limited (e.g., Schottky emission, Fowler−Nordheim and direct tunneling, and thermionic field emission) and bulk-limited (e.g., Poole−Frenkel emission, electron hopping, Ohmic conduction, and space-charge-limited conduction) conduction mechanisms.[11] Electrochemical reactions must be strictly prohibited for dielectric applications, especially under high voltages. In general, small polar molecules and ions are susceptible to electrochemical reactions, whereas nonpolar molecules and polymers do not readily undergo electrochemical reactions unless they are contaminated with small polar molecules and ions. Therefore, it is highly desired that polymer dielectrics be free of moisture and/or impurity ions. Therefore, when we consider which types of polarizations to enhance the dielectric constant of a polymer dielectric, we shall always bear in mind that more than one type of loss mechanism may work at the same time.

2.2 Mechanisms for electrical breakdown

Another important criterion we need to consider is breakdown strength. As voltage across the material increases, there comes a point at which so much electric energy releases quickly, making the materials burn out in the breakdown region between the electrodes. This potential is the breakdown field, defined as the maximum electric field strength that the insulating material can withstand without breakdown. The dielectric breakdown of insulating materials has been a subject of experimental and theoretical investigations for many decades because of its technical importance. Breakdown mechanisms are complex as they are dominated by many extrinsic factors not inherent to the material, such as impurities, cavities, variations in morphology and microstructure. Most of the computational contribution is about the intrinsic breakdown of the material, a

quantity that can be viewed as an intrinsic material property which provides the upper bound to the dielectric breakdown field.

The basic mechanism of electrical breakdown, more precisely the low-level degradation model described electrical breakdown can be divided into: electric, thermal, electromechanical, and partial discharge breakdown.[12] It seems like that the intrinsic breakdown strength is governed by this electric breakdown mechanism which is primarily associated with the electrode-polymer interface rather than properties intrinsic to the insulator. This mechanism can be explained in terms of electron-avalanche theory, which depends on the presence and creation of charge carriers capable of migration through the dielectric. Electrons gain energy from an external electric field between successive collisions with phonons. At low electric fields, the electron energy distribution achieves steady state, as the energy gain from the external electric field is balanced by energy loss from collisions with phonons. At a sufficiently high electric field, the electron energy increases indefinitely until a threshold is reached at which a high-energy electron ionizes the lattice, leading to carrier multiplication. This process is referred to as impact ionization, and the ensuing avalanche of electrons can damage the material (e.g., through bond breakage). The general features of electron avalanche breakdown theory include the acceleration of a conduction electron by the electric field, the loss of energy from electron to phonons, the generation of a second conduction electron accompanied by a loss of kinetic energy of the first electron through impaction ionization, and the repetition of impact ionization until the electron concentration is sufficient to damage the material. It was found that the intrinsic breakdown strength tends to increase with the band gap, or the material with higher band gap tends to have higher intrinsic breakdown strength, as a

material with a greater band gap will display a higher threshold for impact ionization.[13] Therefore in this dissertation work, we set band gap as one of the direct criteria for both computational and experimental efforts.

Thermal breakdown occurs when the heat input cannot be balanced by the heat losses from the insulation either macroscopically or, more usually, in a small area. As power is dissipated by the insulation, heating occurs which usually causes an exponential increase in the electrical conductivity as more carriers become available for conduction. Alternatively the increased segmental motion may increase the mobility for intrinsic ionic conduction. If the electrical stress is maintained, the current density increases in the area of elevated temperature. This serves to further increase the local temperature through Joule heating and hence the conductivity. The thermal breakdown mechanism is the usual mechanism in polyimides and possibly PVDF.

Electromechanical breakdown occurs due to the electrostatic attraction of the electrodes which decreases the width of the insulation by an amount depending on the Young's modulus. If the applied voltage is maintained, the field increases due to the decrease in thickness thereby increasing the attraction further. The effect is exacerbated by the local heating and consequent softening which is likely to occur in this region. This breakdown mechanism is likely to be of only limited technological significance since polymers used in the insulating systems are either not usually used above their softening point, or, if they are (such as may be the case in a polyethylene power cable under very high load conditions), then they are usually crosslinked and sufficiently thick for this effect to be negligible.

Small voids inevitably occur in polymeric insulation even in the most carefully prepared materials. Since these are filled with gas they have a lower permittivity than the surrounding polymer and so field intensification occurs at the end walls in the direction of the local field. Depending on the gas pressure and other factors the enhanced field may cause the gas to become ionized; i.e. breakdown or discharge within the void. Because this does not necessarily cause the whole polymer insulation to breakdown (and discharge) immediately, this is known as partial discharging. The carriers produced by the ionization are accelerated across the void and, if they acquire sufficient energy from the field, may cause erosion as they impact on the opposite wall of the void. In thin insulating systems this may quickly lead to failure. However in thicker insulators, in which larger voids are more likely to occur but less likely to be detected, these partial discharges may produce electrical trees. In this case the partial discharging acts more as a degradation mechanism with breakdown not occurring immediately. In some systems the eventual breakdown due to partial discharges is so delayed that it is beyond the economic life.

In this dissertation work, we set high thermal stability and durability as one of the criteria for material screening. Not only are we attempting to avoid thermal breakdown from happening, we are minimizing the relaxation loss at higher temperature due to thermal transition. Another important requirement mentioned above is to look for a synthesis and processing method to minimize the impurity content and to optimize the polymer film formation.

2.3 Scalable synthesis and thin film processing

For a newly designed polymer material, their synthetic route and processing condition is extremely important in affecting the final performance of the material. In the area of

dielectrics, as mentioned above, the impurity content needs to be at the minimum to keep low dielectric loss and high breakdown strength. For this requirement, a synthetic route that requires no or minimum amount of catalyst and produce no or minimum amount of byproduct is preferred. If considering scale-up process and the final cost for the whole capacitor, one should design the synthesis route to be simple with minimum steps. The reactive compounds should possess high reactivity to shorten the reaction time. Polypropylene (PP) used for dielectric applications are synthesized using metallocene catalysts, in order to achieve regular orientation (usually isotactic) for the purpose of improved crystallinity. The complete removal of the catalyst which contains metal compound would be a problem for dielectric applications, same as PVDF as mentioned earlier. Therefore, for all the work in this dissertation, we chose to prepare new polymer materials through condensation polymerization, in which the reaction produces no byproduct or simply water. For the organometallic polymers we investigated, the sodium chloride salt as the byproduct stays in the reaction solution whereas our main products precipitate out of the reaction system.

Another step to a real applicable dielectric film is processing, in which we are fabricating polymer thin films with good uniformity and low defects and cavity counts. And the films should be flexible to be able to roll up in the capacitor. The common processing techniques to prepare polymer films consist of solution casting (film applicator, spin coating, spraying coating, etc.) and melt processing (extrusion and blowing). Compared with solution casting, melt processing does not require large amount of solvent, which reduces the cost of the process. It can be problematic to completely remove the solvent used during solution casting, which will function as impurity and

sacrifice the performance of the polymer dielectric film. However, in the lab scale, solution casting is preferred for a fast screening process. And spin-coating, film applicator and simple drop-casting were used in this work to demonstrate the performance of new materials synthesized.

2.4 Characterization methods of polymer dielectrics

Summarized here are the techniques used in this dissertation work to characterize the materials' dielectric properties, with specific details listed in each following chapters for separate works based on different materials.

2.4.1 Dielectric spectroscopy

Dielectric spectroscopy is an ideal tool to study molecular dynamics and charge transport. In its modern form, it is broadband in frequency and covers the range from 10^{-16} Hz to 10^{12} Hz. To span this huge frequency window a variety of different measurement techniques have to be combined, as summarized in Figure 2.2.

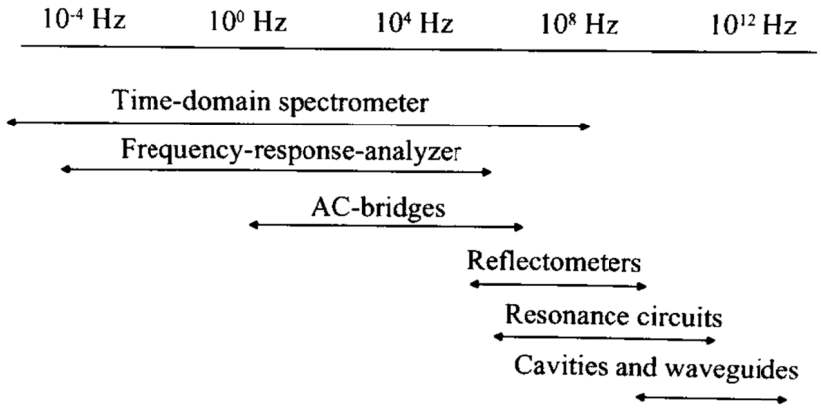

Figure 2.2 Summary of various types of dielectric measurements techniques

On the low frequency side of the dielectric spectrum, time-domain techniques are often employed. At time t=0, a voltage step is applied and the polarization current is

recorded. To obtain the dielectric relaxation spectrum, Fourier transform techniques have to be applied. An alternative way to measure dielectric properties in the time domain is applying a certain displacement *D* at t=0 and acquiring the time-dependent voltage or field *E* (t). In this case, the results refer to the dielectric modulus. Time-domain measurement can be extended to frequencies up to 20GHz, but with a less accurate resolution in comparison to the network analyzer approach. In this technique, a rectangular step voltage pulse is applied to the sample, and the changes in the characteristics of the pulse after the reflection from a section of a coaxial line filled with the sample being tested are monitored. The response of the sample to a fast voltage change is recorded in the time domain and converted to a complex frequency response. Mopsik first published his invention of the time-domain dielectric spectrometer (TDS) in 1984, Figure 2.3.[1] With the improvement of solid state electronics a spectrometer could be achieved with an accuracy of 0.1% and a minimum loss resolution in tan δ of 10^{-5} within a frequency range of 10^{-3} to 10^{4} Hz. If the loss resolution was reduced by an order of magnitude then the frequency range could be brought down to 10^{-4} Hz.

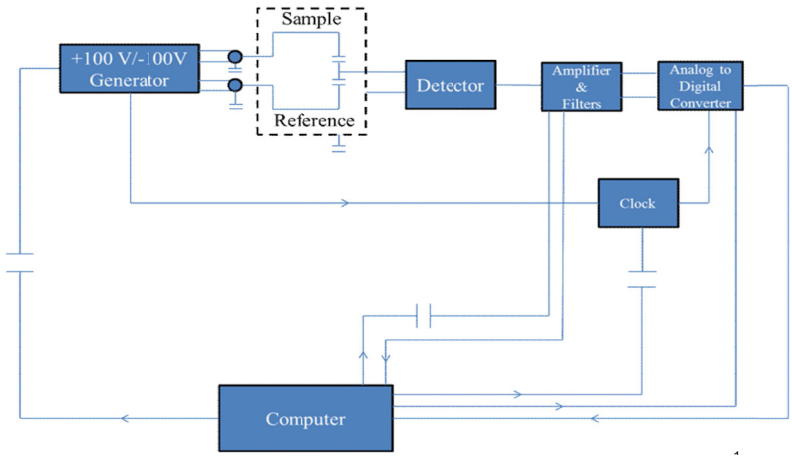

Figure 2.3 Block diagram of Mopsik's time-domain dielectric spectrometer

The time-domain dielectric spectrometer used to gather the data reported in this dissertation is an IMASS TDS. The sample is placed in a sample holder (Figure 2.4) developed by the EIRC at the University of Connecticut. The sample is sandwiched in between two conductive silicon electrodes with an area of 0.78 cm^2 with a Teflon guard around the electrode. The TDS is attached with longer leads to allow for dielectric measurements to be done at various temperatures in an external oven.

Figure 2.4 Sample holder for measuring dielectric spectrum developed by the EIRC

To compliment TDS, dielectric measurements are performed at higher frequencies, 20-106 Hz, using an LCR (Inductance, Capacitance, Resistance) meter, in which an AC current is measured through the sample. The frequency domain measurements performed in this dissertation are done on an Agilent 4284A Precision LCR meter. The sample is placed in the same holder as used for the TDS measurements. The dielectric constant of the material is then calculated from measured capacitance. Again the measurements can be conducted in an air circulated oven.

2.4.2 Band gap measurement and UV-Vis spectroscopy

The most common method of determining the band gap is by optical measurements. To measure the band gap, we need to measure the transmission and reflection of a thin film or single crystal or the diffuse reflection of a powder.

To determine the band gap of the insulating materials synthesized in this dissertation, UV-vis spectroscopy is performed. The absorption of UV-vis radiation results in the promotion of electrons from the ground state to the excited state. To measure the band gap a solution of the dielectric materials is drop casted onto a quartz microscope slide. Quartz is used instead of the normal borosilicate glass because the abosorption maximum of quartz occurs below 175 nm. The absorption spectra is collected using a Cary 5000 UV-vis spectrometer over a wavelength range of 175-800 nm with a second quartz slide as a blank. The onset wavelength, λ_{onset}, of absorption is determined from the intersection point of the two extrapolated lines in the spectra. The band gap is then calculated using Planck's relation:

$$E_g = {}^{hc}/_{\lambda}$$

where h is Planck's constant, c is the speed of light and λ is the onset wavelength.

2.4.3 Refractive index and ellipsometry

As already discussed, at high frequencies the dielectric constant is equal to the square of the refractive index of the insulating material, which corresponds to the electronic part of the dielectric constant, ε_{elec}. To measure ε_{elec}, ellipsometry is used since it is highly sensitive to the change in polarization of the sample due to such properties as thickness, refractive index or dielectric function tensor, upon exposure to electromagnetic radiation. The radiation is emitted from a source and linearly polarized by a polarizer. The incident radiation may then be passed through a compensator before hitting the sample at an

incident angle. Upon reflection from the sample the light may pass through another compensator and a second polarizer termed as the analyzer. After passage through the analyzer the light reaches the detector. The detector measures the complex reflectance ratio, ρ, which relates to the amplitude ratio, Ψ, and phase difference, Δ, through the following equation;[14]

$$\rho = \frac{r_p}{r_s} = \tan(\Psi)e^{i\Delta}$$

The amplitude ratio and phase difference represent the optical constants and thickness parameters, but in order to determine the refractive index the data must be modelled. The refractive index data in this dissertation work was evaluated using variable angle spectroscopic ellipsometry (VASE, J.A.Woollam Co., M-2000). General scans were performed over the wavelength range from 350 to 1497 nm, values at 546 nm listed in Table 3. The ellipsometric angles were modelled using a recursive model consisting of the silicon substrate and a Cauchy layer to describe the refractive index of films.

2.4.4 Breakdown field

Breakdown strength measurements discussed in this dissertation were performed using a linear voltage ramp generated by a resistor capacitor (RC) circuit. Figure 2.5 illustrates the sample setup for breakdown measurements. First a strip of a film electrode to ground is placed down with the metallized surface facing up. On top of the first electrode is placed the sample being tested and resting on top of that is a Kapton mask with a 2 cm^2 hole to ensure that breakdown occurs within the uncovered area. Lastly, a second film electrode to high voltage with metalized side facing down is placed over the area of exposed sample and mask. When the first breakdown event occurs, the power supply is shut off through an interlock input by a silicon controlled rectifier (SCR) circuit, which

uses the breakdown-induced ground-rise voltage capacitively coupled to the gate of an SCR. The breakdown voltage of the sample is read from a peak-holding voltmeter. The sample thickness was determined using a thickness gauge (Model LE1000-2, MeasureItAll) as the average of several measurements near the breakdown site. The Weibull distribution, which is based on the weak-link theory, is applied for characterizing data.[38] The Weibull distribution function, F(x), is given as:

$$\begin{cases} F(x)=1-\exp\left[-\left(\frac{x-c}{\eta}\right)^{\beta}\right] & \text{for } x \geq c \\ F(x)=0 & \text{for } x<c \end{cases}$$

where x is the electric field; η is the scale parameter, defined as Weibull characteristic breakdown field here (the breakdown field at 63.2% probability); β is the shape parameter, which is a measure of dispersion in the data; and c is the threshold field below which no breakdown will occur. The 2-parameter Weibull distribution is obtained when c=0 and is employed here.

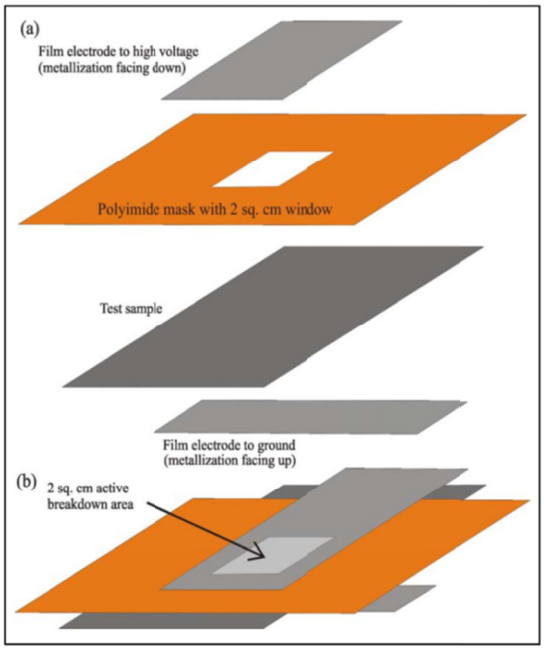

Figure 2.5 Schematic of the sample setup for breakdown measurements

2.4.5 D-E hysteresis loop

The electric displacement change under different voltage is always a great indication of the dielectric behavior of the material, especially under high voltage that the dielectric spectroscopy cannot achieve. The displacement-electric voltage (D-E) hysteresis loops shown in Figure 2.6 illustrate difference types of dielectric behavior from linear dielectric to ferroelectric and several novel types in between. Using D-E hysteresis loop, we can also determine the conduction loss, especially at high voltage.

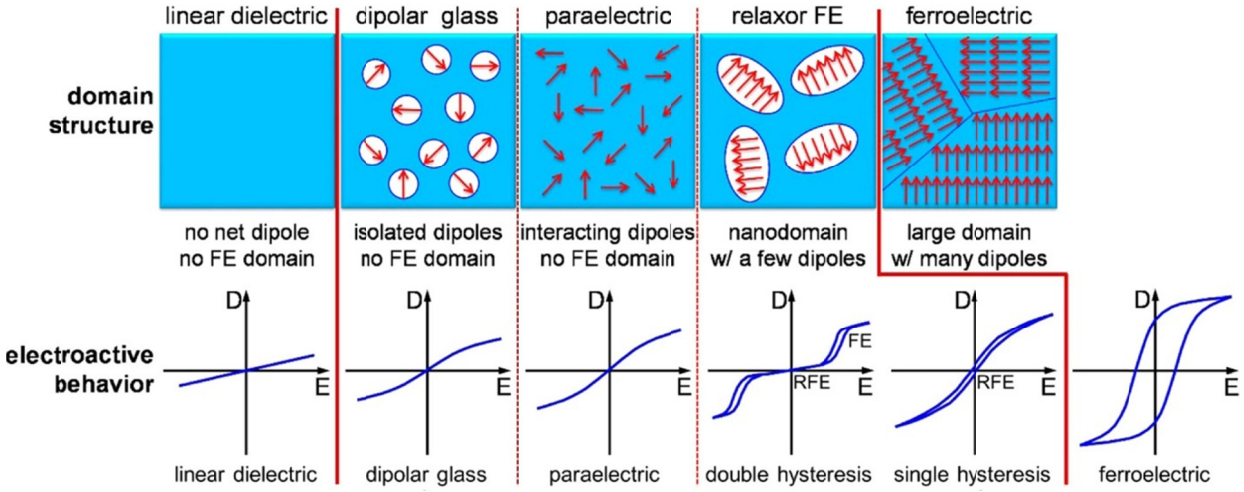

Figure 2.6 Different types of displacement-electric voltage (D-E) behavior[Reprinted with permission from L. Zhu, J. Phys. Chem. Lett. 2014, 5, 3677. Copyright (2014) American Chemical Society]

Here in this dissertation work, the charge-discharge behavior was estimated using D-E hysteresis loop. Polarization measurements were conducted with a modified Sawyer-Tower circuit, employing a Trek Model 10/40 10kV high voltage amplifier and an OPA541 operational amplifier based current to voltage converter. The data obtained were analyzed and plotted using a self-made program by Matlab. As shown in Figure 2.7, the input energy density and released energy density are area I + II and area I, respectively. And the efficiency is calculated as the ratio between area I and total area = I + II.

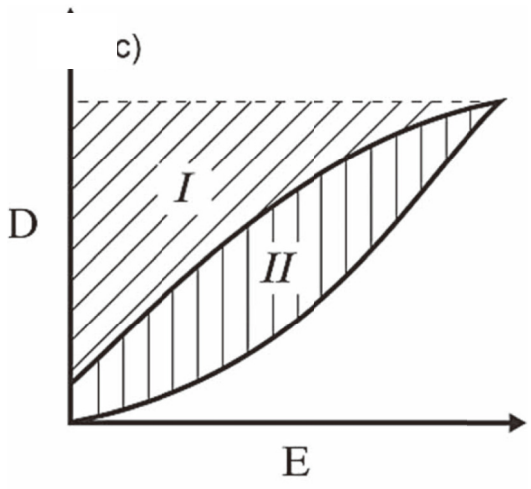

Figure 2.7 Schematic of the discharge efficiency at high field, which is the ratio between area I and total area = I + II (total input energy density)

Reference

1. H. Wang, J. K. Keum, A. Hiltner, E. Baer, B. Freeman, A. Rozanski, A. Galeski, *Science* 2009, **323**, 757.
2. J.-K. Tseng, S. Tang, Z. Zhou, M. Mackey, J. M. Carr, R. Mu, L. Flandin, D. E. Schuele, E. Baer, L. Zhu, *Polymer*, 2014, **55**, 8.
3. M. Mackey, A. Hiltner, E. Baer, L. Flandin, M. A. Wolak, J. S. Shirk, *J. Phys. D: Appl. Phys*. 2009, **42**, 175304.
4. Z. Zhou, M. Mackey, J. Carr, L. Zhu, L. Flandin and E. Baer, *J. Polym. Sci., Part B: Polym. Phys*. 2012, **50**, 993.
5. Z. Zhou, M. Mackey, Y. Yin, L. Zhu, D. Schuele, L. Flandin and E. Baer, *J. Appl. Polym. Sci.* 2013, **131**, 39877.
6. M. Mackey, D. E. Schuele, L. Zhu and E. Baer, *J. Appl. Phys.* 2012, **111**, 113702.
7. L. Yang, E. Allahyarov, F. Guan and Zhu, L. *Macromolecules* 2013, **46**, 9698.

8. J. T. Bendler, C. A. Edmondson, M. C. Wintersgill, D. A. Boyles, T. S. Filipova and J. J. Fontanella, *Eur. Polym. J.* 2012, **48**, 830.
9. J. T. Bendler, D. A. Boyles, C. A. Edmondson, T. Filipova, J. J. Fontanella, M. A. Westgate, M. C. Wintersgill, *Macromolecules* 2013, **46**, 4024.
10. I. Treufeld, D. H. Wang, B. A. Kurish, L.-S. Tan and L. Zhu, *J. Mater. Chem. A,* 2014, **2**, 20683.
11. J. L. Dormann, D. Fiorani and E. Tronc, *Adv. Chem. Phys.,* 1997, **98**, 283.
12. L. A. Dissado and J. C. Fothergill, *Electrical Degradation and Breakdown in Polymers*, Peter Peregrinus Ltd.: London, 1992; Part 3
13. Y. Sun, C. Bealing, S. A. Boggs and R. Ramprasad, *IEEE Electrical Insulation Magazine* 2013, **29**, 8.
14. L. J. Arsov, M. Ramasubramanian, B. N. Popov, *Ellipsometry In Characterization of Materials;* Wiley: Hoboken, New Jersy, 2012, 1135-1146.

Chapter 3

Computational Strategies for Polymer Dielectrics Design

Over the years, the materials design process has been going through major breakthrough, from manually testing materials one-by-one to determine their application, to capturing the property/performance criteria before any synthesis and tests. In the latter half of the 20th century, computations gradually rose in prominence to provide guidance for time-intensive and expensive experiments. Applying many laws of nature, especially the tool of quantum mechanics, solving problems on a computer facilitates is faster and more efficient, and it also provides more fundamental understanding of materials. Computational results/observations started to provide important information for experiments and material design in making crucial preliminary decisions. First principles computations have widely been used in materials discovery and design for a variety of applications. And here we are exploring the application in designing polymer dielectric material.

As mentioned before, there is an increasing demand for new polymer dielectrics. However, the discovery of new materials has largely been guided by expensive and lengthy experimental cycles. The new materials design using computational approaches is increasingly being considered as an attractive alternate option.[1-10] Several classes of computational methods appropriate to model polymer dielectrics have reached a high level of sophistication, accuracy and utility (Figure 3.1).[11]

At the most fundamental level, density functional theory (DFT) based on quantum mechanics can be used to determine dielectric properties at the scale of a crystalline unit cell,[12-15] including structural and thermodynamic details, reasonable estimates of the band gap, electronic dielectric constant, ionic dielectric constant, and intrinsic breakdown field.[16-22] Larger scale chain orientation and morphology difference of polymers can be analyzed using molecular dynamics (MD) based on empirical interatomic potentials or force fields.[23-27] Such simulations can predict crystal structure, semicrystalline morphology and provide rough estimates of glass transition temperature and dielectric loss. Beyond the physics approach, a "data-driven" approach uses various forms of multivariate analysis on experimental or computational data to establish physical relationship to the properties being predicted. Such systems are "trained" on available data and then used to predict properties of interest for polymers for which data are not available. An example of such data-driven approaches is quantitative structure property relationships (QSPR).[28-31]

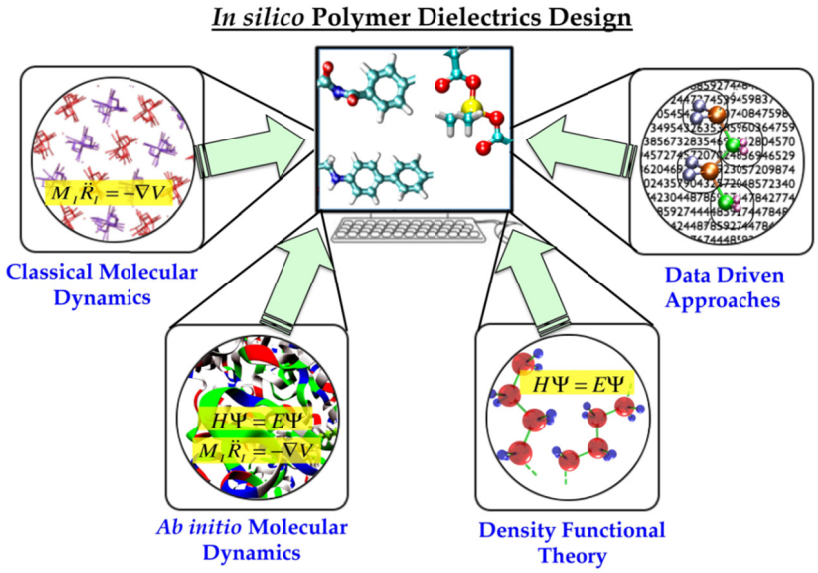

Figure 3.1 Computational strategies for polymer dielectrics design [Reprinted with permission from C.C. Wang et al. Polymer 55 (2014) 979-988. 2014, 5, 3677. Copyright © 2014 Elsevier Ltd.]

By exploring the possibilities for polymer material design (Figure 3.2), we found it is easy to fall into a "forest" so finding a target or starting point becomes extremely important. The computational tools made the discovery possible. In order to facilitate the searching and screening process, we designed a high throughput study of an extensive space, starting with common organic polymers. Our colleagues built up the polymer chain using 4 building blocks using single chain model (Figure 3.3), and carefully chose 7 organic groups for each building blocks. Through combination, we generated an initial database of 267 polymer systems. Isolated polymer chains were placed inside large unit cells, with the polymer repeating infinitely along one direction; the possible van der Waals and other interactions between respective chains were ignored for ease and speed of computations. Density functional theory (DFT) was applied to determine the energies and useful properties for a given collection of atoms. With the idea of selecting promising polymer systems for high energy density applications, the dielectric constant (divided

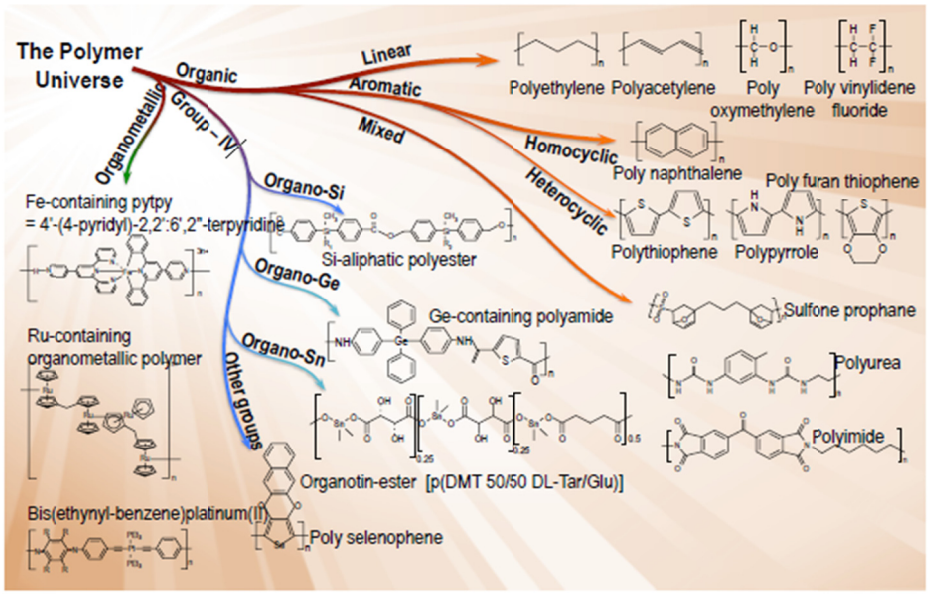

Figure 3.2 New material possibilities in the polymer chemical space

into the electronic and ionic components) and the electronic bandgap were computed and plotted against each other, as shown in Figure 3.3. The ionic dielectric constant refers to all the distribution except for electronic distribution, which is different from the term ionic polarization in Chapter 1. Due to the limitation of the single chain model, the ionic dielectric constant consists of the distribution from atomic polarization and part to the dipolar polarization.

A near perfect inverse Pareto optimal front relationship between the band gap and the electronic dielectric constant can be seen from Figure 3.3, which imposes a theoretical limit on the electronic part of the dielectric constant as a function of band gap, a limit that can be understood by regarding the electronic part of the dielectric response as a sum over electronic transitions from occupied to unoccupied states. On the other hand, the ionic dielectric constant is not correlated with the band gap. This puts a limit on the amount of dielectric constant improvement from the electronic contribution, which correlates the theory we discussed in Chapter 2. Then the ionic dielectric constant can thus be exploited to increase the total dielectric constant without compromising the band gap.

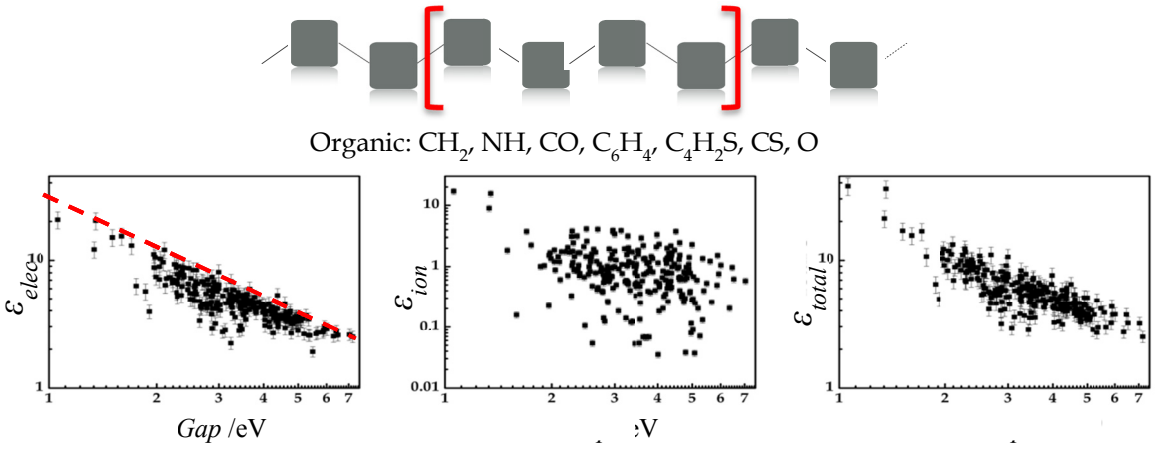

Figure 3.3 The DFT computed values for electronic, ionic and total dielectric constants plotted respectively against the computed bandgap values for the 267 4-block polymers. [Reprinted with permission from C.C. Wang et al. Polymer 55 (2014) 979-988. 2014, 5, 3677. Copyright © 2014 Elsevier Ltd.]

Once a set of promising polymers has been identified, their crystal structures and morphologies must be investigated. If interatomic potentials are available to handle the systems, MD simulations can be used to determine their crystal structure and morphology, for example, using a melt and quench approach.[32-35] An additional option, especially if force fields are not available for the new identified systems, is to use 3-dimensional structure searching schemes to determine the ground state structures based on DFT.[36-41]

In our recently work,[42] we presented a rational design strategy of hierarchical modelling with successive downselection stages, as shown in Figure 3.4. As described above, quantum mechanics-based combinatorial searches of chemical space are used to identify polymer repeat units that could lead to desirable dielectric properties, followed by configurational space searches using evolutionary and classical molecular dynamics schemes to determine the three-dimensional (3D) arrangement of polymers (and their properties) built from the desirable repeat units. Successful synthesis and testing of some of the most promising identified polymers and the measured attractive dielectric properties supports the proposed approach to material selection.

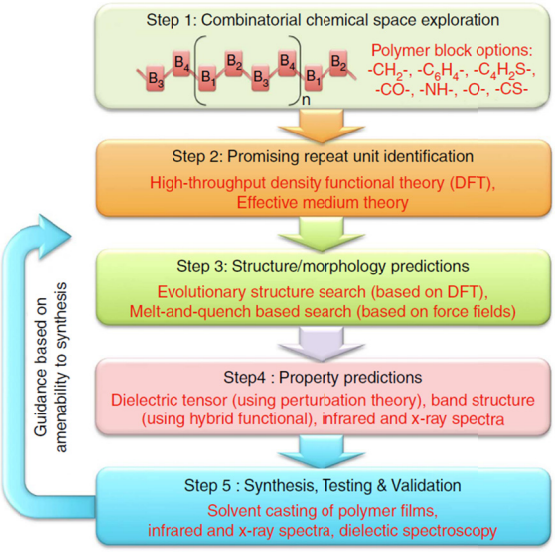

Figure 3.4 Schematic illustration of rational polymer dielectric design strategy

To explore the chemical space and investigate the potential of material for dielectric application to a wider range, we extended our search regime to other elements besides carbon based polymer systems. Starting from Group 14 elements, we investigated silicon[43] and tin based polymers. Further study where we further expanded out search regime to metal containing polymers will be discussed in detail in Chapter 6 and 7.

DFT-based strategies are limited to polymers based on short, periodic chains. For longer chains required to screen larger regions of compositional space, the computational cost associated with DFT rises rapidly. Furthermore, as the system size increases, the number of candidates within the system grows exponentially, which leads to combinatorial explosion. Clearly, exploration of such a vast chemical space using present first principles based approaches is impractical. A new approach is needed for this large class of systems. To effect such large scale explorations, a machine learning approach has been developed and applied to the current systems. Machine learning, also known as data mining, or statistical learning, deals with making predictions from data. It is a field at the intersection of computer science and modern mathematical analysis. The initial dataset was generated using the high throughput DFT calculations, and they were randomly separated to be used for training and testing of the model.

Another important tool as mentioned above is Quantitative Structure-Property Relationship (QSPR) method. We used it here for predicting thermal transitions, especially glass transition temperature of polymers. While QSPR methods cannot generally duplicate the accuracy of physics-based calculations, they are capable of quickly providing remarkably useful results within well-defined domains of applicability when the models are trained using appropriate physics-based descriptors, and are subject

to “best practices” model building and validation criteria. Often, the most important determinant for the usefulness of a QSPR model in any design project is whether the domain of applicability of the model can be defined.

In each of the following chapter, the simulation work applied to specific dielectric property prediction, material screening and discussion of validity compared to experiments are illustrated in detail. With the combination of computational tools and experiment, we are complete a design loop to discover new polymer dielectric materials.

Reference

1. G. Hautier, A. Jain, S. P. Ong, *J. Mater. Sci.* 2012, **47**, 7317.
2. I. E. Castelli, T. Olsen, S. Datta, D. D. Landis, S. Dahl, K. S. Thygesen, K. W. Jacobsen, *Energy Environ Sci* 2012, **5**, 5814.
3. K. Yang, W. Setyawan, S. Wang, M. Buongiorno Nardelli, S. Curtarolo, *Nat. Mater.* 2012, **11**, 614.
4. S. Curtarolo, G. L. W. Hart, M. Buongiorno Nardelli, N. Mingo, S. Sanvito and O. Levy, *Nat. Mater.* 2013, **12**, 191.
5. R. Olivares-Amaya, C. Amador-Bedolla, J. Hachmann, S. Atahan-Evrenk, R. S. Sanchez-Carrera, L. Vogt, A. Aspuru-Guzik, *Energy Environ Sci* 2011, **4**, 4849.
6. J. Hachmann, R. Olivares-Amaya, A. Jinich, A. L. Appleton, M. A. Blood-Forsythe, L. R. Seress, C. Roman-Salgado, K. Trepte, S. Atahan-Evrenk, S. Er, S. Shrestha, R. ondal, A. Sokolov, Z. A. Bao, A. Aspuru-Guzik, *Energy Environ Sci.,* 2013, Advance Article.
7. C. Ortiz, O. Eriksson, M. Klintenberg, *Comput Mater. Sci.* 2009, **113 (12)**, 4932.

8. M. P. Andersson, T. Bligaard, A. Kustov, K. E. Larsen, J. Greeley, T. Johannessen, C. H. Christensen, J. K. Nrskov, *J. Catal.*, 2006, **239**, 501.
9. F. Besenbacher, I. Chorkendor, B. S. Clausen, B. Hammer, A. M. Molenbroek, J. K. Nrskov, I. Stensgaard, *Science* 1998, 279, 1913.
10. R. L. Martin, M. Haranczyk, *J. Chem. Theory. Comput.* 2013, **9 (6)**, 2816.
11. C. C. Wang (2014), Polymer Dielectrics Design Using First Principles Computations And Machine Learning (University of Connecticut, Doctoral Dissertaion)
12. P. Hohenberg, W. Kohn, *Phys. Rev.* 1964, **136**, B864.
13. W. Kohn, L. Sham, *Phys. Rev*. 1965, **140**, A1133.
14. R. O. Jones, O. Gunnarsson, *Rev. Mod. Phys.* 1989, 61, 689.
15. S. Baroni, S. de Gironcoli, A. Dal Corso, P. Giannozzi, *Rev. Mod. Phys.*, 2001, 73, 515.
16. C. C. Wang and R. Ramprasad , *J. Mater. Sci.* 2011, 46, 90.
17. C. C. Wang, G. Pilania and R. Ramprasad, *Phys. Rev. B* 2013, 87, 035103.
18. G. Pilania, C. C. Wang, K. Wu, N. Sukumar, C. Breneman, G. Sotzing, R. Ramprasad, *J. Chem. Inf. Model*, 2013, **53(4)**, 879.
19. Y. Sun, S. A. Boggs and R. Ramprasad, *Appl. Phys. Lett.* 2012, **101**, 132906.
20. Y. Sun, C. Bealing, S. A. Boggs and R. Ramprasad, *IEEE Electr.Insul. M.* 2013, **29**, 8
21. V. Ranjan, M. Buongiorno-Nardelli and J. Bernholc, *Phys. Rev. Lett.*, 2012, 108, 087802.
22. V, Ranjan, L. Yu, M. Buongiorno-Nardelli and J. Bernholc, *Phys. Rev. Lett.*, 2007, 99, 047801.

23. W. L. Jorgensen, J. P. Ulmschneider, J. Tirado-Rives, *J. Phys. Chem. B,* 2004, 108, 16264.

24. J. M. Wang, R. M. Wolf, J. W. Caldwell, P. A. Kollman, D. A. Case, *J. Comp. Chem.,* 2004, 25, 1157.

25. K. Vanommeslaeghe, A. D. Jr. MacKerell, *J. Chem. Inf. Model* 2012, 52, 3144.

26. K. Vanommeslaeghe, E. Prabhu Raman, A. D. Jr. MacKerell, *J. Chem. Inf. Model*, 2012, 52, 3155.

27. H. Sun, *J. Phys. Chem. B*, 1998, **102**, 7338.

28. L. P. Hammett, *J. Am. Chem. Soc.*, 1937, **59(1)**, 96.

29. C. Hansch, R. M. Muir, T. Fujita, P. P. Maloney, F. Geiger, M. Streich, *J. Am. Chem. Soc.*, 1963, 85, 2817.

30. R. W. Taft, *J. Am. Chem. Soc.*, 1952, 74, 3120.

31. A. R. Katritzky, V. S. Lobanov and M. Karelson, *Chem. Soc. Rev.*, 1995, 24, 279.

32. D. Rigby and R. Roe, *J. Chem. Phys.*, 1987, 87, 7285.

33. I. Bitsanis and G. Hadziioannou, *J. Chem. Phys.*, 1990, **92**, 3827.

34. C. Bennemann, W. Paul and K. Binder, *Phys. Rev. E,* 1998, **57**, 843.

35. M. Moreno, M. Casalegno, G. Raos, S. V. Meille, R. Po, *J. Phys. Chem. B*, 2010, **114(4)**, 1591.

36. A. R. Oganov, C. W. Glass. *J. Chem. Phys.* 2006, 124, 244704.

37. A. O. Lyakhov, A. R. Oganov and M. Valle, *Comput. Phys. Commun.*, 201, 181, 1623.

38. A. R. Oganov, *Modern methods of crystal structure prediction.* Berlin:Wiley-VCH; 2010, ISBN 978-3-527-40939-6; 2010.

39. S. Goedecker, *J. Chem. Phys.*, 2004, 120, 9911.

40. M. Amsler and S. Goedecker. *J. Chem. Phys.* 2010, 133, 224104.

41. J. Pannetier, J. Bassas-Alsina, J. Rodriguez-Carvajal, V. Caignae, *Nature* 1990, 346, 343.

42. V. Sharma, C. C. Wang, R. G. Lorenzini, R. Ma, Q. Zhu, D. W. Sinkovits, G. Pilania, A. R. Oganov, S. Kumar, G. A. Sotzing, S. A. Boggs, R. Ramprasad, "Rational Design of All Organic Polymer Dielectrics", *Nature Communications* DOI: 10.1038/ncomms5845.

43. Aaron F. Baldwin (2014). Synthesis of Next Generation Dielectric Materials through Rational Exploration of Chemical Space (University of Connecticut, Doctoral Dissertation)

Chapter 4

Systematic Synthesis, Characterization and Processing of Polyimide as Dielectric Material

4.1 Polyimide as a dielectric material

Polyimide is a high temperature material with excellent dimensional stability, chemical stability and electrical resistance.[1-2] Polyimide was introduced by Du Pont as a result of the fast expansion of aerospace industry after World War II, in which a material that is lightweight, chemically and thermally stable, and with good mechanical properties was highly needed. The continued success of these polymers as commercial materials was due to the availability of inexpensive starting materials and the ability to tailor these polymers to a variety of end uses. The polyimides are recognized by the presence of repeating imide structural units in the polymer backbone. They can be prepared by the reaction of a dianhydride with either a diamine or a diisocyanate, where the former one is most commonly used.

As for the electrical and electronic applications, polyimide has desired properties, such as excellent mechanical strength, flexibility, inertness to solvent and radiation, and high breakdown field. Therefore, they are used in the electronics industry for flexible cables, as an insulating film on magnet wire and for medical tubing. For example, in a laptop computer, the cable that connects the main logic board to the display is often a polyimide base with copper conductors. The semiconductor industry uses polyimide as a

high-temperature adhesive; it is also used as a mechanical stress buffer. Some polyimide can be used like a photoresist; both "positive" and "negative" types of photoresist-like polyimide exist in the market. One of the most important applications of polyimide thin films is used as the inter-level dielectric insulators within integrated circuits (IC) or large scale integration (LSI). The polyimide films are most widely used in the microelectronic industry are the ones with low dielectric constant.[3] In electronic packing, low dielectric materials minimize cross talk and maximize signal propagation speed in devices. Hence, the development of polyimides with increasingly lower dielectric constants has been the focus for microelectronic applications. [4-12]

Here, we investigate polyimide as a dielectric material for energy storage applications, where we are targeting the opposite by seeking structures with high dielectric constant as well as low dissipation factors.

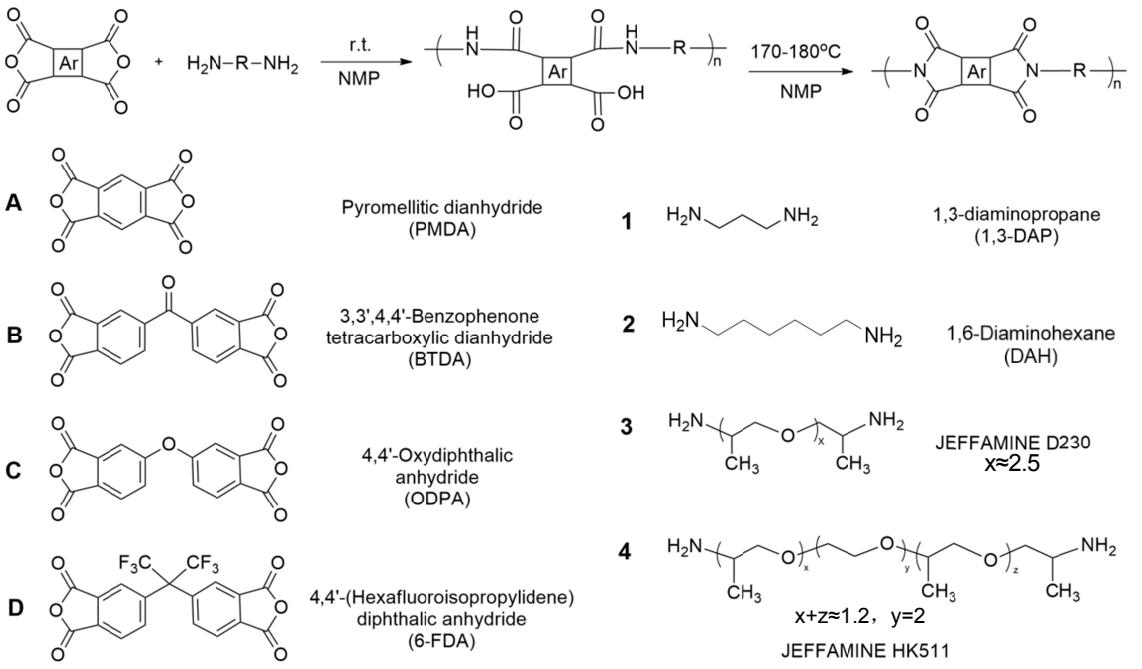

Scheme 4.1 Monomers and Syntheses of Polyimides A1-D4

In attempt to identify the polymers with high dielectric constant and band gap, high-throughput density functional theory (DFT) computations were conducted to perform initial screening, as discussed in Chapter 3. Among the several promising systems, polyimides were chosen to be investigated. Polyimides were generated by polymerization of different aromatic dianhydrides and aliphatic diamines (Scheme 4.1) to increase the dipole density and mobility in the backbone and to improve solubility. With no catalyst and sole production of water in the synthesis procedure, polyimide with higher purity minimizes conduction loss, which is inherent for PVDF prepared from suspension polymerization. Incorporation of different functional groups such as carbonyl, ether works as additional permanent dipole moments, as well as changes the cross-conjugation length, hence alters the delocalization of π-electrons.

4.2 Systematic synthesis based on high throughput DFT screening

Density functional theory (DFT) based quantum mechanical electronic structure method allows for the determination of atomic level interactions accurately, providing both the static (low frequency) and optical (electronic) dielectric constant as well as band gap for given configurations of atoms.[13,14] In order to identify promising structures, we used DFT

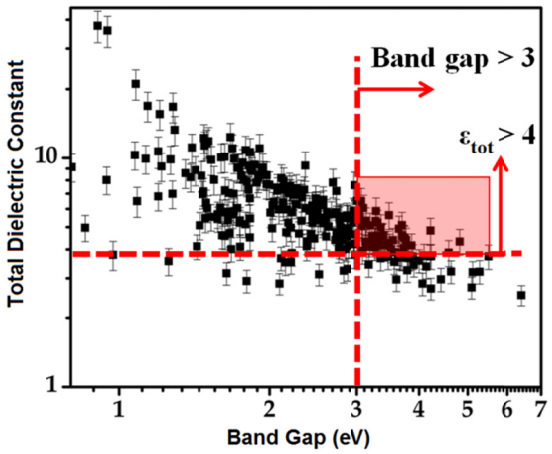

Figure 4.1 DFT based initial screening results

computation in a high-through put mode to conduct an initial combinatorial screening, as discussed in Chapter 3.[15] We considered an all-trans single polymer chain containing four independent blocks with periodic boundary conditions along the chain axis, without interchain interactions being considered. Each block was assigned as one of the following units: $–CH_2–$, –NH–, –C(=O)–, –C(=S)–, –O–, $–C_6H_4–$ (benzene ring) and $–C_4H_2S–$ (thiophene ring). Combination of these blocks forms different types of polymers, including polyimides, polyureas, polyurethanes, polyamides, etc., resulting in 267 unique and reasonable structures. Polymer structures with total dielectric constant (electronic and ionic) > 4 and band gap > 3 were selected as promising candidates, as shown in Figure 4.1. These polymers are found to be composed of aromatic group and polar blocks –NH–, –C(=O)– and –O–. In this Chapter, we focused on the exploration of polyimide by combining various chain segments to tailor dielectric properties.

Polyimides were prepared by two step polycondensation (Scheme 4.1),[16] with NMP as solvent and isopropylamine as the end capping reagent (2 mol % to the total of anhydride group). Poly(amic acid) was formed at room temperature under inert atmosphere followed by imidization at 170-180 ^oC. Syntheses of polyimides based on Jeffamines are described with the structure determination by FTIR, ^1H-NMR and GPC in Experimental part following this Chapter. Table 4.1 lists the thermal properties obtained by TGA and DSC. Polyimides with polyether segments have lower decomposition temperatures, since Jeffamine segments contain methyl group and ether linkage which are more sensitive to thermal degradation.[17] They also exhibit lower glass transition temperature (T_g). Only polyimide **B1** and **B2** were found to be semicrystalline.

Compared to polypropylene, with a low T_g of 0 ^oC but highly crystalline, most of the polyimides here are amorphous which requires a T_g higher than operation temperature.

Table 4.1 Thermal Properties of Polyimides

Polymer	B1	B2	A3	A4	B3	B4	C3	C4	D3	D4
T_g(℃)	174	150	75	53	82	78	72	63	98	81
T_m(℃)	271	234	N/O	N/O	N/O	N/O	N/O	N/O	N/O	N/O
T_o(℃)	350	338	333	313	325	317	354	341	324	283
T_d(℃)	498	482	458	450	452	447	465	461	453	452

T_m: melting temperature; T_g: measured at the midpoint of transition; T_o: onset temperature of degradation; T_d: maximum derivative of weight loss.

The incorporation of a polyether segment improves the solubility of polyimides. Polyimides based on Jeffamines are soluble in THF, DMF, DMAc, DMSO, NMP and m-cresol at room temperature, making solution casting feasible. Films were prepared by casting 10 wt% THF solutions onto stainless steel shim stock, and drying *in vacuo* at 40^{o}C for 10h and then 150 ^{o}C for 10h. Polyimides **B1, B2** only dissolve in m-cresol at room temperature. For these polyimides, 10 wt% m-cresol solutions were used for casting and further drying at 150 ^{o}C for 10h. Polyimide films prepared by the method above were used for dielectric spectroscopy and band gap determination.

Large scale films were made by casting on glass plate followed by same drying process for breakdown strength measurement. **B2** was found to possess the best film forming quality, with large scale films made by using a 3” wide Dr. Blade coater. The blade gap was set to 356 μm. After drying, the film was soaked overnight in a water bath for ease of peeling from the glass substrate. The dried films were then used for breakdown strength measurement.

4.3 Dielectric properties and design strategy

Dielectric properties of polyimides were evaluated by dielectric constant, dissipation factor (tan δ) and their variations with frequency and temperature, as well as band gap and breakdown strength. As discussed before, in order to increase the density of the dipoles and to improve the mobility of the dipoles, we incorporated flexible aliphatic chain segment along with aromatic segment with additional dipoles, and different bridge works to alter the conjugation structure.

In parallel, the calculation based on single chain model was conducted on similar structures as synthesized. Given the structure irregularity of the polyimides based on Jeffamines, the calculation time would be excessive. Therefore, we only considered several similar but more regular structures (Figure 4.2). The results showed that the oxygen added into the structure improves the total dielectric constant, but has limited effect on electronic dielectric constant, which means it works to improve dipolar polarization. In addition, polyimide Ⅱ shows higher dielectric constant than polyimide Ⅴ, which proves that a dipole in the flexible chain segment further enhances polarization than the one placed in the rigid segment. The rule also applies when we place the dipole in between two benzene rings, which represents a rigid segment in the polymer chain. Compared PMDA, the bridge breaks symmetry of the imide ring on the two sides to give a net dipole. Also, the carbonyl bridge improves the polarization further than oxygen as that it's not only breaking symmetry, but also links the conjugation structure better so that the electrons are more delocalized. In terms of band gap, it is obvious that polyimide Ⅴ and Ⅵ have higher band gaps due to less conjugation. However, the calculated values of band gap are lower than the real values, because a well-known deficiency of the DFT

approach is that under the local or semi-local approximations due to the self-interaction error, the lack of long-range correlation effect, and the poor description of the electron-hole interaction in the excited states, DFT underestimate the energy band gap.

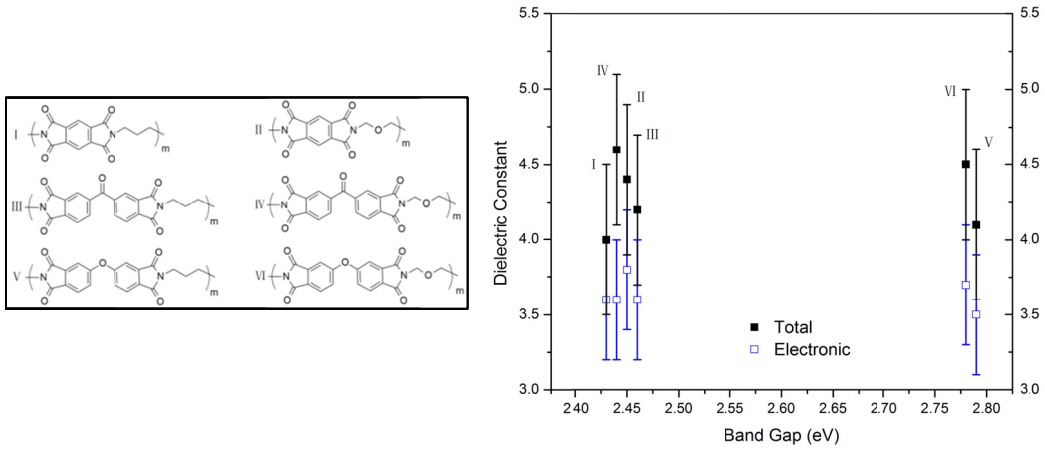

Figure 4.2 DFT calculation results for polyimides

Experimental results of the dielectric constants (room temperature, 1 kHz) and dissipation factors are listed in Table 4.2. All the polyimides have dielectric constants higher than BOPP owing to dipolar polarizability of imide functional group. Higher dielectric constants were achieved compared to common commercial polar polymers, including poly(ether imide) (PEI, dielectric constant of 3.2, dissipation factor of 0.21 %), poly(phenylene sulfide) (PPS, dielectric constant of 3.1, dissipation factor of 0.30 %) and poly(ether ether ketone) (PEEK, dielectric constant of 3.1, dissipation factor of 0.18%) tested at room temperature, 1 kHz.[18] The highest value achieved is 7.8 for **B4**. Incorporation of polyether segment enhances dipolar polarizability, hence increased dielectric constant further, as established by polyimides derived from Jeffamines having higher dielectric constant than the ones derived from diaminopropane and diaminohexane. Similarly, Jeffamine HK511 resulted in higher dielectric constants versus Jeffamine

D230, which fits with calculation results. Although side groups on polymer backbone may possess higher mobility, they increase the free volume of polymer chain, resulting in lower density of dipole moments.

Table 4.2 Dielectric Properties (room temperature) of polyimides

Polymer	B1	B2	A3	A4	B3	B4	C3	C4	D3	D4
ε_{1kHz}	4.01	3.57	4.17	5.44	4.52	7.80	4.37	6.04	2.50	5.26
$\tan \delta_{1kHz} \times 100$	0.255	0.849	0.518	0.660	0.256	0.555	0.166	0.714	1.47	0.791
E_g (eV)	3.79	3.42	3.48	3.39	3.50	3.48	3.62	3.58	3.98	3.93

In addition, the dielectric constant was found to be greatly dependent on the bridge of the dianhydride structure. Comparing **B3** and **C3** to **A3**, a benzophenone or diphenyl ether structure leads to higher dielectric constants as additional dipole moments. However, unlike a carbonyl bridge in benzophenone structure, an ether linkage in diphenyl ether breaks the cross-conjugation between two benzene rings, meaning limited delocalization and lower mobility of π electrons. Therefore, the benzophenone structure exhibits higher polarizability than the diphenyl ether, which also fits with calculation results. Among all the polyimides, **B4**, having the longest cross-conjugated system as well as the longest polyether segment, exhibits the highest dielectric constant among the all. **D3** shows much lower dielectric constant, owing to the bulky trifluoromethyl group which reduces interchain electronic interactions, resulting in a less efficient molecular packing.[19]

The dissipation factors of polyimides here, all stays < 1 % at room temperature, 1 kHz, with the exception of **D3**. Although there is relaxation behavior in the power frequency range between 10^{-3} and 10^{3} Hz,[20] the dissipation factors remain lower than 3 %,

comparable to the values for other polar polymers studied recently for energy storage applications.[21-26]

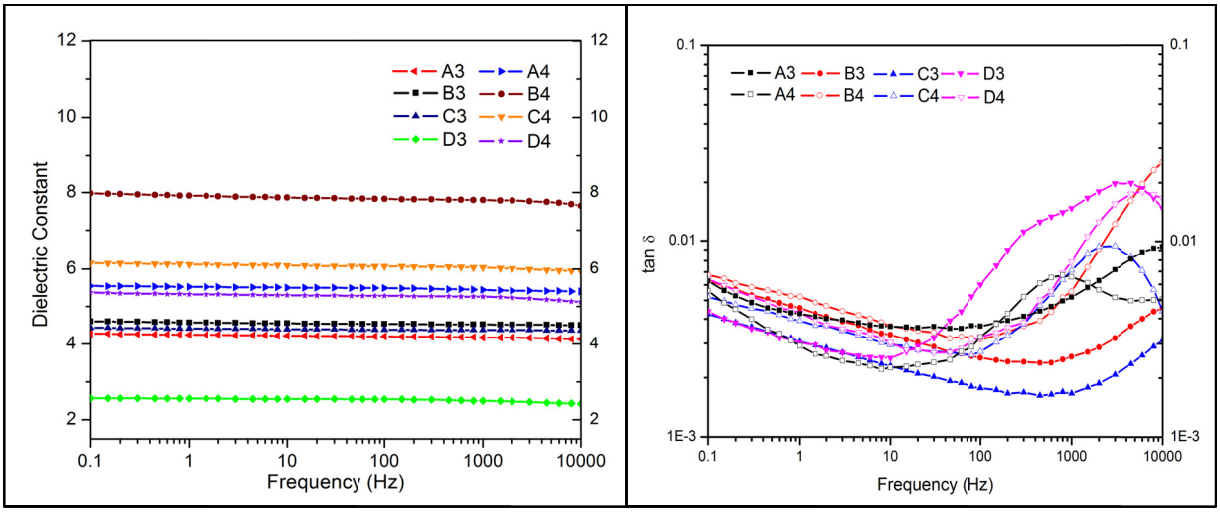

Figure 4.3 Dielectric constant (left) and loss (right) vs. frequency at room temperature (r.t.)

Dielectric constants of polyimides (Figure 4.3, left) decrease with increasing frequency, since the dipoles cannot orient fast enough to keep up with the alternating electric field. Dielectric constant is dependent on electronic, atomic and dipolar polarizations, with dipolar polarization being much slower than the other two. When frequency increases, dipolar polarization decreases, resulting in a slight decrease in dielectric constant. As shown in Figure 4.3 (right), the dissipation factor changes variously for each polyimide with increasing frequency due to relaxation peaks. Polyimides based on Jeffamine HK511 show higher dissipation factor than the ones based on Jeffamine D230 and exhibit relaxation at lower frequencies.

The temperature dependence of dielectric constant and loss was investigated by TDDS also. Figure 4.3 shows TDDS for the polyimide studied here. In general, the dielectric constant remains steady below T_g and increases dramatically after. For

amorphous polar polymers used in power storage capacitors, breakdown strength decreases considerably above T_g.[20] Therefore, in order to increase operation temperature, a high T_g is necessary. For some of the spectrum, for example, B3, there is a slight decrease in dielectric constant when we first started to increase the temperature, which for B3 is to compare the data at 50 ℃ and 75 ℃ to those at room temperature. The variation is insignificant but may be attributed to the loss of water upon heating the films.[25] The dissipation factors are around 1% over most of the frequency range, and increases with increasing temperature. By investigating the transition peaks of all polyimides and comparing with literature,[24,25] the transition peaks on the right hand of the spectrum is defined as β relaxation peak, and they move to higher frequency when temperature increases. At temperatures higher than T_g, a potential α relaxation develops.

For polyimide **D2**, we are able to see two β relaxation peaks around the same frequency range with other polyimides, which could be contributed to different chain segment motion in this polymer system.

Polyimide **A3:**

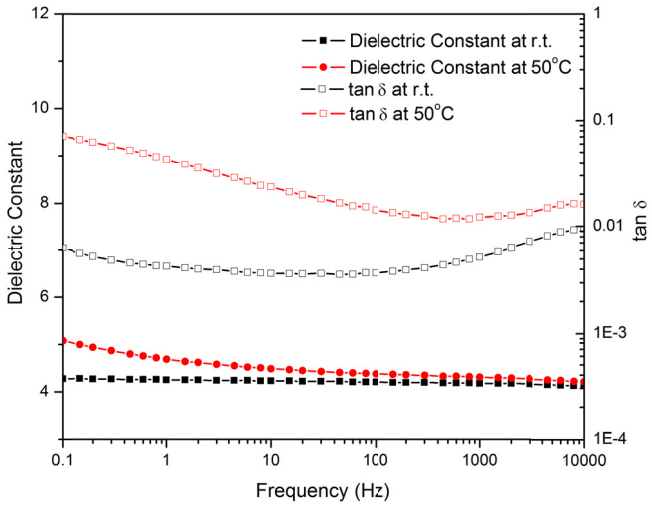

Polyimide **A4:**

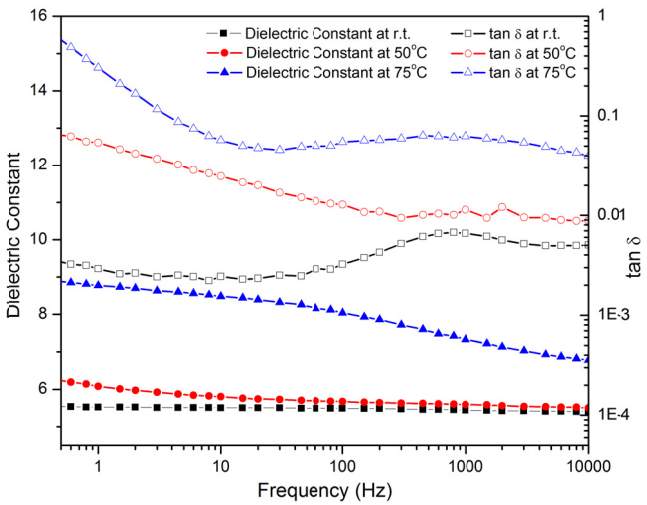

Polyimide **B3:**

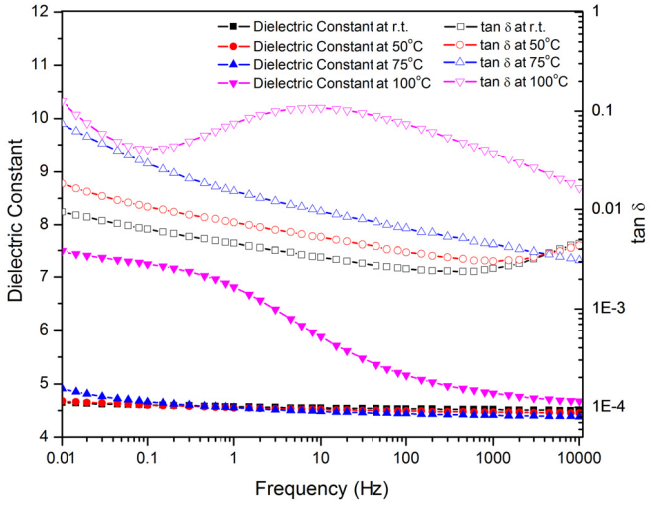

Polyimide **B4:**

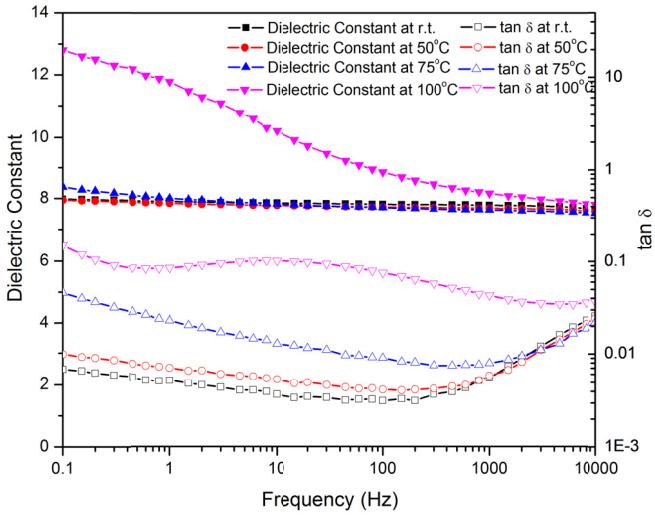

Polyimide **C3:**

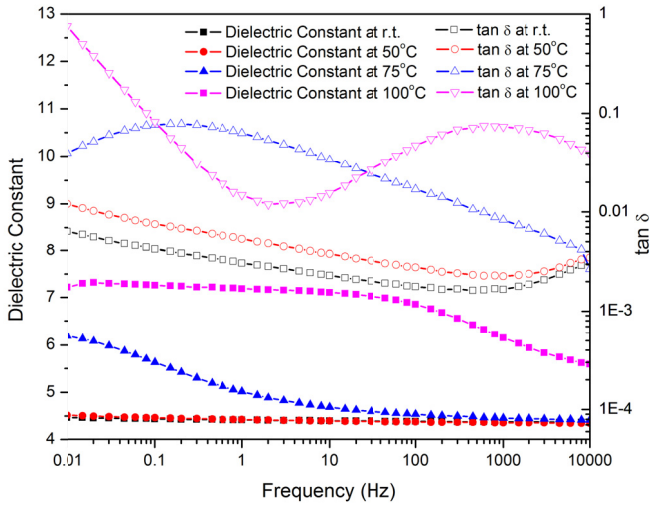

Polyimide **C4:**

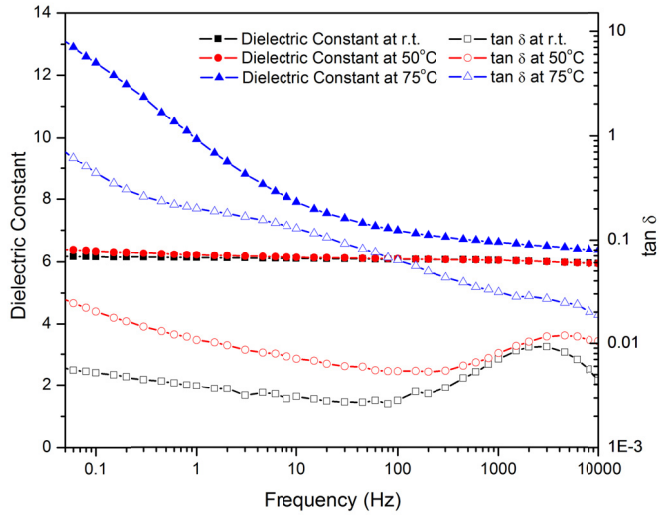

Polyimide **D3:**

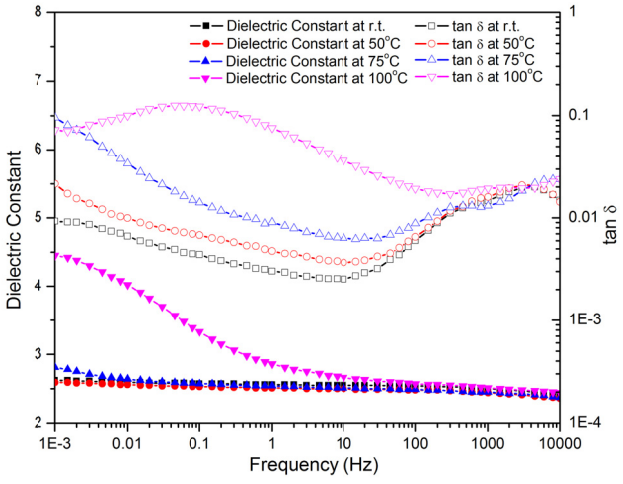

Polyimide **D4:**

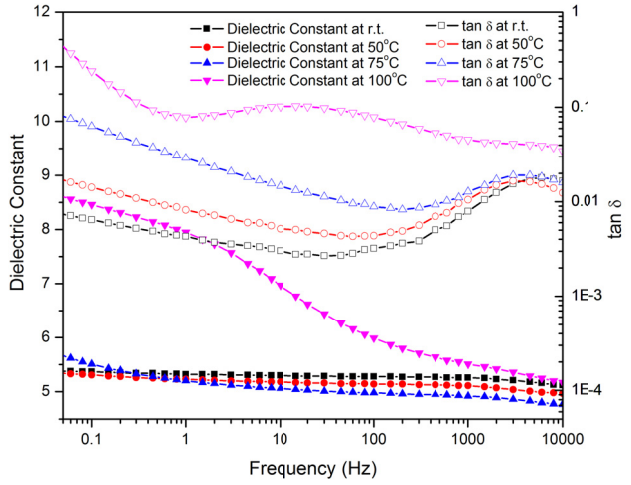

Figure 4.4 Dielectric constant and loss vs. frequency at different temperatures for Jeffamine systems

As discussed in Chapter 1, for an insulator material without defects and impurities, its intrinsic breakdown field should be a fixed value. As a result of impact ionization when electric stress is applied, electrons in the conduction band may transfer to valence band to create an avalanche of electrons at breakdown fields, so the energy band gap indicates the intrinsic breakdown strength. Band gap values obtained from UV absorption are listed in Table 4.2, where polyimide **D3** and **D4** possess highest values followed by **C3** and **C4**. Polyimide with longer ether linkage showed slightly lower band gap. As changing conjugation structure by switching the dianhydride segment, delocalization of electrons affects the band gap to increase as conjugation or cross-conjugation length decreases. Compared to polyimides here, polypropylene as an example of most linear polyolefins has higher band gap of 7.0 eV, but a low dielectric constant as mentioned before. This negative relationship between band gap and dielectric constant is well known for inorganic solids, and is also observed for organic polymer systems.[27]

Intrinsic breakdown is believed to be dependent on band gap, and it is understandable intuitively, as that a material with a larger band gap tends to exhibit a higher threshold for impact ionization. The quantitative relationship between band gap and intrinsic breakdown field was investigated based on the measured maximum breakdown voltage which can be regarded as the approximate value of the intrinsic breakdown.[33-35] A power law dependence was found as the intrinsic breakdown increases when band gap increases. However the relationship appears to differ for different materials.[36] For a polymer material, establishing the relationship between intrinsic breakdown and band gap is more challenging. First the intrinsic breakdown is required to be obtained from a "perfect" material without high field aging. However the "perfection" of polymer materials is

difficult to achieve macroscopically, since they are often amorphous or semicrystalline. Therefore, using the measured maximum breakdown voltage as the intrinsic breakdown is problematic. Second the intrinsic breakdown is defined in terms of electron-avalanche theory, whereas breakdown of polymer usually depends on other mechanisms including thermal breakdown, partial charge and free volume breakdown. As for polyimide, thermal breakdown is believed to be an important mechanism. [28]

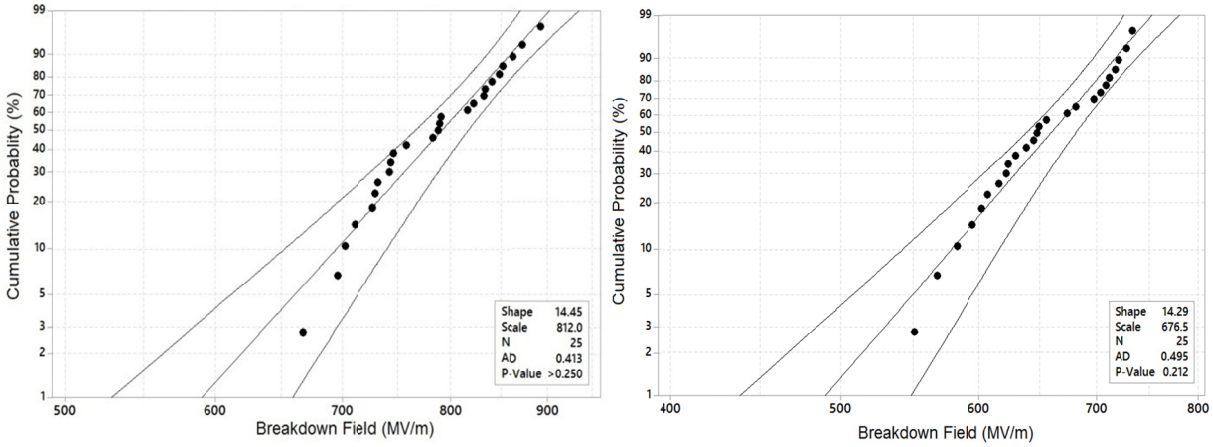

Figure 4.5 Weibull Distribution of Breakdown Field of B2 (left) and B4 (right) at Room Temperature

The engineering DC breakdown was investigated in comparison with band gap values. The measurements were conducted on free standing films in silicone oil using ball bearing electrodes (diameter ¼'') with careful operation. The Weibull distribution, as discussed in Chapter 1 is applied for characterizing data. Measurements were conducted on **B2** which possesses best film forming quality and **B4** which exhibits highest dielectric constant (Figure 4.5). The Weibull characteristic breakdown fields of **B2** and **B4** are 812MV/m and 676MV/m. The Anderson-darling test parameter (critical value = 0.745 for 25 data points) for the fitting of **B4** is higher than that of **B2**. With comparable band

gap, the measured breakdown strength of **B2** is much higher than that of B4. These suggest that the film quality of **B4** needs to be improved by exploring different solvents and casting conditions, which affects the morphology and surface roughness of the films. In addition, the measured breakdown field here indicates a possible extrinsic breakdown, which is not inherent to the material itself, and is affected by chemical impurities, cavities, uniformity in microstructure, etc.

4.4 Processing development and optimization of promising system

Systematic synthesis of polyimide discussed in Section 4.3 reveals how dielectric properties depend on chemical structure, with several promising candidate revealed to have high dielectric constant or high breakdown strength. Polyimide BTDA-HDA described above was found to be melt proccesable and stretchable to a large extent. Figure 6 shows the full dielectric spectrum of this polymer at different temperature. As discussed before in Section 4.3, the dielectric constant decreases as increasing frequency due to decreased contribution of dipolar polarization. We also found the dielectric constant decreases first at 50 ^{o}C to 100 ^{o}C, whereas the dissipation factor always increases as we increase temperature.

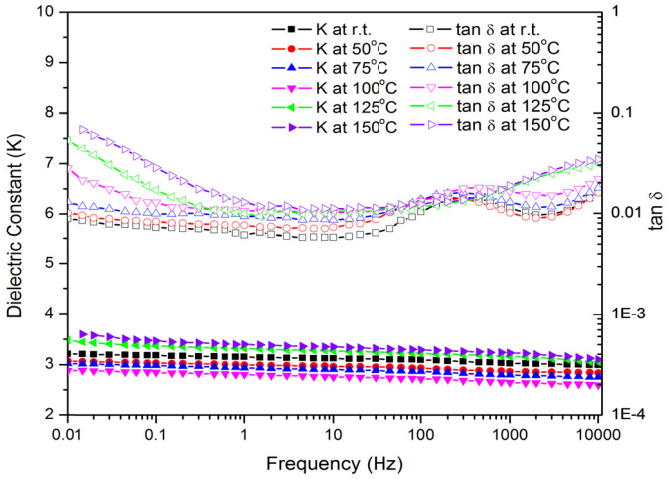

Figure 4.6 Dielectric Constant and Loss for BTDA-HDA

Based on the requirement, we scale up our synthesis and optimized the synthesis procedure to still give a high molecular weight as well as purity. The cost was cut down to $0.24/g. ~1 kg of the polymer was sent to our collaborator in the University of Akron for film melt processing. The film was obtained after biaxially stretching on a compression molded sample. Figure 4.7 shows the dissipation factor data of melt processed sample compared to the one from solution processing, in which a clear depression of loss weak was shown in the frequency range of 100-1000 Hz.

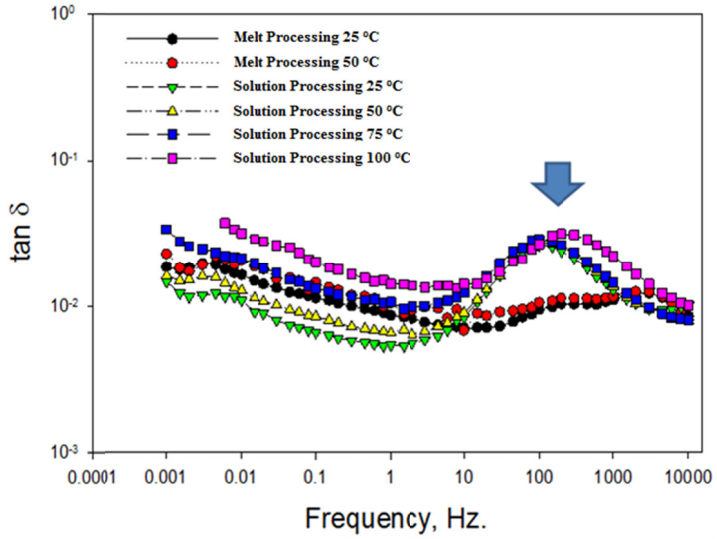

Figure 4.7 Comparison of Dissipation Factor for Solution/Melt Processing

Compared solution casting, melt processing has several advantages: there is no requirement of using large amount of solvent for processing procedure, which will cost down the total cost for film material development; it is easier for melt processing procedure be applied continuously in manufacturing; the procedure of compression molding followed by biaxially stretching was proved to induce the crystallization in the polymer film, which is a key for high breakdown field of BOPP, as discussed in Chapter 1; Here, we show that it also decreases the dielectric loss.

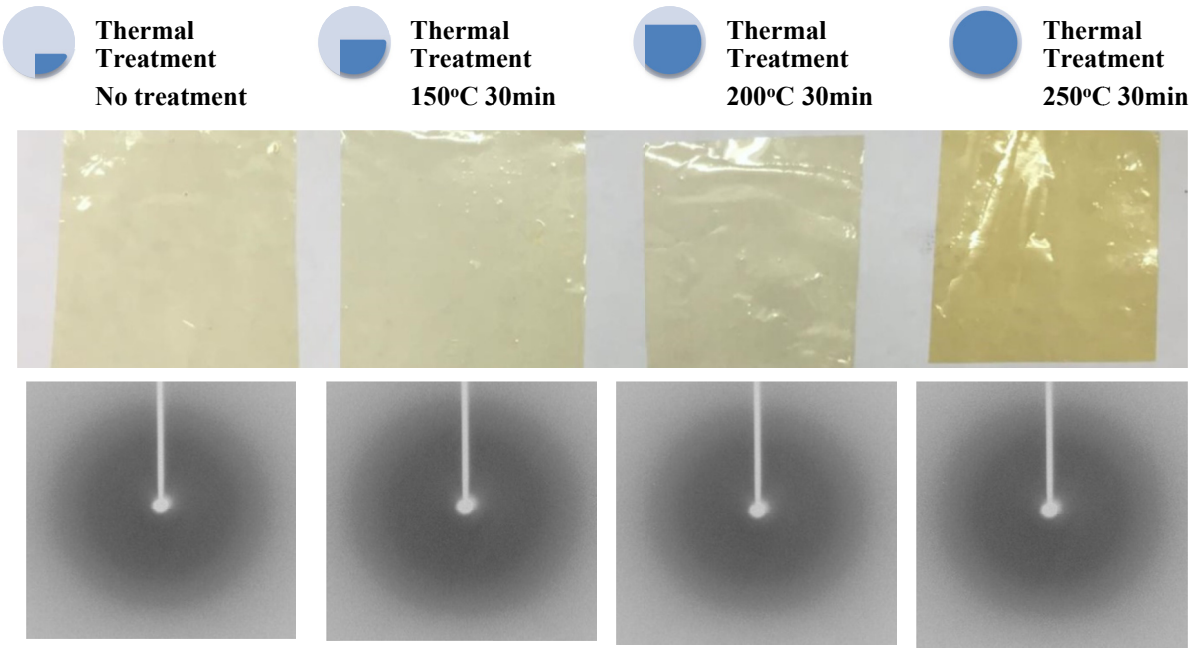

Figure 4.8 Additional Drying of Solution Casted Polyimide Film and Corresponding XRD

However, the question remains, is the reduced loss originated from the less solvent residue through melt processing or the induced crystalline structure in the polymer film? In order to answer this question and further understand the behavior of this polymer, we further dried the polymer film out of solution casting, with the film pictures and corresponding X-ray diffraction pattern shown in Figure 8. Up to 250 ^{o}C of drying, which was considered vigorous enough to remove the residue solvent m-cresol, the TGAs in Figure 4.9 proves that no m-cresol was left in the sample. At the same time, the films still remain amorphous. The dissipation factors measured showed obvious loss peak around 100-1000 Hz as before (Figure 4.10). These results indicate the reduced loss in the melt processed film could be originated from the crystalline structure. To prove this theory, a similar reduced loss should be obtained from a solution casted film with induced crystallization.

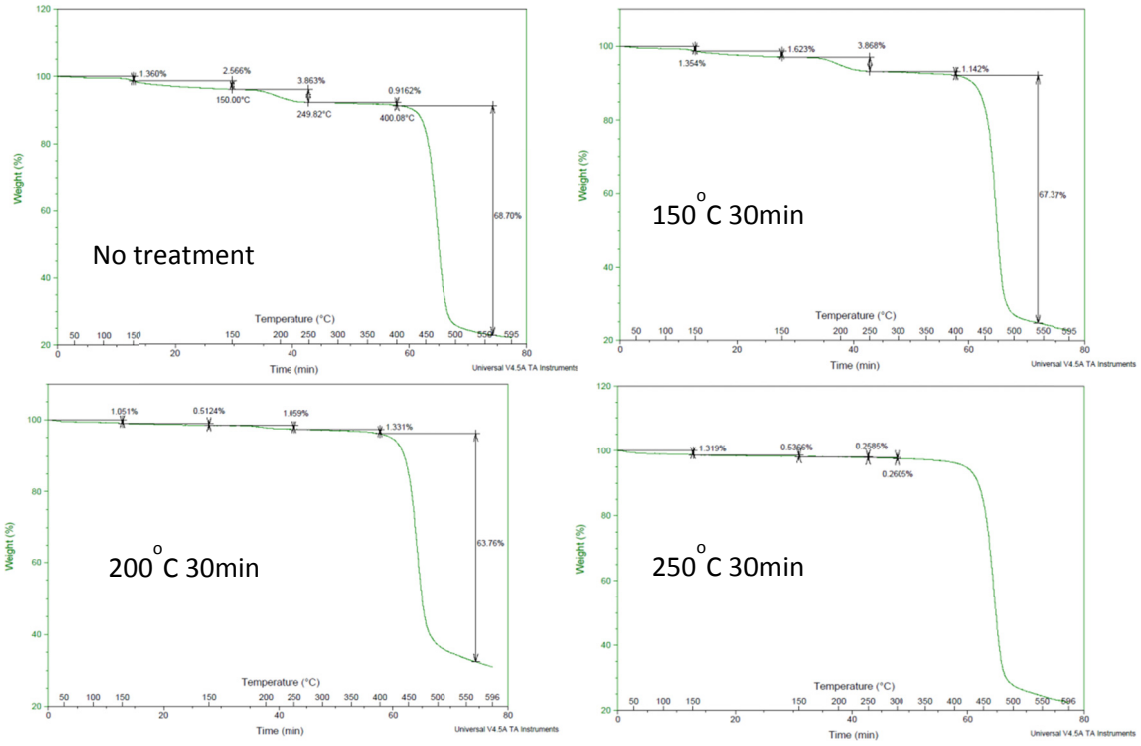

Figure 4.9 TGA of Additional Dried Polyimide Film

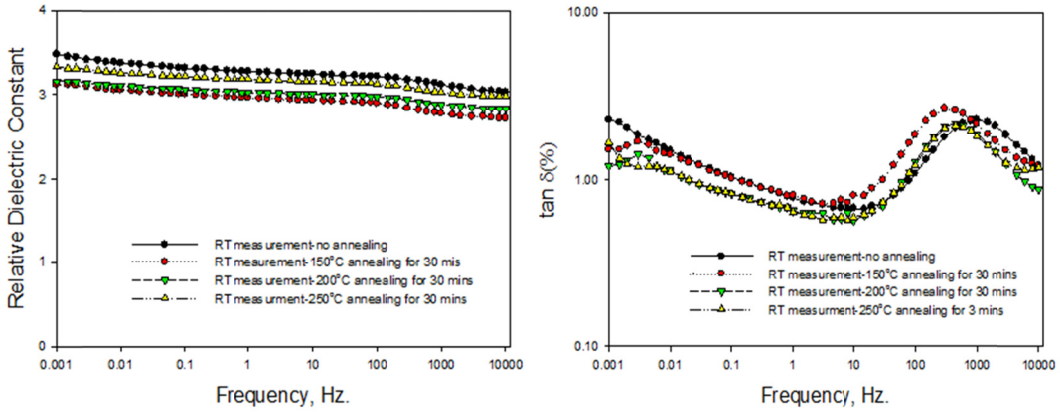

Figure 4.10 Dielectric Spectrum of Additional Dried Polyimide Film

As we know, polymer chains form crystal region above the glass transition temperature, and below the melting point. Thermal treatment in the region of crystallization point may induce the polymer to pack. Different thermal treatments at temperatures close to crystallization point were conducted on polymer fibers first, as in

300°C for 5min then quench to room temperature; 300°C for 5min, 200°C for 60min then quench to room temperature; 300°C for 5min, 170°C for 60min, then quench to room temperature. The temperatures for isothermal annealing were chosen based on a crystallization temperature of 184 °C observed in DSC. The fiber samples were than examined using DSC (Figure 4.11, left) showing melting peaks after thermal treatment. Treatment at 170 °C gave highest degree of crystallization. Same treatment was repeated on polyimide thin films after solution casting and drying (Figure 4.11, right). The crystallization can also be successfully induced in the polymer film, only the DSC showing wider melting peaks. The pictures of the films and corresponding X-ray

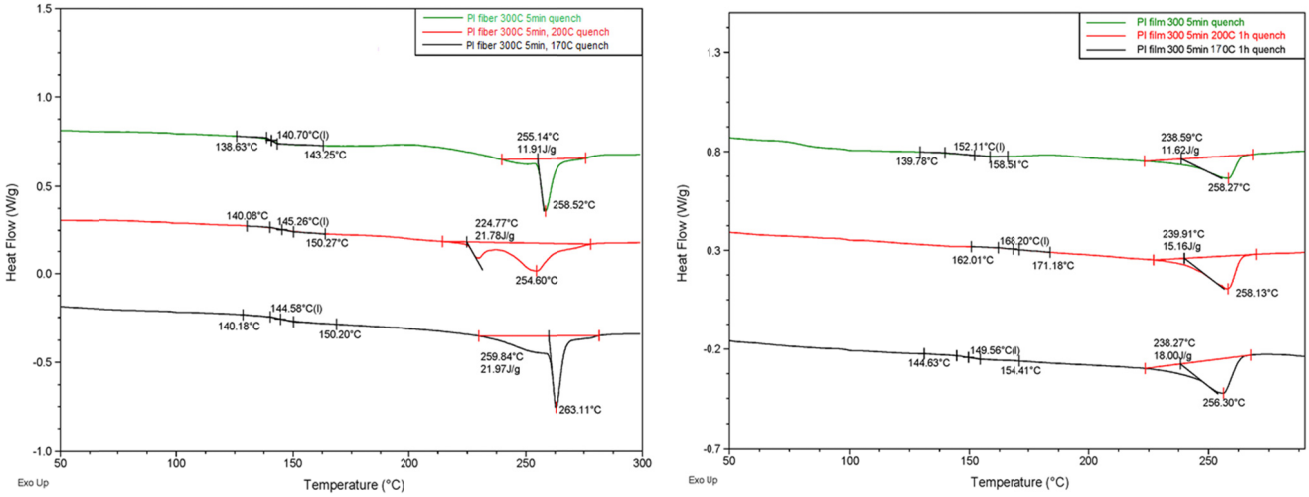

Figure 4.11 DSC of Polyimide BTDA-HDA after Thermal Annealing: Fiber (Left), Film (Right)

diffraction patterns are shown (Figure 4.12) in parallel with samples only treated by additional drying. Clearly, the diffraction pattern again proves the crystalline structure in the polymer film, however, no single crystals and limit degree of crystallinity. For these thermal treatment films, we also found reduced dielectric loss peak, and two relaxations were observed at the same frequency range (Figure 4.13).

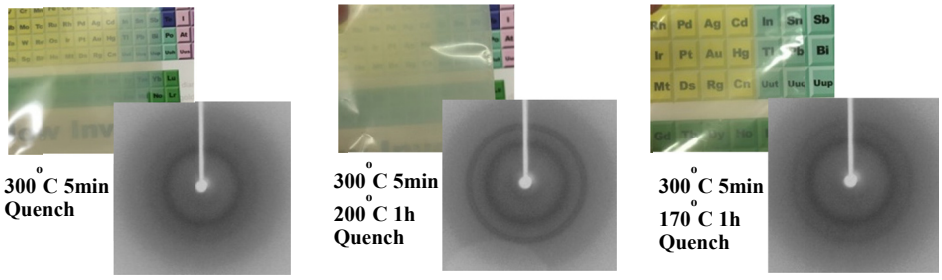

Figure 4.12 Thermal Annealing of the Solution Casted Polyimide Film and Corresponding XRD

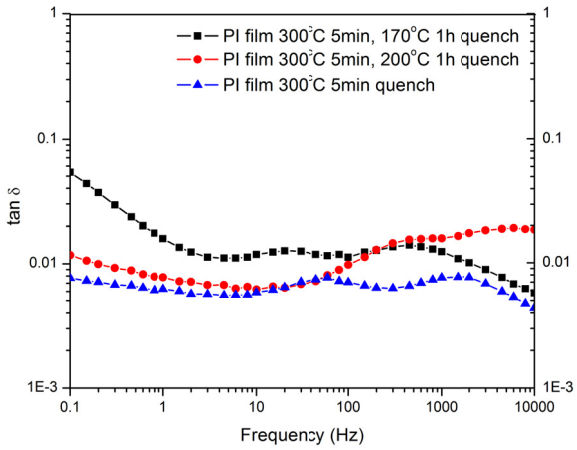

Figure 4.13 Dissipation Factors of the Solution Casted Film

4.5 Copolymerization

Based on the results above, although polyimide **B4** (BTDA-HK511) has high dielectric constant, it does not have a high enough T_g to obtain higher operating temperature. On the other hand, polyimide **B2** (BTDA-HDA) has high T_g as well as excellent processability. With the target to combine good properties together, BTDA copolyimides based on both HDA and Jeffamine HK511 were made.

Synthesis and basic characterizations of copolyimides were conducted similarly as mentioned above. The mole ratio of diamine HDA and HK511 were 25:75, 50:50 and 75:25. Since two diamines were mixed before adding dianhydride, polyimides are random copolymers. Thermal data obtained by TGA and DSC are listed in Table 4.3. As

the percentage of HDA increases, the T_g of the polymer increases. In parallel, the calculated T_g based on Fox equation are also listed. The measured values are in close agreement with calculated value, meaning we have the actual ratios of the two the diamines being similar to the feed ratios. No crystalline structure was found for the copolyimides.

Table 4.3. Thermal and Dielectric Data (at r.t. , 1kHz) of Copolyimides

	T_g (^{o}C)	**Calculated T_g (^{o}C)**	**T_o(^{o}C)**	**T_d(^{o}C)**	ε_{1kHz}	tan δ_{1kHz}
BTDA-HK511	78	---	311	447	7.80	0.555%
BTDA-HDA/HK511(25/75)	85	86.71	324	438	5.60	0.539%
BTDA-HDA/HK511(50/50)	96	99.05	342	453	5.34	0.325%
BTDA-HDA/HK511(75/25)	120	117.85	366	476	4.42	0.460%
BTDA-HDA	150	---	338	482	3.57	0.849%

The dielectric constant and loss of copolyimides at room temperature and 1 kHz are also shown in Table 4.3. All the values are between the dielectric constant of polyimides **B2** and **B4**, which means by copolymerization, we can obtain higher dielectric constant compared to **B2**, and higher T_g value compared to **B4**.

The dielectric constant data for all the copolyimide are shown in Figure 4.14 as an example; the other copolyimides show similar curves. As we can see, dielectric constant stays almost steady up to 100^{o}C for BTDA-HDA/HK511 75/25 system, which gives an increased operation temperature than polyimide **B4**. The dielectric constant of copolymers exhibits the same dependency on frequency, decreasing with increasing frequency. Also, due to the removal of moisture, there is a slight decrease when increasing temperature.

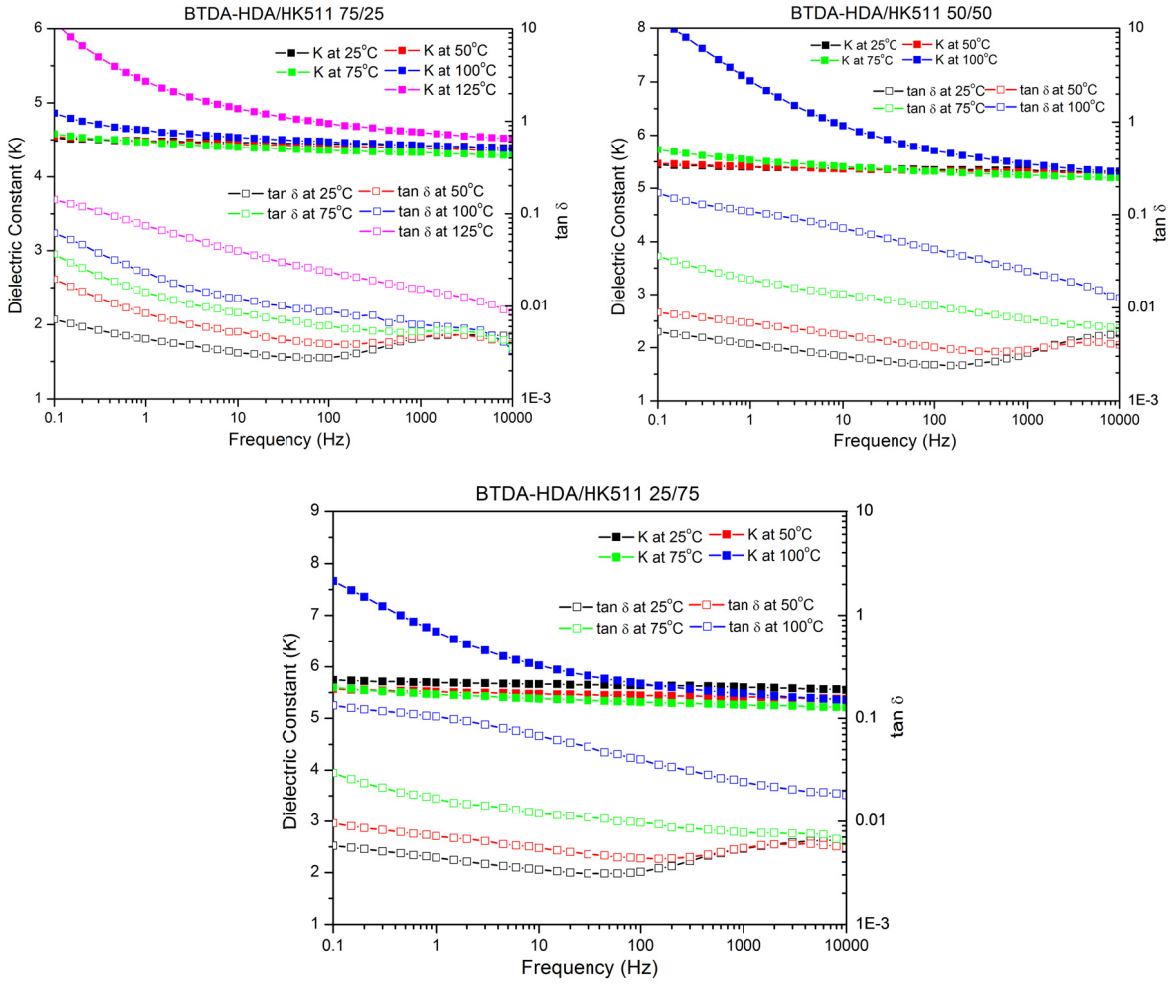

Figure 4.14 Dielectric Spectrum of Copolyimides

As to the dissipation factors for the copolyimides, almost all the tan δ values of copolyimides are below 1% up to 75°C. The β relaxation becomes less significant with lower tan δ value compared to polyimide B4. With the addition of HDA segment, the chain mobility decreases, hence the peak for β relaxation moved to lower frequency range.

Similar to the homopolymers, breakdown strength of the copolyimides was investigated under a DC ramp source and the data was analyzed using Weibull distribution. Figure 4.15 showed the distribution plot with a characteristic breakdown field of 868, 774, 716 MV/m for BTDA-HDA/HK511 75/25, 50/50, and 25/75 respectively. The HDA segment improves the processability of the polymer into higher

quality films, which is believed to be the main reason for higher breakdown strength when increasing the HDA ratio.

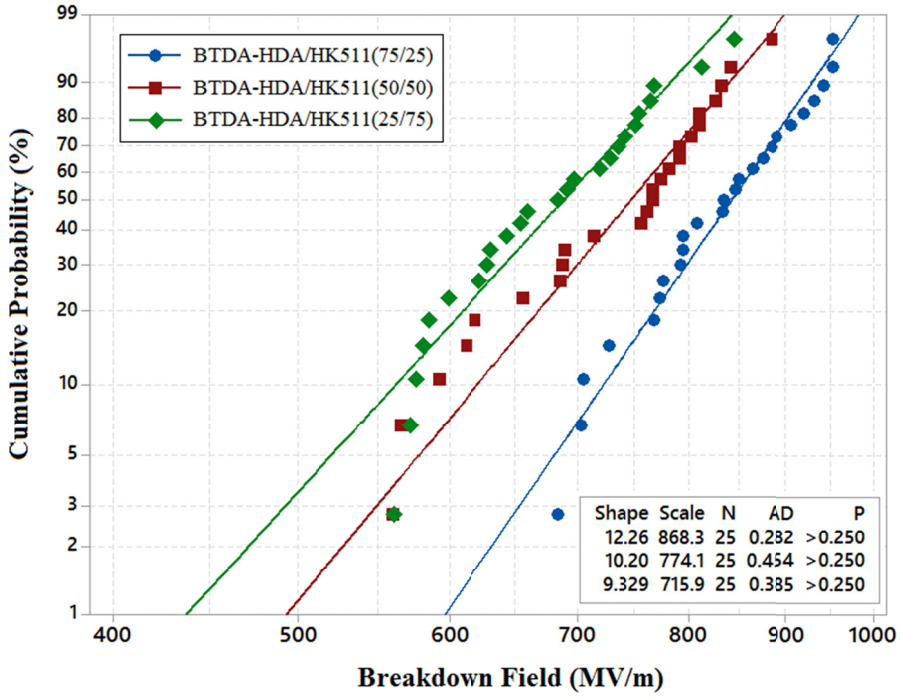

Figure 4.15 Weibull Distribution of Breakdown Field for Copolyimides

In summary, by copolymerization T_g is increased which leads to a higher operation temperature. Although the dielectric constant is sacrificed compared to polyimide B4, it's still higher than Kapton and BOPP. Compared to polyimide B4, copolyimide shows a decreased dielectric loss due to the more rigid polyimide segment. Breakdown field of copolyimides are comparable with the one BTDA-HDA, and with increasing the HDA portion, breakdown field increases.

4.6 Conclusion

Through rational design, polyimides were determined to be a significant class of polymers for study as high-dielectric constant, low-loss materials for energy storage applications. The trends observed in the experimental results were corroborated by the

DFT calculations. In this study, one of the highest dielectric constants of 7.8 for polyimide **B4** was achieved, with a potential energy density of ~15 J/cm^3. This established the importance of the increased dipole volume from the ether linkage as well as the longer conjugation length when a carbonyl spacer was inserted between the benzene rings on the dielectric constant. The thermal limitation of **B4** can be solved through copolymerization with alkyl diamine, for example, diaminohexane to increase the operating temperature, which will be used in the future work. The band gap was used to predict the intrinsic breakdown voltage, with breakdown field measurements on **B4**. This work provided insights into polyether-containing polyimides as promising dielectric materials for achieving a high energy density.

4.7 Experimental and Material

Materials. Pyromellitic dianhydride (PMDA), 3,3',4,4'-benzophenone tetracarboxylic dianhydride (BTDA), 4,4'-oxydiphthalic anhydride (ODPA), 1,3-diaminopropane (1,3-DAP), 1,6-diaminohexane (DAH) and anhydrous N-methyl-2-pyrrolidone (NMP) were purchased from Aldrich Chemical Company and 4,4'-(hexafluoro isopropylidene) diphthalic anhydride (6-FDA) was purchased from TCI America. Jeffamines D230 and HK511 were provided by Huntsman Corporation. Dianhydrides were recrystallized from acetic anhydride before use. Diamines were used as received.

Instruments. Fourier Transform Infrared (FTIR) spectra were recorded with a Nicolet Magna 560 FTIR spectrometer (resolution 0.35 cm^{-1}). Solution ^{1}H NMR was performed on a Bruker DMX500 high resolution digital NMR spectrometer. Gel permeation chromatography (GPC) was conducted using tetrahydrofuran (THF) as the mobile phase and polystyrene standards with the following instrumentations: Waters 1515 HPLC pump,

Waters 717+ autosampler, Waters 2487 dual λ absorbance detector, Varian 380-LC evaporative detector, two mixed bed Jordi Gel DVB columns. Thermogravimetric analysis (TGA) was performed with TA instruments TGA Q500 (heating rate 10 $^{o}C \cdot min^{-1}$ under nitrogen), and differential scanning calorimetry (DSC) analysis was performed by TA instrument DSC Q-100 with glass transition and melting point determined from the second heating cycle at 10 ^{o}C/min. Dielectric spectroscopies were obtained using an IMASS Time Domain Dielectric Spectrometer. Measurements were made in an air circulating oven at constant temperature by taking frequency scans, with 10 volts AC applied. Stainless steel shims purchased from McMaster Carr (diameter 2 ", thickness 0.01 ") were used as the substrates. The UV-Vis spectrum for band gap determination was obtained using Varian Cary UV-VIS 5000. The UV-vis spectra were recorded from 200-800 nm and the onset wavelength of absorption, λ_{onset}, was used to determine the band gap (E_g) from Planck's equation: $E_g = hc/\lambda_{onset}$.

Breakdown strength measurements were performed using a linear voltage ramp generated by a resistor capacitor (RC) circuit. When the first breakdown event occurs, the power supply is shut off through an interlock input by a silicon controlled rectifier (SCR) circuit, which uses the breakdown-induced ground-rise voltage capacitively coupled to the gate of an SCR. The breakdown voltage of the sample is read from a peak-holding voltmeter. The sample thickness was determined using a thickness gauge (Model LE1000-2, MeasureItAll) as the average of several measurements near the breakdown site.

Synthesis and Chemical Structure Determination of Polyimides

Polyimide **B1***:* To a dry 100 ml 3-neck flask 0.741 g (10 mmol) of 1,3-diaminopropane, 0.012 g (0.2 mmol) of isopropylamine, and 20 ml dry NMP were added under nitrogen

with stirring. After well stirred for 30 min, 3.221 g (10 mmol) of BTDA were added. The reaction was carried out at room temperature for 6 h, followed by imidization at 170-180 ^{o}C for 6 h. After cooling to room temperature, the mixture was poured into 150 ml of methanol, filtered and washed with methanol several times, and dried *in vacuo*. Light yellow solid was obtained in 89 % yield (3.206 g). FTIR (cm^{-1}): 2972, 2876, 1773, 1716, 1659, 1455, 1425, 1243, 1098, 1044, 725.

Polyimide **B2***:* The preparation is similar to that of **B1**, with 1.162 g (10 mmol) of 1,6-diaminohexane and 3.221 g (10 mmol) of BTDA. Light yellow solid was obtained in 91 % yield (3.278g). FTIR (cm^{-1}): 2975, 2873, 1769, 1713, 1664, 1456, 1425, 1243, 1097, 1041, 724.

Polyimide **A3***:* To a dry 100 ml 3-neck flask 2.140 g (10 mmol) of Jeffamine D230, 0.012 g (0.2 mmol) of isopropylamine, and 20 ml dry NMP were added under nitrogen with stirring. After well stirred for 30 min, 2.180 g (10 mmol) of PMDA were added. The reaction was carried out at room temperature for 6 h, followed by imidization at 170-180 ^{o}C for 6 h. After cooling to room temperature, the mixture was poured into 150 ml of methanol, filtered and washed with methanol several times, and dried *in vacuo*. Light yellow solid was obtained in 85 % yield (3.362 g).

^{1}H NMR (500MHz, DMSO-d_6, ppm): δ = 1.34 (m, 11H), 3.58 (m, 7H), 4.39 (m, 3H), 8.11 (s, 2H). FTIR (cm^{-1}): 2976, 2878, 1771, 1716, 1460, 1380, 1355, 1265, 1105, 1040, 731. GPC: M_n = 30167 g·mol^{-1}, M_w = 61567 g·mol^{-1}, PDI (polydispersity index) = 2.04.

Polyimide **A4***:* The preparation is similar to that of **A3**, with 2.180 g (10 mmol) of PMDA, 2.316 g (10 mmol) of Jeffamine HK511. Light yellow solid was obtained in 82 % yield (3.381 g).

^{1}H NMR (500MHz, DMSO-d_6, ppm): δ = 1.33 (m, 7H), 3.54 (m, 12H), 4.41 (m, 2H), 8.12 (s, 2H). FTIR (cm^{-1}): 2973, 2870, 1721, 1717, 1458, 1387, 1354, 1264, 1103, 1038, 730. GPC: M_n = 39776 g·mol^{-1}, M_w = 84430 g·mol^{-1}, PDI = 2.12.

Polymer **B3***:* The preparation is similar to that of **A3**, with 3.221 g (10 mmol) of BTDA, 2.140 g (10 mmol) of Jeffamine D230. Orange solid was obtained in 94 % yield (4.714 g).

^{1}H NMR (500MHz, DMSO-d_6, ppm): δ = 1.31 (m, 11H), 3.43 (m, 7H), 4.39 (m, 3H), 7.98 (broad, 4H), 8.12 (s, 2H). FTIR (cm^{-1}): 2974, 2873, 1774, 1712, 1665, 1456, 1427, 1368, 1247, 1097, 1040, 728. GPC: M_n = 41321 g·mol^{-1}, M_w = 88631 g·mol^{-1}, PDI = 2.14.

Polyimide **B4***:* The preparation is similar to that of **A4**, with 3.221 g (10 mmol) of BTDA, 2.316 g (10 mmol) of Jeffamine HK511. Dark orange solid was obtained in 92 % yield (4.763 g).

^{1}H NMR (500MHz, DMSO-d_6, ppm): δ = 1.32 (m, 7H), 3.53 (m, 12H), 4.41 (m, 2H), 7.98 (broad, 4H), 8.12 (s, 2H). FTIR (cm^{-1}): 2972, 2866, 1773, 1716, 1662, 1456, 1428, 1367, 1246, 1092, 1039, 728. GPC: M_n = 46982 g·mol^{-1}, M_w = 80809 g·mol^{-1}, PDI = 1.72.

Polyimide **C3***:* The preparation is similar to that of **A3**, with 3.107 g (10 mmol) of ODPA, 2.140 g (10 mmol) of Jeffamine D230. Orange solid was obtained in 89 % yield of (4.341 g).

^{1}H NMR (500MHz, DMSO-d_6, ppm): δ = 0.84, 1.28 (m, 11H), 3.50 (m, 7H), 4.35 (m, 3H), 7.46 (broad, 4H), 7.96 (s, 2H). FTIR (cm^{-1}): 2975, 2873, 1773, 1716, 1474, 1437, 1363, 1263, 1230, 1091, 1038, 748. GPC: M_n = 39472 g·mol^{-1}, M_w = 72810 g·mol^{-1}, PDI = 1.84.

Polyimide **C4***:* The preparation is similar to that of **A4**, with 3.107 g (10 mmol) of ODPA, 2.316 g (10 mmol) of Jeffamine HK511. Yellow solid was obtained in 87 % yield (4.405 g).

^{1}H NMR (500MHz, DMSO-d_6, ppm): δ = 1.30 (m, 7H), 3.52 (m, 12H), 4.37 (m, 2H), 7.46 (broad, 4H), 7.96 (s, 2H). FTIR (cm^{-1}): 2972, 2868, 1773, 1708, 1475, 1444, 1366, 1263, 1230, 1093, 1038, 748. GPC: M_n = 40398 $g{\cdot}mol^{-1}$, M_w = 74551 $g{\cdot}mol^{-1}$, PDI = 1.85.

Polyimide **D3***:* The preparation is similar to that of **A3**, with 4.446 g (10 mmol) of 6-FDA, 2.140 g (10 mmol) of Jeffamine D230. Yellow solid was obtained in 93 % yield (5.781 g).

^{1}H NMR (500MHz, DMSO-d_6, ppm): δ = 1.27 (m, 11H), 3.49 (m, 7H), 4.38 (m, 3H), 7.62 (broad, 2H), 7.80 (broad, 2H), 7.96 (s, 2H). FTIR (cm^{-1}): 2977, 2880, 1780, 1716, 1439, 1378, 1354, 1256, 1210, 1104, 1043, 748, 721. GPC: M_n = 50296 $g{\cdot}mol^{-1}$, M_w = 85653 $g{\cdot}mol^{-1}$, PDI = 1.70.

Polyimide **D4***:* The preparation is similar to that of **A4**, with 4.446 g (10 mmol) of 6-FDA, 2.316 g (10 mmol) of Jeffamine HK511. Yellow solid was obtained in 90 % yield (5.752 g).

^{1}H NMR (500MHz, DMSO-d_6, ppm): δ = 1.30 (m, 7H), 3.51 (m, 12H), 4.35 (m, 2H), 7.63 (broad, 2H), 7.80 (broad, 2H), 7.98 (s, 2H). FTIR (cm^{-1}): 2975, 2875, 1779, 1716, 1439, 1378, 1355, 1256, 1211, 1105, 1044, 748, 722. GPC: M_n = 53662 $g{\cdot}mol^{-1}$, M_w = 112443 $g{\cdot}mol^{-1}$, PDI = 2.09.

References

1. M. K. Ghosh and K. L. Mittal, *Polyimides, fundamentals and applications.* New York: Mercel-Dekker; 1996.

2. K. Fukushima, Y. Ikeda, T. Hayashi, N. Kikuchi, E. Kusano, A. Kinbara, *Thin Solid Films* 2001, **392**, 254.
3. G. Hougham, G. Tesero and J. Shaw *Macromolecules* 1994, 27, 3642.
4. G. Hougham, G. Tesero, A. Viehbeck, J. D. Chapple-Sokol. *Macromolecules* 1994, **27**, 5964.
5. E. J. Onah, U. Oertel, C. Froeck, T. Kratzmuller, V. Steinert and T. Bayer, *Macromol Mater Eng* 2002, **287**, 412.
6. H. G. Boston, V. S. Reddy, P. E. Cassidy,J. W. Fitch, D. Stoakley and A. K. Clair, *High Perform Polym* 1997.
7. Y. T. Chern. *Macromolecules* 1998, **31**, 5837.
8. Y. T. Chern, H-C. Shiue, *Macromolecules* 1997, **30**, 4646.
9. Y. T. Chern, H-C. Shiue, *Macromolecules* 1997, **30**, 5766.
10. B. Gonzalo, J. L. Vilas, T. Breczewski, M. A. Pèrez-Jubindo, M. R. De La Fuente, M. Rodriguez, L. M. Lèon, *J. Poly. Sci., Part A: Poly. Chem.* 2009, **47**, 722.
11. M. A. B. Meador, S. Wright, A. Sandberg, B. N. Nguyen, F. W. Van Keuls, C. H. Mueller, R. Rodríguez-Solís, F. A. Miranda, *ACS Appl. Mater. Interfaces* 2012, **4**, 6346.
12. T. Miyagawa, T. Fukushima, T. Oyama, T. Iijima, M. Tomoi, *J. Poly. Sci., Part A: Poly. Chem.* 2003, **41**, 861.
13. G. Kresse and J. Furthmuller, *Phys. Rev. B: Condens. Matter* 1996, **54**, 11169.
14. N. Shi and R. Ramprasad, *IEEE Trans. Dielectr. Electr. Insul.* 2008, **15**, 170.
15. C.C. Wang, G. Pilania, S. A. Boggs, S. Kumar, C. Breneman and R. Ramprasad, *Polymer* 2014, **55**, 979.

16. C. Koning, L. Teuwen, E. W. Meijer and J. Moonen, *Polymer* 1994, **35**, 4889.

17. S. H. Hsiao, C. P. Yang and K. Y. Chu, *Macromolecules* 1997, **30(2),** 165.

18. J. Ho and T. R. Jow, *Characterization of High Temperature Polymer Thin Films for Power Conditioning Capacitors.* Army Research Laboratory: Adelphi, MD, **2009**; ARL-TR-4880.

19. M. Ree, K. Kim, S. H. Woo, H. Chang, *J. Appl. Phys.* 1997, **81 (2)**, 15.

20. L. Zhu and Q. Wang, *Macromolecules* 2012, **45**, 2937.

21. Y. Wang, X. Zhou, Q. Chen, B. Chu and Q. Zhang, *IEEE Trans. Dielectr. Electr. Insul.* 2010, **17**, 1036.

22. J. R. MacDonald, M. A. Schneider, J. B. Ennis, F. W. MacDougall and X. H. Yang, *Proc. IEEE Electrical Conf., Montreal, QC, Canada* 2009, 306-309.

23. S. Wu, W. Li, M. Lin, Q. Burlingame, Q. Chen, A. Payzant, K. Xiao, Q. M. Zhang, *Adv. Mater.* 2013, **25**, 1734.

24. J. D. Jacobs, M. J. Arlen, D. H. Wang, Z. Ounaies, R. Berry, L. S. Tan, P. H. Garrett and R. A. Vaia, *Polymer* 2010, **51**, 3139.

25. S. Chisca, V. E. Musteata, I. Sava and M. Bruma, *Eur. Polym. J.* 2011, **47**, 1186.

26. I. Treufeld, D. H. Wang, B. A. Kurish, L.-S. Tan, L. Zhu. *J. Mater. Chem. A,* 2014, **2,** 20683.

27. Y. Ohki, N. Fuse and T. Arai, *Conf. Electr. Insul. Dielectr. Phenom.,West Lafayette, USA* **2010,** 660.

28. C. Ku and R. Liepins, *Electrical Properties of Polymers: Chemical principles*, Hanser Publishers: New York, 1987; Chapter 4, pp 150-151.

Chapter 5

Systematic Synthesis, Characterization and Processing of Polythiourea as Dielectric Material

5.1 Polythiourea and Dielectric Properties

Thiourea is usually used as a comonomer in polycondensation, like urea. The interest in design the polymers with thiourea functional group originated from the fact that thiourea crystals are a well-known ferroelectric material.[1] Studies on a variety of electrical properties such as temperature and frequency dependent dielectric behavior, spontaneous polarization, and ferroelectric effects showed that thiourea single crystal to be an interesting organic ferroelectric. Thiourea has a chemical structure H_2N-CS-NH_2, in which the amino group is electron-donating and CS is electron-withdrawing. This gives the dipole moment of ~ 4.89 D,[2] which will potentially lead to high dielectric constant. Therefore, it is promising to incorporate thiourea as a part of the polymer chain to study their dielectric properties. A linear polythiourea, with thiourea functional group in the polymer main chain, can be prepared by polycondensation of thiourea with formaldehyde to achieve the simple structure -NH-CS-NH-CH_2-; or the reaction of a diamine with carbon disulfide, thiophosgene, or diisothiocyanate.

The first work on polythioureas in the field of ferroelectrics was published in 1978 using a thiourea-formaldehyde condensation polymer with the repeat unit of –NH-CS-NH-CH_2-, however the molecular weight was rather low.[3] The dielectric measurements

were done by preparing a powder pellet, which showed a ten-fold dielectric constant increase at 145^{o}C. This polymer exhibit ferroelectric transition as well as the cooperative orientational change of thiourea segments. Ohishi et al.[4] studied aliphatic polythioureas synthesized by condensation of diamine with carbon disulfide with variation of aliphatic chain length. Similar the behavior of ferroelectric nylons, odd-numbered polythioureas were selected in order to obtain a polar chain and their packing. It is proved in this work that these polymers possessing large thiourea dipoles are able to have a polar structure with hydrogen bonding. Hydrogen bonding, generally, is stronger than van der Waals force, and it assists in forming crystalline structure, hence stabilizes the remnant polarization. Usually only a small amount of chains can form sufficient hydrogen bonding, while a large part of chains remain non-hydrogen-bonded. Through molecular design, the quality and the quantity of hydrogen bonding can be controlled by changing the chemical structure, consequently altering the dielectric relaxation of polythioureas.

Recently, an aromatic polythiourea[5,6] was reported to have a high breakdown strength and low loss at high electric fields (10% at 1 GV/m), which has great potential in energy storage applications. This aromatic polythiourea was synthesized via a microwave-assisted polycondensation of 4,4'-diphenylmethanediamine with thiourea. The polymer was casted into film through spin coating a polymer solution, and the thin film was found to be amorphous without long-range crystalline ordering. The high breakdown field was explained by the presence of random dipoles in an amorphous structure which provide substantially stronger scattering to charge carriers. However, due to the synthesis method, the polymer has relatively low molecular weight and cannot be processed into free standing films. In order to better understand polythiourea as a dielectric material and how

it can be different from the ferroelectric analogs, a close investigation on chemical and micro-structure of different types of polythiourea and their corresponding electrical properties is necessary. Further study can provide guidance for molecular design of polythiourea as a potential dielectric for capacitive applications.

As discussed in Chapter 3, the current design and selection of polymer dielectrics are dominated by trial and error strategies, which could be significantly more efficient by using the tools of advanced computational screening. We recently proposed a hierarchical modelling strategy[7,8] to accelerate the identification of polymer dielectrics with successive downselection steps: Combinatorial chemical space exploration using four independent building blocks; Identification of promising repeat unit based on band gap and dielectric constant estimates; 3D structure predictions of polymers composed of the downselected repeat units; Property predictions of the 3D systems. Combined with experimental results, we determined polythiourea as one of the promising systems with a repeat unit of -NH-CS-NH-C_6H_4-, with the other two being polyimide -CO-NH-CO-C_6H_4-, and polyurea -NH-CO-NH-C_6H_4-. The polymers have a band gap higher than 3.5 eV, as well as a dielectric constant from 4 to 6. The structures of polymers were predicted in terms of IR spectrum as well as X-ray diffraction patterns. The correspondence between the measured IR spectrum and predicted ones are uniformly good, since the IR peaks are dominated by intra-chain “bonded” interactions. We also discovered matching crystal structure for the synthesized polymer with the predicted based on XRD patterns. The polymer studied here has a simple structure beneficial for calculation process, but it showed limited solubility and processability. Therefore, further modification and optimization needs to be conducted on the experimental side.

Here, a systematic synthesis and processing study on polythiourea was conducted in combination with our hierarchical modeling strategy to provide a clear structure – dielectric property relationship. To further improve the dielectric property and processability, different chain segment including aromatic, aliphatic and polyether with various additional dipoles were incorporated into the basic polythiourea backbone. Scalable synthetic procedures were one of the materials selection criteria making these systems the potential candidates for industrial scale manufacturing of thin films and capacitor assembling.

5.2 Systematic synthesis as modification of promising system

Molecular structures were inspired by a simple polythiourea structure identified by calculation results.[7] The polymer with a repeat unit of -NH-CS-NH-C_6H_4- (also listed here as PDTC-PhDA) showed promising dielectric properties, but had limited solubility and processability in that it only dissolves in hot DMSO, and only low molecular weights were achieved due to early precipitation during a condensation polymerization.

With the exception of one synthesis, polymerizations shown in Scheme 5.1 were carried out by the reaction of a diamine with a diisothiocyanate. In order to reproduce the polythiourea reported by Wu *et al*.[5], polymerization was carried out between a diamine and thiophosgene, which can be scaled up with a reasonable cost. Polymers precipitated out of the reaction solution in the form of white fibers, which was a first indication that these polymers had achieved a high degree of polymerization. The polythioureas were characterized by proton nuclear magnetic resonance spectroscopy (^{1}H-NMR), infrared spectroscopy (IR), and powder x-ray diffraction for structure determination and by

thermogravimetric analysis (TGA), and differential scanning calorimetry (DSC) for thermal properties.

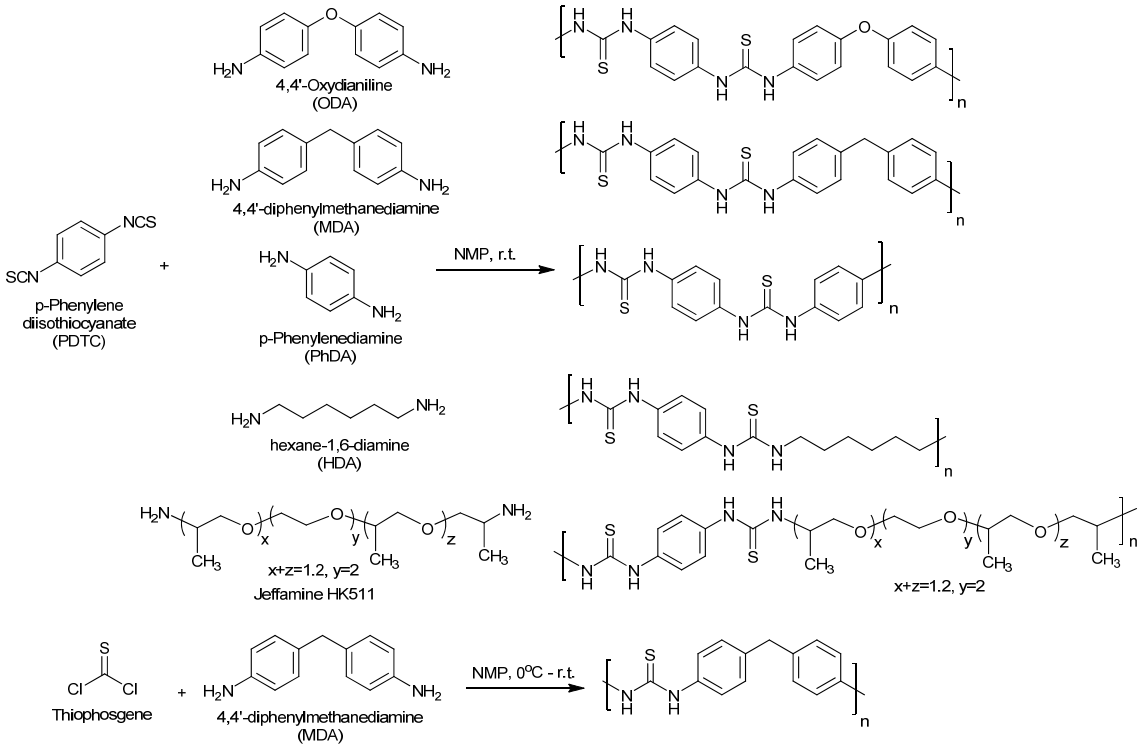

Scheme 5.1 Polythiourea synthetic route and structures

The number average molecular weight reported in Table 5.1 was calculated using end group analysis from ^{1}H-NMR (the details of synthesis and characterizations are listed in the Experimental section in this chapter). All newly synthesized polythioureas showed high molecular weight (Table 5.1) and improved solubility compared to PDTC-PhDA.[22] PDTC-MDA, PDTC-HDA and PDTC-HK511 are soluble in N,N-dimethylformamide (DMF), N,N-dimethylacetamide (DMAc), dimethyl sulfoxide (DMSO) and N-methylpyrolidinone (NMP). In addition to these solvents, PDTC-HK511 is also soluble in tetrahydrofuran (THF). PDTC-ODA and Thiophosgene-MDA, on the other hand, show limited solubility in DMF, DMAc and NMP, but a good solubility in DMSO at room

temperature. Thermal properties play an important role in polymer thin film processing and dielectric properties at elevated temperature. The occurrence of a phase transition, such as a glass transition, within the operating temperature range of a capacitor can be detrimental since polymer chain segmental motion increases dielectric loss, and reduces energy storage efficiency. PDTC-HDA and PDTC-HK511 show glass transition temperatures of 139 ^{o}C and 92 ^{o}C, respectively, due to flexible chain segments. All other polythioureas did not exhibit any observable T_g, and, generally have high degradation temperatures.

Table 5.1: Molecular Weight and Thermal Properties

Polymer	M_n (g/mol)	T_g (^{o}C)	T_d (^{o}C)
PDTC-ODA	21500	N/O	246
PDTC-MDA	56400	N/O	228
PDTC-PhDA	N/A	N/O	276
PDTC-HDA	85100	139	275
PDTC-HK511	25900	92	294
Thiophosgene-MDA	44600	N/O	311

5.3 Dielectric properties and their dependence on chemical structure and morphology

From rational design, polythiourea was identified to have desirable electrical properties from a first level screen involving a 1-dimensional catenation of repeat units into a polymer chain.[7] The second step of determining a 3-dimensional structure helped to provide more accurate prediction of dielectric properties. As described in Chapter 2, the structure search was conducted with an evolutionary algorithm based method[9-11] specially modified to handle repeat units rather than atoms as the building blocks using DFT energetics.

Table 5.2 Dielectric Properties: Predicted Structure and Experiment (Exp.)

	PDTC-ODA						PDTC-MDA						PDTC-HDA			
Structure	S1	S2	S3	S4	S5	Exp.	S1	S2	S3	S4	S5	Exp.	S1	S2	S3	Exp.
E_g (eV)	3.31	3.07	3.06	3.44	3.45	3.22	3.25	3.69	3.47	3.25	3.41	3.16	3.68	3.81	3.77	3.70
K_e	3.78	3.94	3.90	3.86	3.84	3.20	3.31	3.71	3.78	3.88	3.79	3.28	3.33	3.35	3.18	2.92
Refractive Index	---					1.79	---					1.81	---			1.69
K_t	5.68	5.05	6.81	4.82	4.74	4.52	4.08	4.35	4.52	4.83	5.15	4.08	3.98	4.00	4.05	3.67

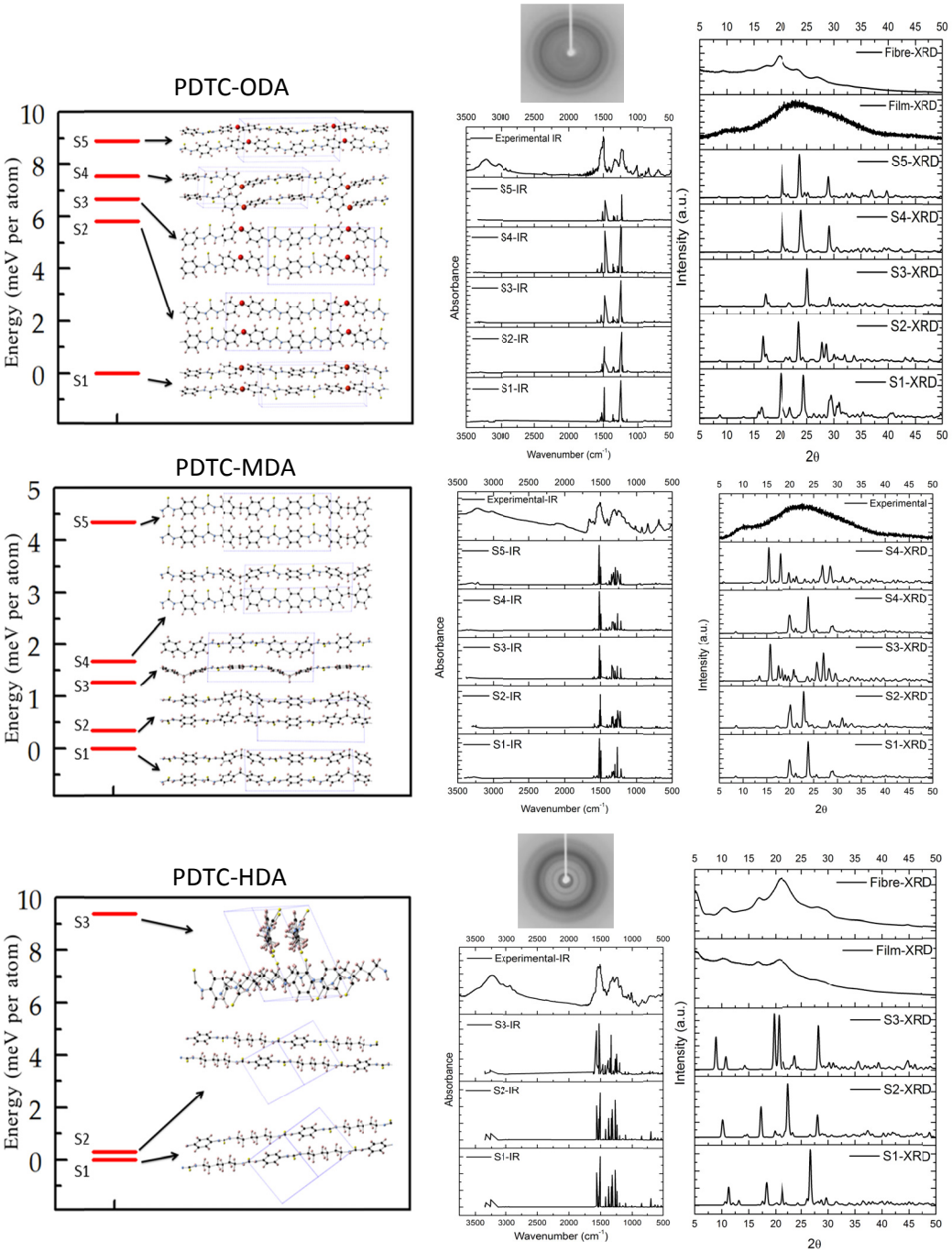

Figure 5.1 Calculated and experimental structures of PDTC-ODA (Top), PDTC-MDA (Middle) PDTC-HDA (Bottom)

To predict the crystal structure of these polymers we applied a constrained evolutionary search algorithm embodied in USPEX code where each monomeric unit is treated as one motif with fixed connectivity. During the course of evolutionary optimization, fixing the chemical connectivity greatly reduces the search space and allows the initial structure generation with different packing to identify the most stable packing of monomers. The diversity in initial structures is maintained by allowing a certain degree of variation in the rotation and translation of polymers along the chain direction. Low energy configurations of the polymers were identified and further studied for computing the electronic and dielectric properties. The predicted low energy crystal structures for PDTC-ODA and PDTC-HDA, as well as the corresponding infrared (IR) spectra and X-ray diffraction (XRD) patterns, all numerically computed, are shown in Figure 5.1, along with the experimentally determined IR spectra and XRD patterns. For each predicted crystal structure, the numerically calculated values of the band gap (E_g), total (K_t) and electronic (K_e) part of dielectric constants for PDTC-ODA, PDTC-MDA, and PDTC-HDA are summarized in Table 5.1, along with experimentally determined band gap (E_g), total (K_t) dielectric constant. The measured electronic (K_e) part of dielectric constant was determined indirectly from the refractive index measured from the ellipsometry.

The correspondence between the measured IR spectrum and that of the predicted structures is uniformly good, except for some details that are not able to be shown in experimental results. The IR peaks are dominated by chemical bonds and hence consistently reproduced for all predicted structures to show similar IR

spectrum. In terms of morphology, PDTC-HDA fiber and film are both semicrystalline, whose XRD diffraction pattern is in agreement with predicted structure S2 (Figure 5.1, bottom), computationally identified as one of the structures with lowest energy. Dielectric constants are close for all three computationally derived structures. With regards to the discrepancy in the calculated and experimentally derived dielectric constants, the experimental dielectric constant values reflect an average of both amorphous and crystalline phases, whereas the calculated structures represent only the purely crystalline form (Table 5.2). After solution processing, PDTC-ODA films were found to be amorphous (Figure 5.1, top), whereas fibers show an obvious diffraction pattern, similar to that of predicted structure 1. Therefore, the lower dielectric constant for the film versus the value derived from computation is expected. PDTC-MDA (Figure 5.1, middle) is amorphous in both fiber and film as that there is no significant XRD diffraction pattern. All polymers show high refractive indices, which will be discussed later in this chapter. Aliphatic polythioureas exhibit a lower refractive index than their aromatic analogues.

Dielectric properties were evaluated experimentally in terms of dielectric constant, loss, band gap, DC breakdown strength, and charge-discharge behavior determined from a D-E hysteresis loop. Dielectric constant and dissipation factors (tan δ) are listed in Table 5.3. Dielectric constants are all higher than BOPP, and comparable with the polythiourea reported recently by Wu *et al.*[7] Higher dielectric constants were achieved by addition of permanent dipoles such as diphenyl ether, and polyether segments which enhance polarization, resulting in higher dielectric

constants for PDTC-ODA and PDTC-HK511. Dielectric constant increases with increasing conjugation length, which is attributed to the enhanced π electron mobility. Even with the high dielectric constant, and increased conjugation in these systems, tan δ remains at approximately 2% which is also comparable to the loss factor reported recently for other polythioureas.[7]

Table 5.3 Dielectric Properties, Experimental

Polymer	K (r.t. 1kHz)	tan δ (r.t. 1kHz)	E_g (eV)	Refractive Index
PDTC-ODA	4.52	0.0233	3.22	1.79
PDTC-MDA	4.08	0.0348	3.16	1.81
PDTC-PhDA	4.89	0.0144	3.07	N/A*
PDTC-HDA	3.67	0.0267	3.53	1.71
PDTC-HK511	6.09	0.0115	3.51	1.64
Thiophosgene-MDA	3.84	0.0226	3.30	1.74

Dependence of K and tan δ on temperature and frequency were evaluated by time domain dielectric spectroscopy, with all the spectra shown in Figure 5.2. In general, the dielectric constant increases as temperature increases due to improved chain mobility, which enhances the dipole alignment along the applied electric field. The trend that the dielectric constant first decreases then increases for polyimide was not observed here, which indicates the polythioureas are not sensitive to moisture nor absorb obvious amount of moisture. However, in the high frequency regime, the dielectric constant slowly decreases due to relatively slow segmental motion of dipoles in the polymer chain. In general, dielectric constant remains steady over a wide frequency range suggesting a relatively fast polarization response. For PDTC-MDA, HDA, HK511 and thiophosgene-MDA, tan δ shows a weak peak at *ca.* 1 kHz. As temperature increases tan δ slightly increases and this peak shifts to higher frequencies, which can be explained by increased dipole mobility. For PDTC-PhDA, which has lower chain mobility, the

similar peak cannot be observed. Therefore, the peak can be assigned to the motion of diamine segment. The relaxation peak for PDTC-HDA and HK511 show at higher frequency compared to aromatic systems, since aliphatic systems have higher chain mobility than the aromatic ones.

The energy density is proportional to the square of the electric field and therefore is limited by the breakdown field of the polymer dielectric. By operating at a high electric field, the significantly higher energy density can be achieved. The fundamental mechanism of polymer breakdown lies in the electronic breakdown, which is often explained by electron avalanche theory[12], which depends on the presence and creation of charge carriers capable of migration through the dielectric. Electrons gain energy from an external electric field between successive collisions with phonons. At low electric fields, the energy gain from the external electric field is balanced by energy loss from collision with phonons. However, at a sufficient high electric field, the electron energy increases indefinitely until a threshold is reached at which a high-energy electron ionizes the lattice, leading to carrier multiplication. And this is referred to as the impact ionization. Band gap is believed to be the basic property related to the intrinsic breakdown where a larger band gap implies a higher threshold for impact ionization. The band gaps of polythiourea, that are highly dependent upon chemical structure, were evaluated by UV absorption (Table 5.3). The highest band gap was achieved for polythioureas containing aliphatic segments whereas the presence of extensive π conjugation lowers the band gap due to electron delocalization.

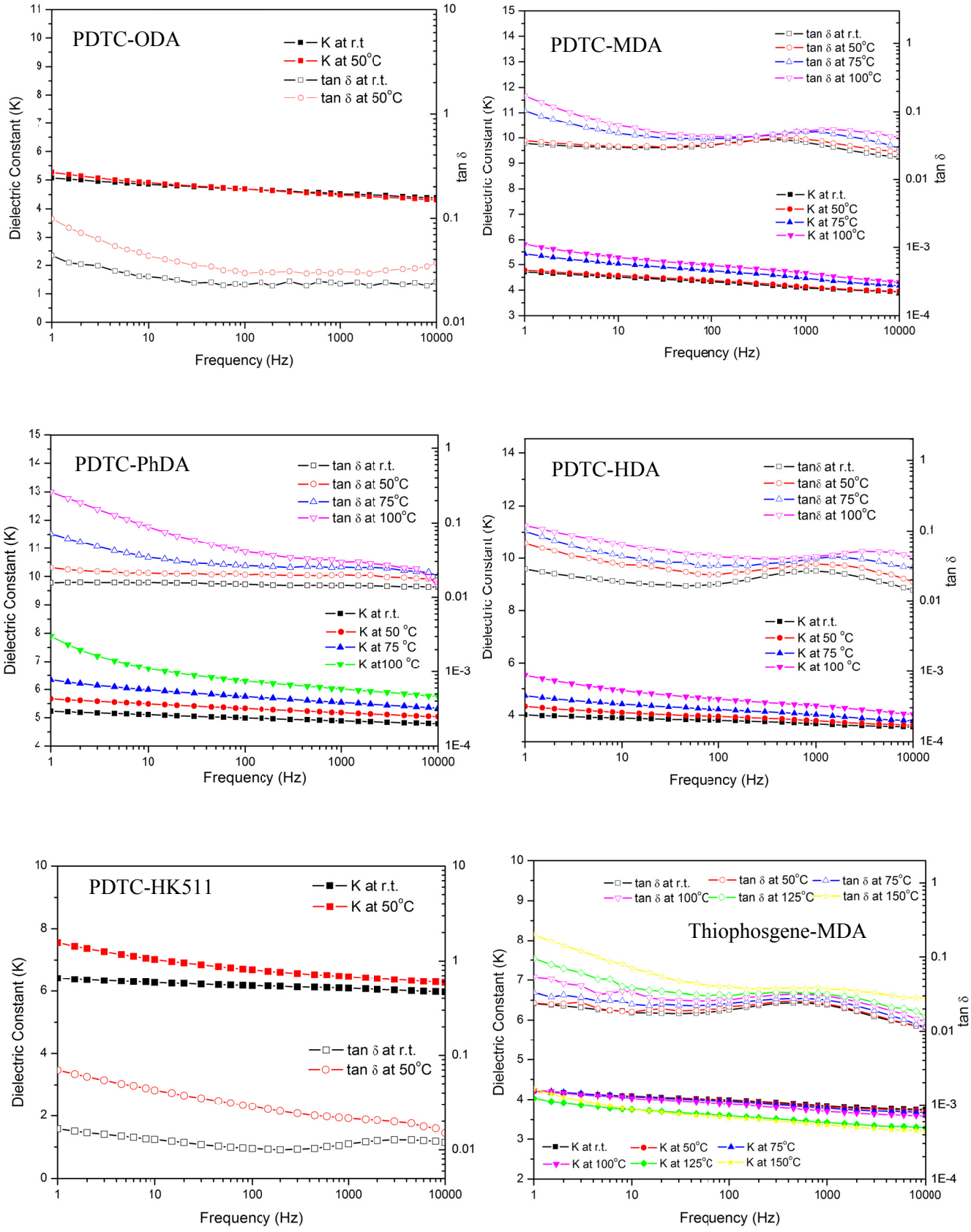

Figure 5.2 Dielectric Spectra of Polythioureas

Table 5.4 Weibull Breakdown Field Measurement

Polymer	Weibull Characteristic Breakdown Field (MV/m)	Slope	Quality of Fit (R^2)	Number of samples
PDTC-ODA	789	9.517	0.965	30
PDTC-MDA	707	10.30	0.923	30
PDTC-HDA	667	20.95	0.955	30
PDTC-HK511	602	6.03	0.971	30
Thiophosgene-MDA	677	19.24	0.927	30

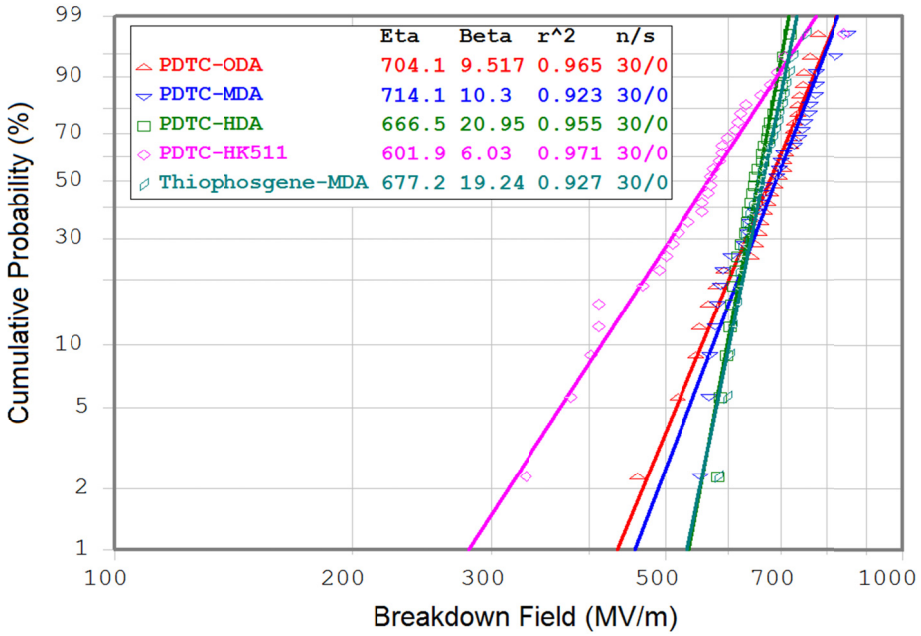

Figure 5.3 Weibull Distribution of Breakdown Field of Polythioureas

The higher band gap of PDTC-HDA and HK511 implies a higher intrinsic breakdown strength than that for PDTC-ODA and PDTC-MDA. However, the measured engineering DC breakdown is shown to differ, as PDTC-ODA, MDA have a higher breakdown field than PDTC-HDA. First, the relationship of band gap and intrinsic breakdown is not well established for polymer, much worse for engineering breakdown strength which is dominated by "extrinsic" factors not inherent to the material such as imperfections (e.g., chemical impurities at the

atomic level, and cavities at the microscopic and macroscopic scales) as well as statistical variations in morphology and microstructure. Second, polymer breakdown phenomenon also depends on other mechanisms besides electronic breakdown including thermal breakdown, partial charge and free volume breakdown.[13]

It has been proposed that the presence of random dipoles in amorphous polar polymers provide electron-dipole scattering in addition to electron-phonon scattering to stabilize electron energy and hence, prevent dielectric breakdown.[14] Here for the polythiourea systems, amorphous films of PDTC-ODA and PDTC-MDA show higher dc breakdown voltages than the semicrystalline films of PDTC-HDA confirming that there might be an advantage to polar polymers being in an amorphous state. Another advantage is that the amorphous material is more homogenous than a semicrystalline one, and fluctuations of electrical properties will occur on a much smaller scale. The breakdown field of PDTC-HK511 is lower than all the other polythioureas due to poor film quality. The T_g of PDTC-HK511 is lower than the drying temperature of the film causing unevenness and defects in the free-standing films that were obtained.

5.4 Processing optimization in increasing high field performance

Charge-discharge behavior was estimated using D-E hysteresis loop. Film samples were prepared in the same way as for the breakdown measurement. Breakdown fields achieved through D-E hysteresis loop is comparable with the value from linear DC voltage ramp in Table 5.4. The hysteresis loop and the corresponding releasing energy and efficiency are shown in Figure 5.4 for each polythiourea. For all the polythioureas investigated here, a

high releasing energy density of ~ 10 J/cc was achieved at breakdown strength of 550-750 MV/m. Hysteresis observed in the D-E loops is believed to be originated from conduction loss at high voltage, which can be attributed to residue solvent and other impurities. PDTC-HK511 showed much higher efficiency than the other systems due to much less solvent residue. The films for this particular polymer were dried above its glass transition temperature, above which the chain mobility is highly improved so that the solvent is much easier to be removed.

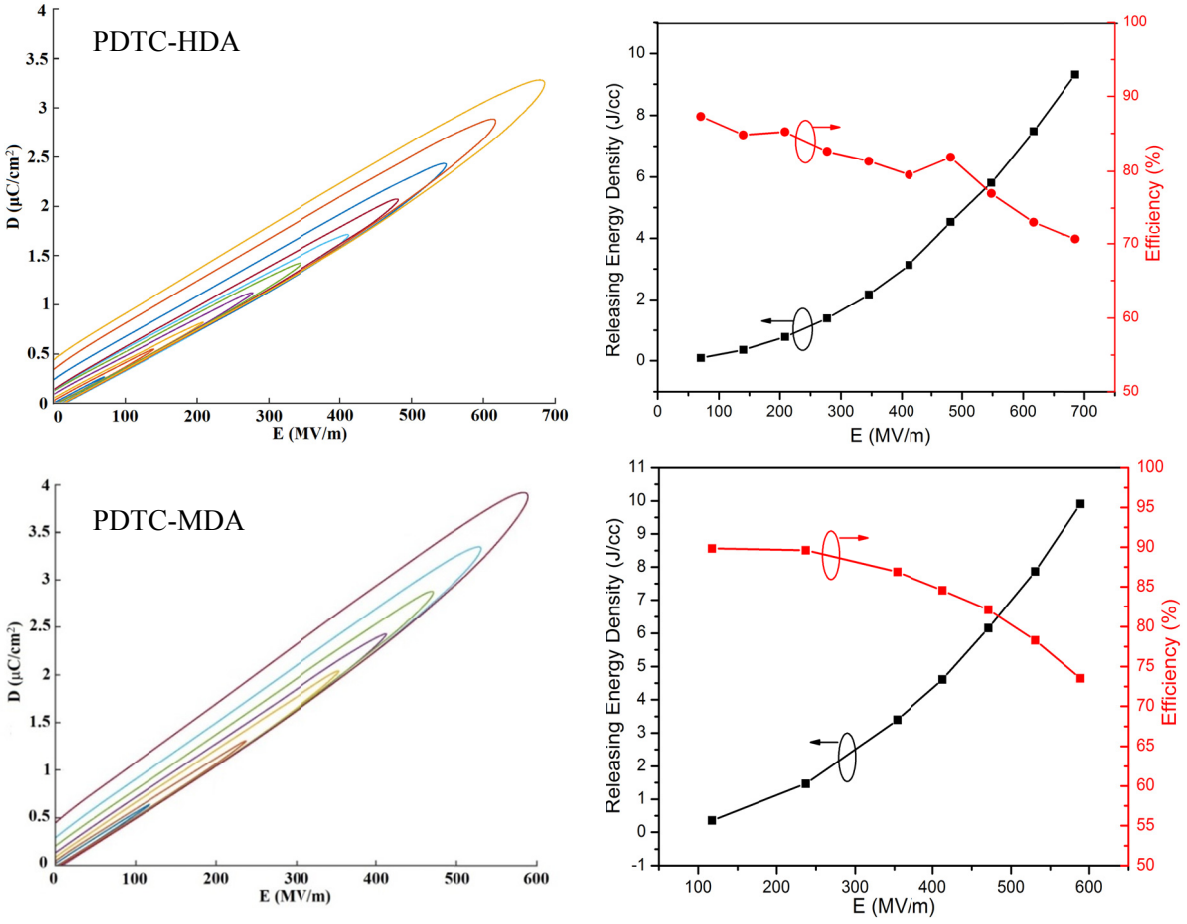

Figure 5.4 D-E Hysteresis Loop of Polythioureas

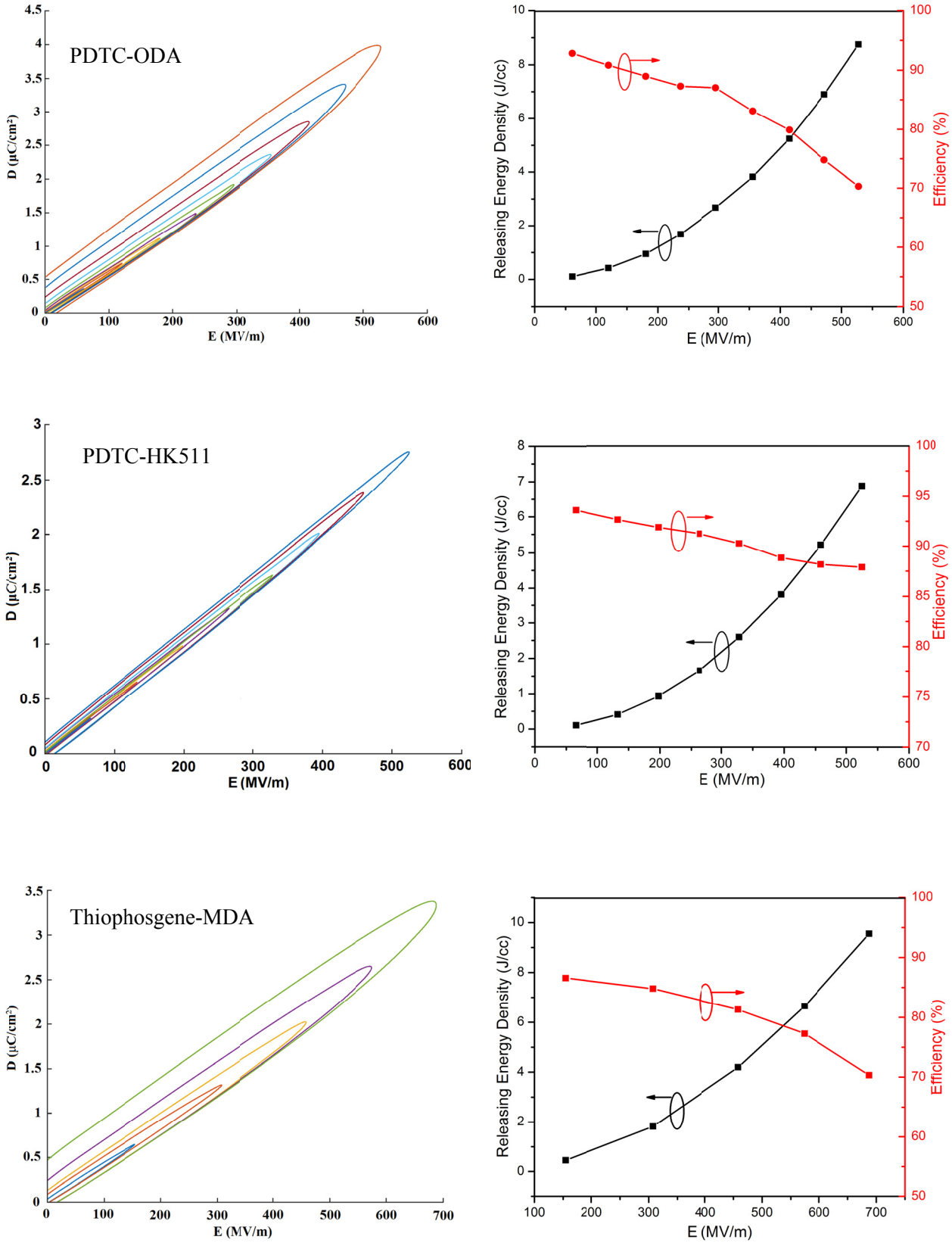

Figure 5.4 D-E Hysteresis Loop of Polythioureas (Following Page)

The films were prepared through industrial scale processing, which produces large scale free standing films. The casting speed, drying condition and thermal annealing all lead to different surface structure and defect levels. Large scale processing brought a higher level of surface roughness and more defects and impurities, which reduced efficiency and breakdown voltage. However, large scale free standing films are required for capacitor assembling. Further optimization of processing conditions will be conducted to improve the overall performance. Refined high field conduction study will be performed to champion the thin film processing optimization.

5.5 High Refractive Indices of Polythiourea and Potential Optical Applications

Another interesting data observed in this study is the high refractive indices of the polythioureas here. With refractive indices as high as 1.81 (Table 5.5) for solution casted colorless films, these polythioureas could be promising for optical devices.

Table 5.5 Refractive Indices for Polythioureas

	546 (Green light)	632 (Red light)
PDTC-ODA	1.79	1.76
PDTC-MDA	1.81	1.79
PDTC-HK511	1.64	1.63
PDTC-HDA	1.71	1.70

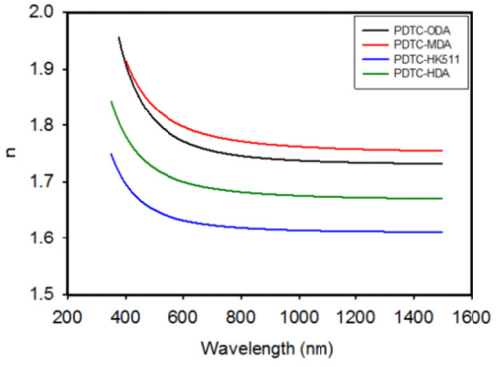

Figure 5.5 Refractive Indices of Polythiourea at Different Frequency

Achievements of new functions in advanced optical devices are becoming increasingly dependent on the availability of new functional materials. And high refractive index polymers (HRIPs) are very important in advanced optoelectronic fabrications, such as high performance substrates for advanced display devices,[15] optical adhesives or encapsulants for organic lightemitting diode devices (OLEDs),[16] antireflective coatings for advanced optical applications,[17] photoresists for 193-nm immersion lithography,[18] and microlens components for charge coupled devices (CCD) or complementary metal oxide semiconductor (CMOS) image sensors (CIS).[19] Typical refractive indices (n) of conventional polymers are often in the range of 1.30–1.70. However, in practical applications, a higher refractive index is frequently desired. For example in high-brightness LED fabrications, the mismatch of the n values between the semiconductor dies (n of 2.50 to 3.50) and the polymer encapsulants (n of 1.40 to 1.60) often causes total internal reflection when light travels from the die into the encapsulant at certain incident angles, resulting in low light extraction efficiency of the device. The desired n value of the encapsulant layers is at least 1.80 over the entire visible region and preferably in the range of 1.80–2.50.[16] Since many optoelectronic devices are based on components with high refractive indices, molecular tailoring of conventional polymers is greatly desired. Fortunately, the ever-increasing demands of HRIPs greatly promote extensive research in this field and impressive scientific and technological progress has been achieved in the past decade. However, the upper limitation of the refractive indices of organic polymers which have been reported up to now in the literature is usually below 1.80.[20] With the

rapid development of nano-science and technology, nanocomposites consisting of highly refractive inorganic nanoparticles and organic polymer matrixes could easily achieve an n value higher than 1.80. However, such polymer nanocomposites sometimes suffer from storage stability, higher optical loss and poor processability.

From the molecular design point of view, the way to increase the refractive index is to introduce the substituents with high molar refractions and low molar volumes.[20] Aromatic rings, halogen atoms except fluorine, and sulfur atoms are effective in increasing the refractive indices of polymers. In addition, metal elements and highly polarizable p-conjugated functionalities are also beneficial for increasing the refractive indices of polymers. In practice, these substituents are usually combined into one polymer, whose n values can often be increased by the synergic effects of the groups. Here in our systems, the thiocarbonyl (C=S) group has a molar refraction of 7.97 and phenyl group has a value of 25.46.[21] The measured refractive indices for our system was obtained using an ellipsometer. Due to the sulfur species and the aromaticity, the polythioureas here showed high refractive indices. Polymer PDTC-HK511 has the lowest value among the four, since the repeat unit has higher molecular weight than the other and the free volume created by the side methyl groups increases the molar volume. The refractive indices in the range of 400 to 1400 nm wavelength decrease as the wavelength increases, but stabilized after the point of ~800 nm. The drop from 400 to 800 nm indicates band gap of the material. Because of the low absorption

wavelength, the material appears to be colorless, which is beneficial for the polymer films to be used in optical devices for display.

5.6 Conclusion

A systematic study on polythioureas was conducted as a prospective dielectric layer by implementation of a high throughput hierarchical modelling with combinatorial exploration and successive screening, followed by an evolutionary structure search based on density functional theory (DFT). From a downselection, a series of polythioureas were synthesized and investigated in terms of dielectric constant and loss, band gap, charge-discharge behaviour and DC breakdown strength. A dielectric constant of ~ 4.5 and a corresponding energy density of ~ 10 J/cc were achieved in accordance with Weibull characteristic breakdown voltage of ~ 700MV/m. With the incorporation of various chain segments, including aromatic, aliphatic and polyether, we were able to tune dielectric properties by means of introducing additional permanent dipoles, altering conjugation length, controlling morphology, etc. Crystalline structures in solution casted films were observed by WAXD (Wide Angle X-ray Diffraction), which were in great agreement with DFT predicted diffraction patterns. The effects of crystalline structure, microstructure and processing conditions on high voltage conduction loss and breakdown strength were also discussed.

5.7 Experimental, Materials

5.7.1 Materials and Synthesis

Para-phenylene diisothiocyanate (PDTC), thiophosgene, 1,4-diazabicyclo [2.2.2]octane (DABCO), 4,4'-Oxydianiline (ODA), 4,4'-diphenylmethanediamine (MDA), 1,4-diaminobenzene (PhDA), 1,6-diaminohexane (HDA) and anhydrous N-methyl-2-pyrrolidone (NMP), dimethyl sulfoxide (DMSO), dimethylacetamide (DMAc) were all purchased from Sigma-Aldrich Chemical Company. DABCO was recrystallized from petroleum ether before use, whereas all other chemicals were used as received.

Polythioureas were prepared through two synthetic methods: (1) the reaction of diamine with diisothiocyanate or (2) the reaction of diamine with thiophosgene. For method (1), p-phenylene diisothiocyanate was added in the NMP solution of diamine while stirring under inert atmosphere. After 6h at room temperature, the reaction mixture was poured into methanol with fibre-like precipitation, followed by washing with methanol and dried at 50^{o}C *in vacuo* overnight. For method (2), the reaction was carried out in a completely dried four neck flask equipped with dropping funnel, distillation and safety trap. Thiophosgene was carefully and slowly added to the mixture of DABCO and diamine in NMP at 0^{o}C. The reaction was carried out at room temperature for 24h after reactants were well mixed. Deionized water and methanol was used for precipitation and washing. Polymer was obtained after purification and drying 50^{o}C *in vacuo*. Detailed synthesis and characterizations are listed below.

PDTA-ODA: To a dry 50ml 3-neck flask, 0.961g (5mmol) of para-phenylene diisothiocyanate 1.001g (5mmol) 4,4'-oxydianiline and 20ml NMP were added under inert atmosphere with stirring. After 6h at room temperature, the reaction mixture was

poured into methanol with fibre-like precipitation, followed by washing with methanol and dried at 50°C *in vacuo* overnight. White precipitate was obtained in 91% yield (1.78g). FTIR: ν_{max}/cm^{-1} 3210 (N-H st), 3030 (ar C-H st), 1510 (ar C-C), 1340 (C-N st), 1240 (C=S st), 1160 and 1010 (ar C-O-C st). ^{1}H NMR δ_H(500 MHz; DMSO-d^6) 6.99 (4 H, d, benzene), 7.43 (4 H, s, benzene), 7.46 (4 H, d, benzene) and 9.72 (4 H, s, NH). Chain end: 4.98 (0.0736 H, s, NH_2), M_n=21537 g/mol.

PDTC-MDA: The preparation is similar to that of PDTC-ODA, with 0.961g (5mmol) of para-phenylene diisothiocyanate and 0.991g (5mmol) of 4,4'-diphenylmethanediamine. White fibre-like solid was obtained in 94 % yield (1.84g). FTIR: ν_{max}/cm^{-1} 3220 (N-H st), 3020 (ar C-H st), 1510 (ar C-C), 1300 (C-N st), 1250 (C=S st). ^{1}H NMR δ_H(500 MHz; DMSO-d^6) 3.88 (2 H, s, CH_2), 7.20 (4 H, d, benzene), 7.37 (4 H, s, benzene), 7.41 (4 H, d, benzene) and 9.71 (4 H, s, NH). Chain end: 5.24 (0.0280 H, s, NH_2), M_n=56360 g/mol.

PDTC-PhDA: The preparation is similar to that of PDTC-ODA, with 0.961g (5mmol) of para-phenylene diisothiocyanate and 0.991g (5mmol) of 4,4'-diphenylmethanediamine. White fibre-like solid was obtained in 94 % yield (1.84g). FTIR: ν_{max}/cm^{-1} 3220 (N-H st), 3020 (ar C-H st), 1510 (ar C-C), 1310 (C-N st), 1250 (C=S st).

PDTC-HDA: The preparation is similar to that of PDTC-ODA, with 0.961g (5mmol) of para-phenylene diisothiocyanate and 0.581g (5mmol) of 1,6-diaminohexane. White fibre-like solid was obtained in 93 % yield (1.43g). FTIR: ν_{max}/cm^{-1} 3220 (N-H st), 3020 (ar C-H st), 2930 (C-H st), 1510 (ar C-C), 1310 (C-N st), 1230 (C=S st). ^{1}H NMR δ_H(500 MHz; DMSO-d^6) 1.32 (4 H, m, CH_2), 1.54 (4 H, m, CH_2), 3.45 (4 H, m, CH_2), 7.33 (4 H, s, benzene), 7.65 (2 H, s, NH), and 9.39 (2 H, s, NH). Chain end: 1.96 (0.0150 H, s, NH_2), M_n = 85121 g/mol.

PDTC-HK511: The preparation is similar to that of PDTC-ODA, with 0.961g (5mmol) of para-phenylene diisothiocyanate and 1.10g (5mmol) of Jeffamine HK511. White fibre-like solid was obtained in 87 % yield (1.80g). FTIR: ν_{max}/cm^{-1} 3230 (N-H st), 3040 (ar C-H st), 2973 (C-H st), 1510 (ar C-C), 1310 (C-N st), 1230 (C=S st), 1103 and 1038 (ar C-O-C st). ^{1}H NMR δ_H(500 MHz; DMSO-d^6) 1.06-1.13 (7 H, m, Me), 3.52-3.56 (12 H, m, CH_2), 4.49 (2 H, m, CH), 7.36 (4 H, s, benzene), 7.52 (2 H, s, NH), and 9.44 (2 H, s, NH). Chain end: 1.27 (0.0641 H, s, NH_2), M_n = 25975 g/mol.

Thiophosgene-MDA: To a completely dried four neck flask equipped with dropping funnel, distillation and a safety trap, 3.96g 4,4'-diphenylmethanediamine and 2.26g 1,4-diazabicyclo [2.2.2]octane (DABCO) were well mixed then cooled with ice bath. 2.30g thiophosgene was carefully and slowly added to the mixture through dropping funnel at 0^{o}C. The reaction was then carried out at room temperature for 24h. Deionized water and methanol was used for precipitation and washing, followed by drying 50^{o}C *in vacuo*. Light yellow fibre like polymer was obtained after purification in 85% yield (4.10g). FTIR: ν_{max}/cm^{-1} 3210 (N-H st), 3020 (ar C-H st), 1510 (ar C-C), 1320 (C-N st), 1250 (C=S st). ^{1}H NMR δ_H(500 MHz; DMSO-d^6) 3.86 (2 H, s, CH_2), 7.18 (4 H, d, benzene), 7.35 (4 H, d, NH), and 9.67 (2 H, s, NH). Chain end: 6.93 (0.0931 H, m, two benzene), M_n=44615 g/mol.

5.7.2 Measurements and Instruments

Fourier Transform Infrared (FTIR) spectra were recorded with a Nicolet Magna 560 FTIR spectrometer (resolution 0.35 cm^{-1}). Solution ^{1}H NMR was performed on a Bruker DMX500 high resolution digital NMR spectrometer. Thermogravimetric analysis (TGA) was performed with TA instruments TGA Q500 (heating rate 10 ^{o}C·min^{-1} under nitrogen),

and differential scanning calorimetry (DSC) analysis was performed by TA instrument DSC Q-100 with the glass transition and melting point determined from the second heating cycle at 10 ^{o}C/min. The diffraction data was recorded on an Oxford Diffraction Xcalibur PX Ultra with a Cu-Kα (λ= 0.15418 nm).

Polythiourea films with thickness ~10μm were prepared by casting solution on borosilicate glass plates using Erichsen CoatMaster Film Applicator with fixed blade gaps for different polymers. Free standing films peeled off of the glass substrate were dried *in vacuo* to remove residue solvent and anneal (detailed description for each polythiourea in Supplementary Information)

Dielectric spectroscopies were obtained using an IMASS Time Domain Dielectric Spectrometer. Measurements were made in an air circulating oven at constant temperature by taking frequency scans, with 10 volts AC applied. Polarization measurements were conducted with a modified Sawyer-Tower circuit, employing a Trek Model 10/40 10kV high voltage amplifier and an OPA541 operational amplifier based current to voltage converter. The samples were sputtered with Au/Pd 80/20 wt% electrodes of 0.07 cm^2. The UV-Vis spectrum for band gap determination was obtained using Varian Cary UV-VIS 5000. The UV-vis spectra were recorded from 200-800 nm and the onset wavelength of absorption, λ_{onset}, was used to determine the band gap (E_g) from Planck's equation: $E_g = hc/\lambda_{onset}$. The refractive index was evaluated using variable angle spectroscopic ellipsometry (VASE, J.A.Woollam Co., M-2000). General scans were performed over the wavelength range from 350 to 1497 nm, values at 546 nm listed in Table 5.3. The ellipsometric angles were modelled using a recursive model consisting of the silicon substrate and a Cauchy layer to describe the refractive index of films.

Breakdown strength measurements were performed using a linear voltage ramp generated by a resistor capacitor (RC) circuit. When the first breakdown event occurs, the power supply is shut off through an interlock input by a silicon controlled rectifier (SCR) circuit, which uses the breakdown-induced ground-rise voltage capacitively coupled to the gate of an SCR. The breakdown voltage of the sample is read from a peak-holding voltmeter. The sample thickness was determined using a thickness gauge (Model LE1000-2, MeasureItAll) as the average of several measurements near the breakdown site.

5.7.3 Thin Film Processing

PDTC-ODA: A 10wt% DMSO solution was used for casting large scale film on a borosilicate glass substrate by Dr. Blade Film Applicator. The blade gap was 254μm. Films were casted at 80 ^{o}C followed by drying on the hot plate at 100 ^{o}C for 6h. After peeling off the glass, films were dried under vacuum at 120 ^{o}C overnight. The film thickness is 13-14μm.

PDTC-MDA: A 10wt% DMAc solution was used for casting large scale film on a borosilicate glass substrate by Dr. Blade Film Applicator. The blade gap was 254μm. Films were casted at 60 ^{o}C followed by drying on the hot plate at 80 ^{o}C for 6h. After peeling off the glass, films were dried under vacuum at 100 ^{o}C overnight. The film thickness is 13-14μm.

PDTC-HDA: A 10wt% DMAc solution was used for casting large scale film on a borosilicate glass substrate by Dr. Blade Film Applicator. The blade gap was 500μm. Films were casted at 60 ^{o}C followed by drying on the hot plate at 80 ^{o}C for 6h. After peeling off the glass, films were dried under vacuum at 100 ^{o}C overnight. The film thickness is 9-10μm.

PDTC-HK511: A 15wt% DMAc solution was used for casting large scale film on a borosilicate glass substrate by Dr. Blade Film Applicator. The blade gap was 500μm. Films were casted at 70 ^{o}C followed by drying on the hot plate at 75 ^{o}C for 6h. After peeling off the glass, films were dried under vacuum at 100 ^{o}C overnight. The film thickness is 12-14μm.

Thiophosgene-MDA: A 15wt% DMSO solution was used for casting large scale film on a borosilicate glass substrate by Dr. Blade Film Applicator. The blade gap was 254μm. Films were casted at 80 ^{o}C followed by drying on the hot plate at 100 ^{o}C for 6h. After peeling off the glass, films were dried under vacuum at 100 ^{o}C overnight. The film thickness is 11-13μm.

References

1. H. S. Nalwa, *Ferroelectric Polymers: Chemistry: Physics, and Applications (Plastics Engineering)* Marcel Dekker, New York 1995, Part 1: 8.
2. H. S. Nalwa, *Handbook of Low and High Dielectric Constant Materials and Their Applications. Volume 1: Materials and Processing. Volume 2: Phenomena, Properties and Applications*, Academic Press, New York 1999.
3. P. Vasudevan, H. S. Nalwa, K.L. Taneje and U. S. Tewari, *J. Appl. Phys.* 1979, **50**, 4324.
4. K. Ohishi, S. Tasaka, N. Inagaki, *Polymer Prep. Jpn.* 1993, **42**, 1430.
5. S. Wu, Dr. W. Li, Dr. M. Lin, Q. Burlingame and Q. M. Zhang, *Adv. Mater.* 2013, **25**, 1734.
6. Q. Burlingame, S. Wu, M. Lin, Q. M. Zhang Advanced Energy Materials, 2013, **3**, 1051-1055.

7. V. Sharma, C. Wang, R. G. Lorenzini, R. Ma, Q. Zhu, D. W. Sinkovits, G. Pilania, A. R. Oganov, S. Kumar, G. A. Sotzing, S. A. Boggs and R. Ramprasad, *Nat. Commun.*, 2014, **5**, 4845.
8. C. C. Wang, G. Pilania, S.A. Boggs, S. Kumar, C. Breneman, R. Ramprasad, *Polymer* 2014, **55**, 979.
9. A. R. Oganov, *Modern Methods of Crystal Structure Prediction* Wiley-VCH, 2011.
10. A. R. Oganov and C. W. Glass, *J. Chem. Phys.*, 2006, **124**, 244704.
11. Q. Zhu, V. Sharma, A. R. Oganov, and R. Ramprasad *J. Chem. Phys.*, 2014, **141**, 154102.
12. Y. Sun, C. Bealing, S. A. Boggs and R. Ramprasad, *IEEE Electrical Insulation Magazin*e 2013, **29**, 8.
13. L. A. Dissado and J. C. Fothergill, *Electrical Degradation and Breakdown in Polymers*, Peter Peregrinus Ltd.: London, 1992; Part 3.
14. Y. Sun, S.A. Boggs, and R. Ramprasad, The Effect of Dipole Scattering on Intrinsic Breakdown Strength of Polymers, Accepted by IEEE Trans. DEI., June 2014.
15. T. Nakamura, H. Fujii, N. Juni and N. Tsutsumi, *Opt. Rev*., 2006, **13**, 104.
16. D. W. Mosley, K. Auld, D. Conner, J. Gregory, X. Q. Liu, A. Pedicini, D. Thorsen, M. Wills, G. Khanarian and E. S. Simon, *Proc. SPIE*, 2008, **6910**, 691017.
17. K. C. Krogman, T. Druffel and M. K. Sunkara, *Nanotechnology,* 2005, **16**, S338.
18. R. D. Allen, G. M. Wallraff, D. C. Hofer and R. R. Kunz, *IBM Res. Develop.,* 1997, **41**, 95.
19. J. L. Regolini, D. Benoit and P. Morin, *Microelectron. Reliab.,* 2007, **47**, 739.
20. J. Liub, and M. Ueda, *J. Mater. Chem.*, 2009, **19**, 8907.
21. J. G. Speight, Lange's Handbook of Chemistry (16th Edition), McGraw-Hill, 2005.

Chapter 6

Exploration of Chemical Space and Organotin Polyesters as Dielectric Material

6.1 Exploration of chemical space---Group 14 elements

With the primary objective to discover, design and develop new polymers appropriate for dielectric application, an efficient and rational strategy is necessary to explore a wide chemical space with a reasonable starting point. The unique tool which was made available to this study is to utilize the computational strategy to guide the material design, which was largely taking place through experimental efforts solely. Our colleague, R. Ramprasad and coworkers considered modifications of polyethylene with the intent to improve dielectric properties by replacing CH_2 with Group 14 halides in a systematic manner, as shown in Figure 6.1.[1-3] The chemical trends in Group 14 elements are

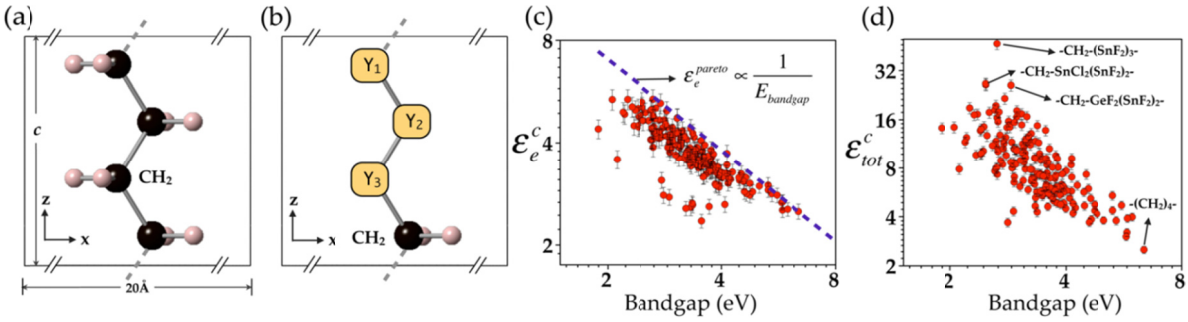

Figure 6.1 (a) Atomistic model of a polyethylene chain containing four independent CH_2 units. (b) Schematic representation of the general model for DFT computations by filling up Y1, Y2, Y3 any of the seven CH_2, SiF_2, $SiCl_2$, GeF_2, $GeCl_2$, SnF_2, and $SnCl_2$ units. The DFT computed (c) electronic and (d) total (dielectric constants as a function of the computed DFT bandgap for the 175 systems. [Reprinted with permission from (J. Chem. Inf. Model., 2013, 53 (4), 879). Copyright (2013) American Chemical Society]

interesting because of their unique placement, right between the metals on the left and nonmetals on the right. By moving from carbon to Tin, we are crossing the line of nonmetal and metal. Another motivation of substituting carbon with other Group 14 elements is to place more polarizable chemical bond and at the same time preserve the local chemical environment to ensure the chemical compatibility. In addition, atoms like F and Cl can provide large dipole moment that will contribute to the orientational polarization. The computations were performed using Density Functional Theory and the results suggest that incorporation of contiguous SnF_2 or GeF_2 is expected to give excellent dielectric constants. A further study on Group 14 halides crystals also revealed the advantages of introducing such structural units into existing structures to tune dielectric constants and band gap.[2] Figure 6.2 showed that not only the electronic dielectric constant increases from C to Pb, the total dielectric constant goes very high in cases with large ionic components.

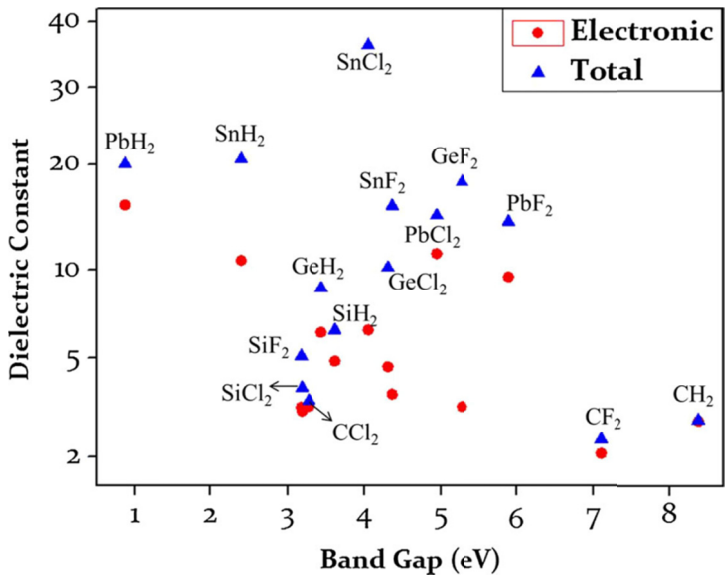

Figure 6.2 Dielectric constant versus band gap for the Group 14 halide systems

A clear inverse relationship between the electronic part of dielectric constant and band gap was observed, just as for the organic building systems (Chapter 3 and 4) as well as oxide systems. They also found that the electronic part of the dielectric constant is strongly correlated with the sum of polarizabilities of all the atoms in the system and is inversely proportional to the van der Waals volume. This means that a compact system with large atomic polarizability will lead to higher electronic dielectric constant. For ionic dielectric constant, it depends on the presence of large dipole moments as well as the ability of those dipoles to reorient easily along the applied electric field. Among all the systems, they found that Sn-F has the largest dipole moment and the Sn-Sn bond is the softest. This explains the promising system identified in Figure 6.1 (d). In order to provide guidance to synthesis effort to achieve large dielectric constant and band gap simultaneously, our colleagues also investigated the preferred composition range for three unique systems, as shown in Figure 6.3. In general, as we go from Si to Ge to Sn, the total dielectric constant increases, and the band gap decreases. The highlighted composition range was defined as total dielectric constant > 5 and band gap > 3, which broadens and shifts to the left from C to Sn. So it is apparent from this analysis that in

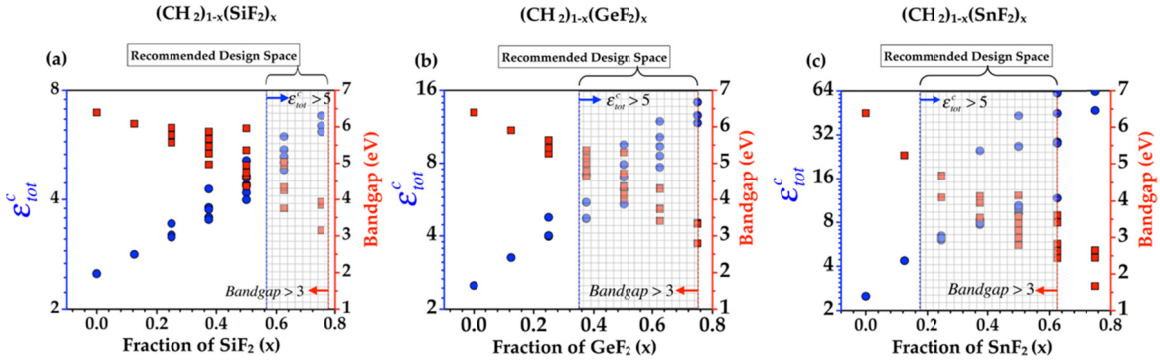

Figure 6.3 Variation between the total dielectric constant and the bandgap as a function of composition x for three classes of systems as predicted by the property expansion approach. [Reprinted with permission from (J. Chem. Inf. Model., 2013, 53 (4), 879). Copyright (2013) American Chemical Society]

order to achieve the desired space, one would need to incorporate ~ 17 mol% of SnF_2 units in polyethylene structure, or 33 mol% GeF_2, 55 mol% SiF_2.

Since the desired hybrid system is tin incorporated, most of the efforts in our synthesis side of study focused on exploring incorporation of tin covalently into the polymer chain. Dr. Aaron F. Baldwin has investigated several synthetic routes to "dope" polyethylene with SnF_2.[4] The first proposed method was to produce a linear polymer by ADMET from a dibutyl attached diene. The difficulty of this method was to substitute butyl group with fluoride, in which process the reagent will degrade the polymer main chain. Other methods were explored afterwards with the similar problems of achieving high molecular weight, which is essential for thin film casting. Therefore, other types of tin polymers were investigated instead of "doped" polyethylene.

Zilkha et. al. reported the synthesis of organotin polyesters through an interfacial polymerization technique between a dialkyldichlorotin and diacid in the mid-1960s. Carraher continued work on this polymerization technique but also expanded it to other types of difunctional monomers such as diols, diamines, etherdiamines, etc. to form organotin ether, amine and etheramine polymers, respectively.[5-7] After screening from some polymers in this three types, organotin polyesters were proved to have sufficiently solubility and high enough molecular weight for film casting and dielectric testing. The detailed synthesis and characterizations can be found in our earlier work,[4] in which the organotin polyesters were synthesized through the interfacial polymerization between a diacid and dimethyltin dichloride within a basic atmosphere (Scheme 6.1).[8-10] In this study, we investigated the amount of tin loading withing the polymer backbone by

varying the length of the aliphatic diacid segment. We also studied the conjugation structure and chirality effect on the dielectric properties, as shown in Scheme 6.1.

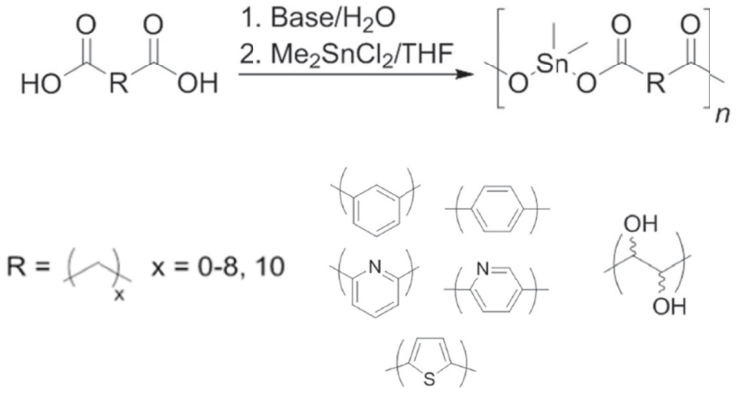

Scheme 6.1 Synthetic route for organotin polyesters

This study provides a novel point of view in increasing the permittivity by incorporation of metal atoms covalently into the polymer backbone. As discussed in Section 1.2, the addition of high-dielectric-constant nanoparticles increases dielectric constant, however facing the issues of a large volume threshold of nanoparticles and agglomeration and poor interface between polymer matrix and nanoparticles at such mixing ratio.

6.2 Structural effect on dielectric properties of organotin polyesters as dielectric material, experimental and simulation

The first system that was thoroughly studied has an aliphatic segment where n is equal to three in Scheme 6.1, named pDMTGlu. The synthesized polymer was proved to have high molecular weight by NMR and good thermal stability.[8] The detailed atomic level structure exploration was conducted using the DFT as implemented in the Vienna ab initio simulation package.[11-13] DFT calculations are essentially based on first principles, making them versatile, but computationally expensive. Even though polymers,

in general, display complex morphologies, they are usually modelled as ideal crystals or infinite single chains at the DFT level.[14-17] Such a simplified approach seems to be powerful in capturing several of the properties of our interest, e.g., energy band gap and dielectric constant.[11,16,18-20] In this work, we modeled our polymer system as ideal, three-dimensional crystalline materials. Even that, the process can be challenging. Our colleagues predicted the possible stable structures using the minima-hopping method.[21-23] To start the prediction process, the initial structure was manually assembled by placing two methyl (CH_3) groups and two carboxyl (C(=O)O) groups with a tin atom. A chain of CH_2 groups was then added to link the obtained dimethyltin dicarboxylate groups. From this starting point, different low-energy structures can readily be predicted with the minima-hopping method. And the same method was applied to the polymers systems with n equals to 0- to 8 and 10.

It has been reported that the coordination number of tin within organic ligands can be four, five, six or seven.[24] And in our case, the tin atom are coordinated by six atoms, including two carbon atoms from two methyl groups and four oxygen atoms from the

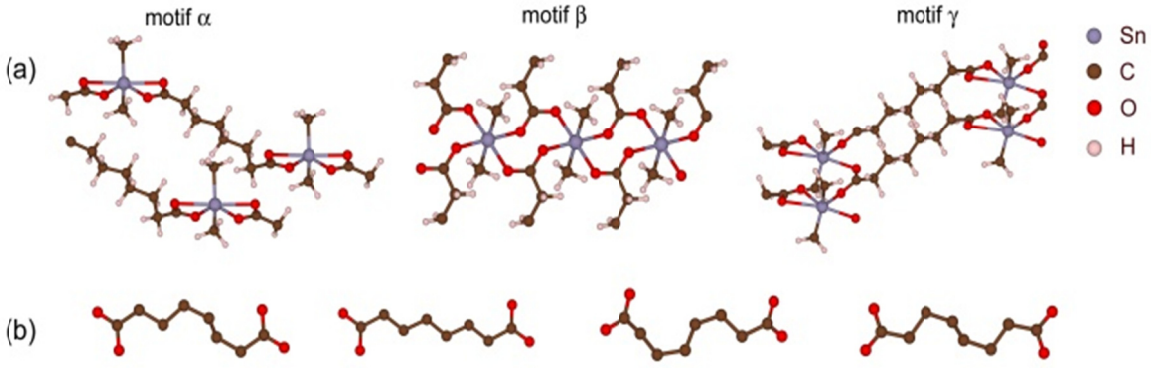

Figure 6.4 (a) Lowest-energy structures of α (intra-chain), β (inter-chain) and γ (hybrid) motifs predicted for p(DMTSub) and (b) four (out of numerous) folding geometries of the chains of methylene groups acting as organic linkers in p(DMTSub). In the figure, tin atoms (gray spheres) are six-fold coordinated by four oxygen atoms (red spheres) from ester groups and two carbon atoms (dark-brown) from two methyl groups. Hydrogen atoms are shown as pink spheres.

surrounding carboxyl groups. It is worth noticing that based on how the tin atoms are coordinating with the oxygen, there are three structural motifs, namely here α, β and γ (Figure 6.4a). In motif α, the two carboxyl groups from the same repeat unit are bonded to the central tin atom by four Sn-O bonds, so it's called intra-chain coordination. In the motif β, which is the inter-chain instead, four Sn-O bonds link the central tin atom with four different carboxyl groups, two of them belonging to the same chain (repeat unit) while the other two bonds come from other chains. A new motif, called γ, was also predicted, combining the essential characteristics of motifs α and β.

For each member of the polymer family examined, many low-energy structures of the same motif were predicted, differing only by the folding geometry of the methylene chains (Figure 6.4b). The energetic information for the most stable structures of each motif indicates these motifs are slightly different by a few meV per atom. For each motif, the number of folding geometries of the methylene chains increases dramatically with the n, generating an "energy spectrum" and these spectra heavily overlap, it is suggested that all of these motifs may easily coexist in the experimental samples under ambient conditions. Among all the predicted structures, motif β was found to be most stable.

Experimentally, based on different coordination mode and structural motifs obtained from the calculation, we should expect different bindings of oxygen to tin existing in polymer systems simultaneously due to pretty close energy difference. However, as the length of CH_2 unit increases, the binding mode should prefer one over the other. FTIR was used to determine the binding mode. The IR stretching frequency of carboxylate groups are very important for determining their structures, in this case when there are interactions between the carbonyl oxygen atoms of the carboxylate groups and the tin

atom. The carboxylates generally have two strongly coupled C=O bonds with band strengths intermediate between C=O and C-O. These give a strong asymmetric stretching band near 1545-1598 cm^{-1} and a weaker symmetrical stretching band near 1400 cm^{-1}. The $\Delta\upsilon$ values [$\Delta\upsilon = \upsilon_{as}(COO)-\nu_s(COO)$] were used to predict the mode of tin carboxylate interaction. The differences $\Delta\upsilon$ between $\upsilon_{as}(COO)$ and ν_s (COO) are more than 200 cm^{-1}, indicating the covalent nature of the metal-oxygen bond, and unidentate coordination of the carboxylic groups bonding to the metal must therefore be assumed. The bridging carboxylate in organotin compound is observed when $\Delta\upsilon$ is less than 200 cm^{-1}.[25-29] For the case of intra-chain binding motif, the difference will be much smaller. For the aliphatic systems, we listed the asymmetric and symmetric stretching of carboxylate group in Table 6.1. Except for the one polymer originated from oxalic acid, all other polymers showed bidentate coordination for the carboxylate to tin. And most of them

Table 6.1 IR determined binding mode for organotin polyesters

	$\nu_{as}COO^-$ (cm^{-1})	$\nu_s COO^-$ (cm^{-1})	$\Delta\nu$ (cm^{-1})	Type
Oxalic (0 CH_2)	1620	1350	270	Unidentate
Malonic (1 CH_2)	1590	1400	190	Bidentate---Inter-chain
		1380	210	Unidentate
Succinic (2 CH_2)	1560	1420	140	Bidentate
		1410	150	Bidentate
		1380	180	Bidentate---Inter-chain
Glutaric (3 CH_2)	1560	1450	110	Bidentate---Intra-chain
		1410	150	Bidentate
		1380	180	Bidentate---Inter-chain
Adipic (4 CH_2)	1570	1460	110	Bidentate---Intra-chain
		1420	150	Bidentate
		1380	190	Bidentate---Inter-chain
Pimelic (5 CH_2)	1570	1420	150	Bidentate
		1380	190	Bidentate---Inter-chain
Suberic (6 CH_2)	1560	1420	140	Bidentate
		1380	180	Bidentate---Inter-chain
Azelaic (7 CH_2)	1560	1420	140	Bidentate
		1380	180	Bidentate---Inter-chain
Sebacate (8 CH_2)	1560	1430	130	Bidentate
		1380	180	Bidentate---Inter-chain
Sebacic (10 CH_2)	1560	1420	140	Bidentate
		1380	180	Bidentate---Inter-chain

have both inter-chain and intra-chain motifs. Starting from Malonic acid system, the tin-oxygen exists in either unibendate or bidentate mode. As the chain length increases by the number of CH_2, bidentate coordination dominates. Since the carboxylate oxygen can bind with the tin on the other chain that is already in either inter-chain mode or intra chain mode, the IRs are showing multiple peaks around 1400 cm^{-1}, and they correspond to the hybrid binding mode. As the chain length increases, inter-chain motif becomes more favorable, with the $\Delta\upsilon$ value around 110 cm^{-1} disappears.

X-ray diffraction (XRD) was performed on the polymer powders to verify the structure of these polymers, which were proved to be a complex crystal nature and combinations of different motifs, as shown in Figure 6.5. Due to the complicated combination of various binding modes, the actual X-ray diffraction pattern moved to lower angle, meaning a larger unit cell. It is clear that the pattern is a combination of different crystal structures.

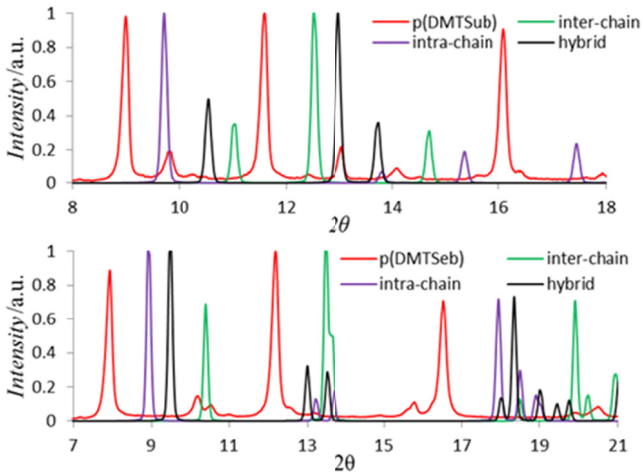

Figure 6.5 Experimental XRD of poly(dimethyltin suberate) and poly(dimethyl sebacate) with predicted diffraction patterns of the intra-chain (α), inter-chain (β) and hybrid (γ) motifs

Dielectric properties were evaluated in terms of dielectric constant (ε, electronic, ionic and total value) and band gap. Theoretically, dielectric constant of the most stable

structures of the motifs predicted for p[DMT(CH_2)$_n$] is shown in Figure 6.6 to be heavily motif dependent. Overall, the general trend is that ε decreases as n becomes large. The total dielectric constant of the interchain motif is higher than that of intrachain motif. As n increases, the dielectric constant follows the even-odd trend as observed for physical properties of alkanes. The dependence of ε on n mostly originates from ε_{ion} because $\varepsilon_{el} \approx$ 2.7-3.0 for all of the examined values of n. The difference in the theoretical and experimental values can be attributed to the DFT calculations being performed on systems on fully crystalline materials at 0 K. What is more intriguing is that as the number of methylene units is increased from 0 to 3 there is a decrease in the dielectric constant and then there is a spike in the dielectric constant to a second maxima at six methylene groups. For the inter-chain motif, the maxima shows up at five methylene groups. The experimental results correlate better with the hybrid motif, which was also proved by IR and XRD results. Dielectric loss for most of the systems stay below 1% (average value), and in general, as n increases, the dielectric loss decreases. It is a standard fact that E_g is usually underestimated by conventional DFT calculations with the PBE XC functional.[30] Using the HSE06 hybrid functional for the XC energies is much more computationally expensive but is also commonly known to be a better option for estimating E_g. With this functional, our calculated band gap is clearly improved. In this work, we will not rule out PBE results in our discussion because both approaches include many approximations that are hard to control. The experimental band gap, which was obtained by the UV-Vis spectra of polymer films, also showed a maximum at six methylene groups. However, the predicted value does not see the same trend. As n increases, the predicted band gap increases until it reaches a plateau. Unlike the

dielectric constant value, band gap of the intra-chain motif was found to be higher than that of inter-chain motif, with the hybrid mode lies in between.

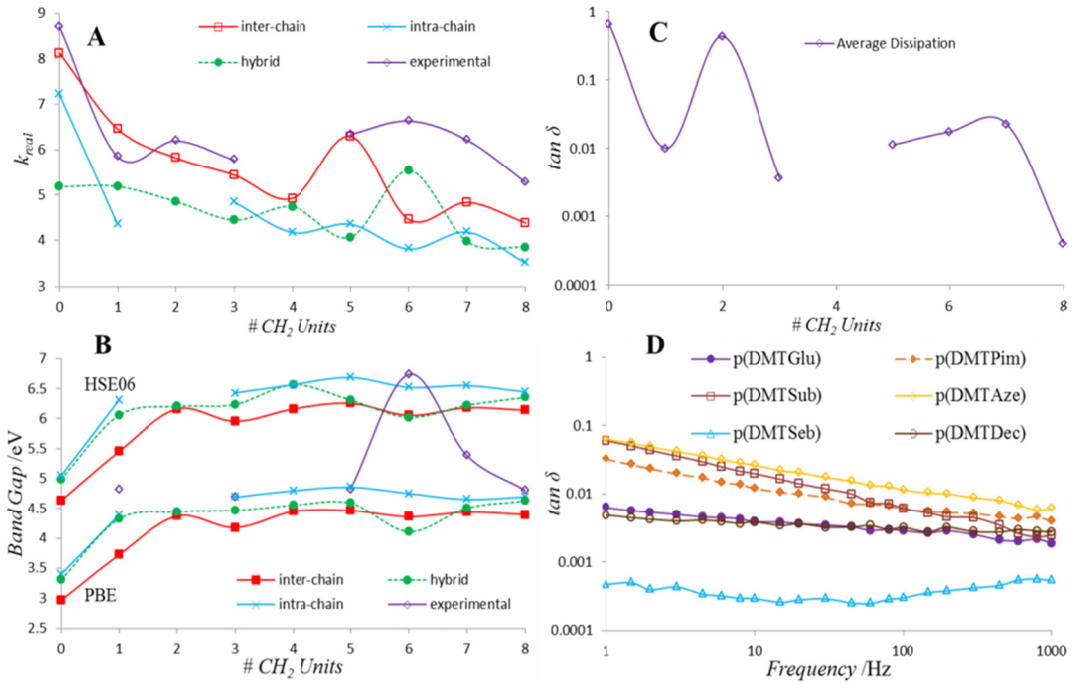

Figure 6.6 Theoretical and experimental values of dielectric constant (A) and band gap (B) of poly(dimethyltin esters). Averaged (1-1000 Hz) experimental dissipation factor (C) for poly(dimethyltin esters) and experimental dissipation factor of poly(dimethyltin esters) with #CH_2 units = 3,5-8,10 (D).

6.3 3D structure prediction and proposed enforced coordination

As discussed above, we found the dielectric properties are highly motif dependent. Especially for ε_{ion}. A typical example for this strong dependence is the case of p(DMTPim), where ε_{ion} is calculated to be 1.74 and 3.44 for intra- and inter-chain motif, respectively. To clarify this large difference, our colleague determined the vibration mode that most significantly contributes to ε_{ion} of each motif (Figure 6.7). For α, all four highly polarized Sn-O bonds are in bending vibrations while for β, two of these bonds are clearly in their stretching modes. It is worth noting that because of the two-dimensional

nature of motif β, the orientations of the four Sn-O bonds are "more isotropic" than motif α, thus stretching vibrations are more likely to occur. Because these stretching vibrations generally lead to larger changes in the Sn-O bond length, one can expect that motif β is more polarizable with a higher ε_{ion}.

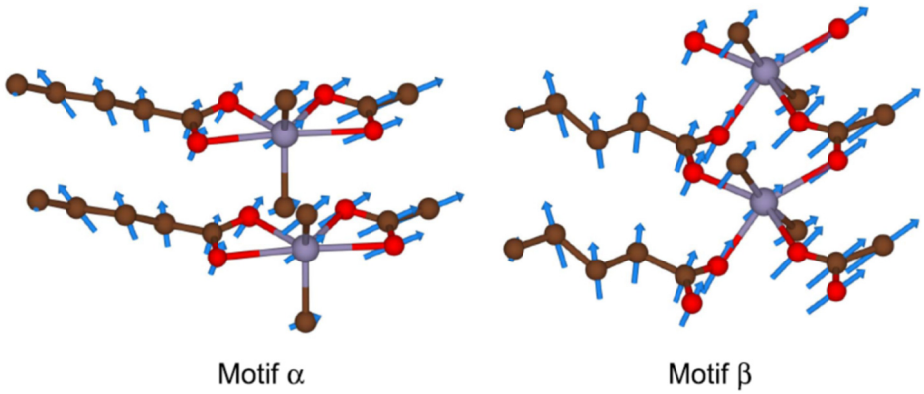

Figure 6.7 The vibration mode that has the most significant contribution to ε_{ion} of the most stable structures of motifs α and β of p(DMTPim). Atom types are indicated in color the same was as above. Between motif α and β, arrows describing the amplitude and direction of atomic displacements, are scaled using the same unit.

Since both computational and experimental results support the fact that a inter-chain binding mode will be favorable in improving dielectric properties, we need to understand how to force such coordination to occur in molecular design. As we know, tin dioxide (SnO_2) has a high dielectric constant of 9.86 as well as a relatively wide band gap of 3.57 eV compared to other semiconductor material. Therefore, it is important to understand the difference between our polymer systems and SnO_2. Our collegues studied the coordination structures of our three basic motifs and noticed that the inter-chain motif is the most similar to the structure of SnO_2, which explains the higher dielectric constant of inter-chain motif systems. However, there still is a difference of the O-Sn-O bond angle between inter-chain motif and SnO_2. Therefore, a structure that can widen the O-Sn-O should be proposed. Another suggestion from this analysis was to increase the number of

oxygen surrounding tin. A similarity with SnO_2 was achieved by one structure (Figure 6.8), with a predicted band gap of ~3.5 and dielectric constant ~8. An six membered ring was added into the polymer main chain to force the coordination. This proposed structure provided a new way for tuning dielectric properties by forced coordination.

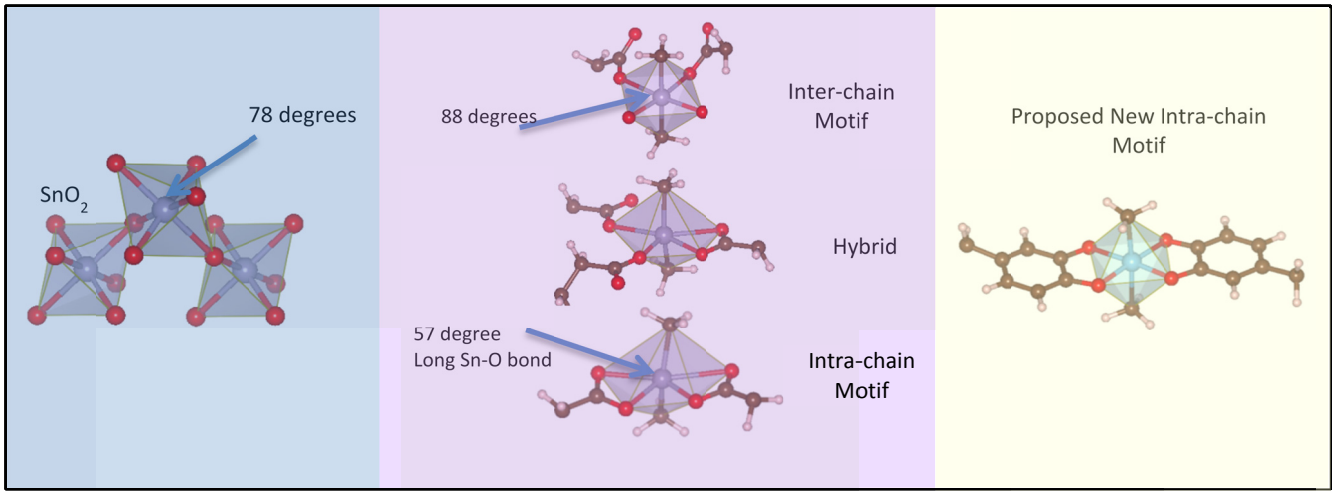

Figure 6.8 O-Sn-O binding mode and bond angle for three basic motifs, comparison with SnO_2, proposed new structure

6.4 Control of crystallinity through processing approach

The shortcoming of the aliphatic poly(dimethyltin esters) is that they form large crystals upon drying, and produce polymer films with obvious defects. We also found that the size of the crystal is dependent upon the length of the methylene linker. The idea to break the large crystal was first landed on using monomers with side chains. A organotin polyester, poly(dimethyltin 3,3-dimethylglutarate) (p(DMTDMG), Scheme 6.2) was chosen, where upon the two pendant methyl groups attached to the diacid can give rise to sufficient chain disruption leading to very small crystal size and better adhesion to the stainless steel shim stock.

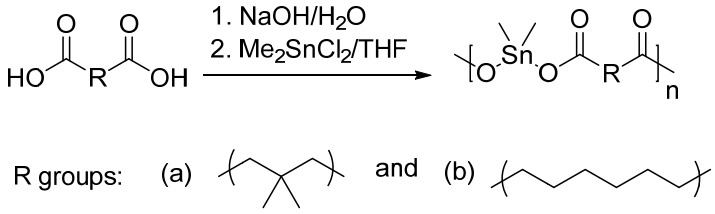

Scheme 6.2 Structure of p(DMTSub) and p(DMTDMG) tin ester homopolymers

The new tin polyester p(DMTDMG) was also studied structurally by XRD and FTIR. These results were compared to DFT calculated results (Figure 6.9). Tin polyesters were previously shown to have 3 different motifs of metal-oxygen bonds, intrachain, interchain, and hybrid structures, and those motifs are confirmed to be present in the new tin polyester as well. The FTIR showed a strong tendency for hybrid structure formation in p(DMTDMG. In addition, analysis of symmetrical and asymmetrical carboxylate stretching frequencies mimics previous results that show both the oxygen atoms in the

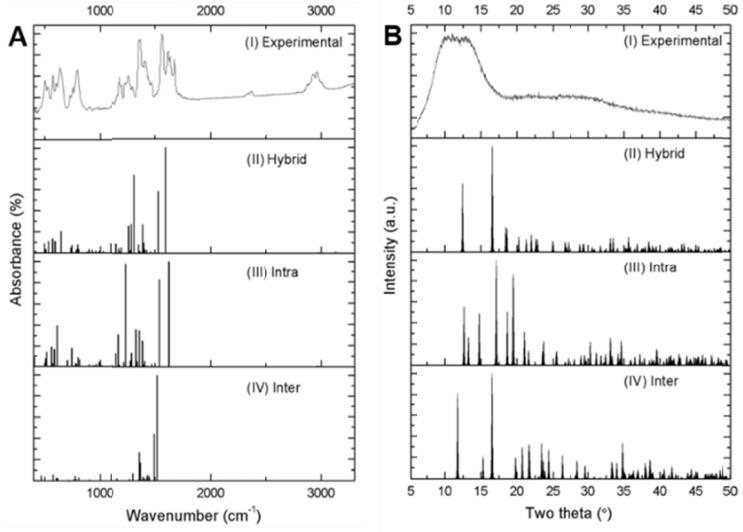

Figure 6.9 Comparison of p(DMTDMG) FTIR (A) and XRD (B). DFT results for the 3 different motifs are compared beneath the experimental results.

carboxylates are involved in bonding to the metal atoms. This is possible since the tin atom is able to exist in both the tetrahedral and octahedral configuration. The XRD

results confirm what can be seen while casting films. Films made from p(DMTDMG) are clear and amorphous while p(DMTSub) films are opaque and crystalline.

P(DMTDMG) was then used for blending with aliphatic organotin polyesters above to achieve good film formation. Poly(dimethyltin suberate), p(DMTSub), was chosen for further study as it has the highest reported dielectric constant of the aliphatic organotin polyesters studied here. The polymers were blended together by dissolving m-cresol at 10% increments from 100% p(DMTDMG) to 50/50 p(DMTDMG)/p(DMTSub). Films were than cast onto glass slides and stainless steel shim stocks for structural and electrical analysis.

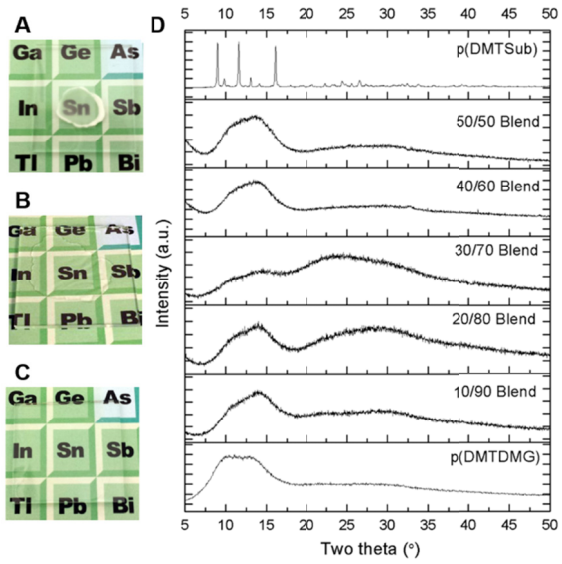

Figure 6.10 Organotin Polyester films cast on microscope slides: (A) p(DMTSub), (B) blend of 30% p(DMTSub) and 70% p(DMTDMG), (C) p(DMTDMG) and (D) film XRD of homopolymers and blends with p(DMTSub) : p(DMTDMG) ratio listed

Figure 6.10 showed the blend film pictures casted on glass slides compared to the two homopolymers. By blending p(DMTSub) with p(DMTDMG), we are able to control the crystal growth and crystal size and allowing for the formation of amorphous films. As

shown in Figure 6.10 (a, b, c), films casted out of the blended solution were clear and uniform.

Dielectric constants and loss were obtained from the frequency domain spectra. Figure 6.11 shows dielectric constant and dissipation factor tan δ as a function of frequency. Surprisingly, two of the blends ratio showed higher dielectric constant than the two homopolymers. The highest value shown for the blends at a standard frequency for 10kHz is 6.84 for the 10/90 blend of p(DMTSub)/p(DMTDMG) while a 20/80 blend was close behind at 6.61. When the ratio of p(DMTSub) in the blend was increased past 20% a decrease in dielectric constant was observed down to the 50/50 blend which was lower than both homopolymers. The dielectric data gives an unexpected result, that not only will blend produce dielectric constants between the parent homopolymers but that at low ratios of p(DMTSub) the blends actually exceed their performance.

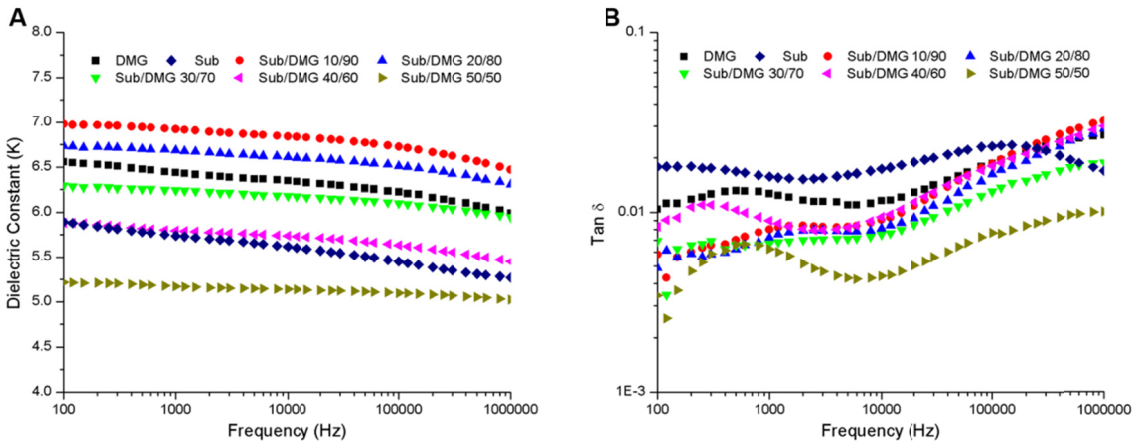

Figure 6.11 Dielectric Constant (A) and Tan δ (B) for p(DMTSub) and p(DMTDMG) homopolymers and blends at ambient conditions.

In order to confirm the blending effect on the morphology of the polymers, a parallel study to was conducted on copolymers. These copolymers were synthesized by varying the mole ratios of suberic acid and 3,3-dimethylglutaric acid in the same ratios as the

blends. Thus a blend consisting of 10% p(DMTSub) and 90% is equivalent to the copolymer p(DMT Sub-co-DMG 10/90). The reactions were carried out in the same manner as the homopolymers, by first dissolving the diacids and sodium hydroxide in the aqueous phase and adding dimethyltin dichloride in THF to the stirred solution. Stirring continued until a white polymer precipitate was formed which was then isolated and analyzed by NMR and IR. Films were then cast onto glass slides and stainless steel shim stocks for structural and electrical analysis.

The FTIR spectrums of the copolymers were very similar to that of previously studied homopolymers as they all showed a high degree of hybrid motif formation. The spectrum also shows that the carboxylates in the copolymers continue to favor bidentate attachment to the tin atom putting it in an octahedral configuration. Due to computational limitations DFT is unable to be done on the copolymer systems for FTIR and XRD comparison. Figure 6.12 shows the XRD patterns for both the polymer powders (A) and their respective films (B). Interestingly, it is clear in the XRD pattern that the copolymer

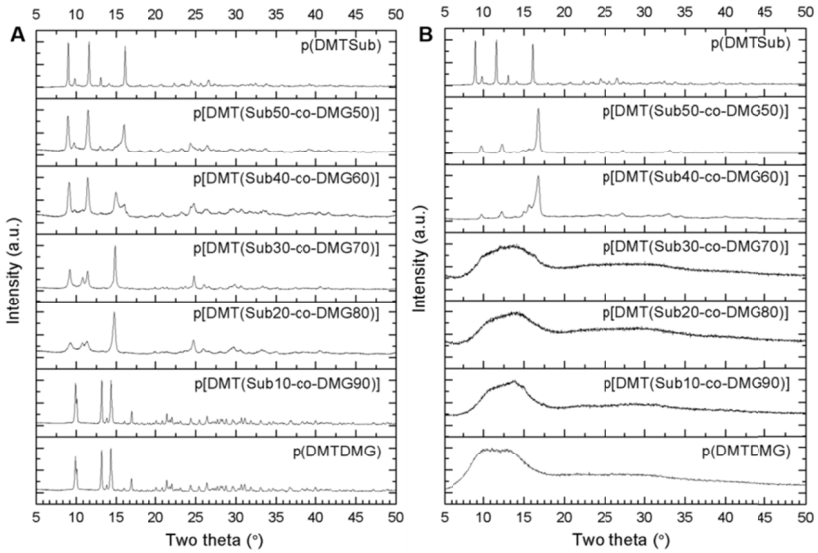

Figure 6.12 Copolymer XRD from powder (A) and films (B)

powder switched from the structure of p(DMTSub) to p(DMTDMG), with the structure of p[DMT(Sub10-co-DMG90)] stayed similar to that of p(DMTDMG) and p[DMT(Sub50-co-DMG50)] similar p(DMTSub). And then for p[DMT(Sub40-co-DMG60)] to p[DMT(Sub20-co-DMG80)], intermediate structures showed up. As for the copolymer films, they are visually clear and amorphous by XRD up to 30 percent suberate content. After that point the films produced are opaque and crystalline but they still retain good film forming capabilities.

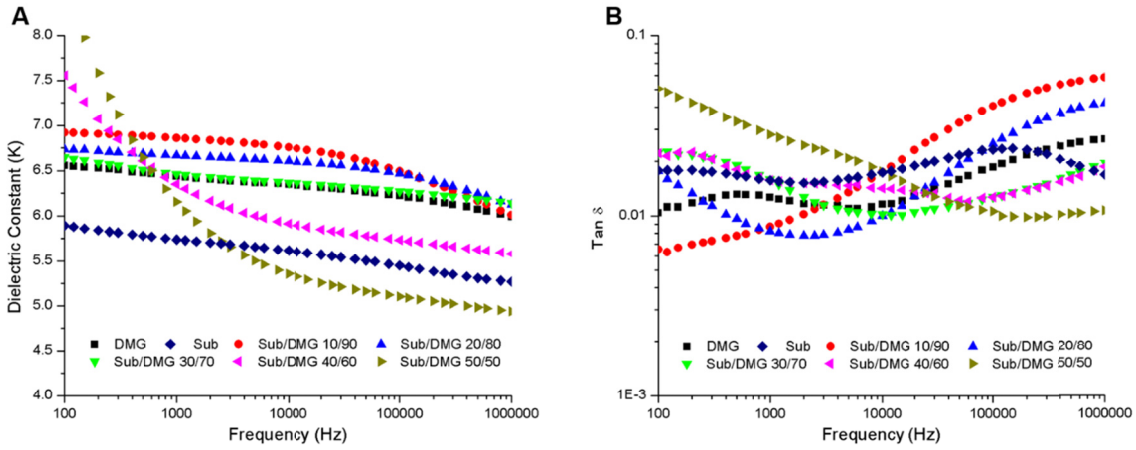

Figure 6.13 Dielectric Constant (A) and tan δ (B) for p(DMTSub) and p(DMTDMG) homopolymers and copolymers at room temperature

The band gaps of all the copolymers were found to be similar to the bandgap of p(DMTDMG) within experimental error. While p(DMTSub) has the highest bandgap of all tested tin polyester at 6.5 eV the value for the p(DMTDMG) and the copolymers was found to be between around 4.8. This matches the expectation that the bandgap of the copolymer would match with the lowest bandgap of two homopolymers especially considering that p(DMTDMG) is at least 50% of the copolymer composition. Dielectric spectroscopy measurements were carried out same to the blend study and had comparable results as shown in Figure 6.13. The copolymer p(DMT Sub10-co-DMG90) has the

highest K value of 6.75 at 10kHz with p(DMT Sub20-co-DMG80) close behind at 6.6. Also as with the tin blends, p(DMT Sub50-co-DMG50) had the lowest k value of 5.3 at 10kHz below that of pure p(DMTSub). These results corroborate the theory that mixing the linear and hindered diacids together affects the film morphology to give an increase in dielectric properties compared to the pure homopolymers. The reason was believed to be the change of the dipole mobility. In an amorphous system, the dipoles are more flexible to move along the applied electric field, which will give a higher permittivity.

Since now a uniform polymer film can be produced, we can then study the electrical behavior under higher voltage. The charge discharge of the 20/80 p(DMTSub)/p(DMTDMG) blend was determined through measurement of D-E hysteresis loops and is depicted in Figure 6.14. The maximum breakdown field achieved was ca. 300 kV mm^{-1}, which resulted in an energy density of ca. 4 J cm^{-3} and a corresponding efficiency of 90%. Based on the hysteresis loop, the loss at high field is due to conduction rather than remnant polarization. The blending provided a means to prepare improved quality of the films, which allow us to better understand the property of

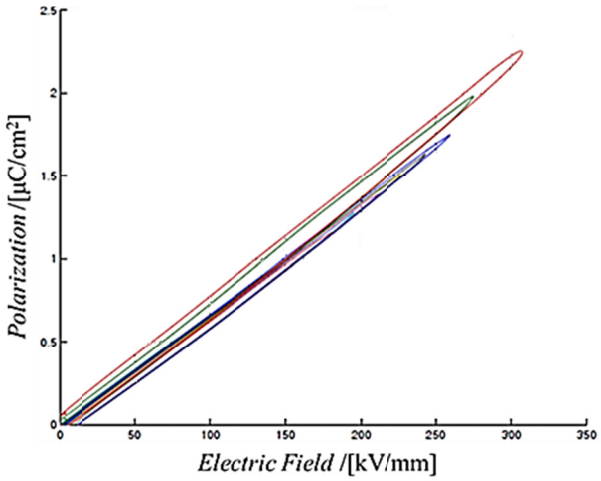

Figure 6.14 D-E loop of 20/80 p(DMTSub)/p(DMTDMG) blend

material itself. And the organotin polyesters can be classified within this voltage range as a linear dielectric. More study needs to be done to further improve the film quality as the breakdown field is obviously lower than those of organic polymers can achieve.

To further expand the dielectric space opened up by poly(dimethyltin esters), the effect on dielectric properties for aromatic and chiral groups was also investigated by using aromatic diacids, as shown in Scheme 6.1. Once again, the experimental and computational IR and XRD patterns match, confirming both the formation of the polymers and the three complexes that they form with tin. The aromatic polymers were insoluble in most common solvents and were pressed into pellets for dielectric testing. All tin polyesters exhibited high dielectric constant and low loss with high thermal stability past 250˚C. Three types of aromatic systems were tested: electron neutral benzene rings, electron withdrawing pyridine rings, and electron donating thiophene rings. The three polymers that are meta-positioned, namely poly(dimethyltin 2,6-dipicolinate) (p(DMT 2,6-DPA)), poly(dimethyltin isophthalate) (p(DMTIso)) and poly(dimethyltin 2,5-thiophenedicarboxylate) (p(DMT 2,5-TDC)), had the highest dielectric constants. Pyridine was higher than benzene which was higher than thiophene with dielectric constants of 5.64, 5.52, and 5.08 respectively. The para-positioned rings both had dielectric constants below 5 with poly(dimethyltin 2,5-dipicolinate) (p(DMT 2,5-DPA)) and poly(dimethyltin terephthalate) (p(DMTTer)) having $\varepsilon = 4.81$ and 4.71 respectively, following the same trend of pyridine being higher than benzene. The relatively higher losses on some of the aromatic polymers are due to residual absorbed water as evident by TGA analysis. These findings give experimental evidence that the

electron withdrawing aromatic rings are a positive structural unit for design of dielectric polymers.

Poly(dimethyltin esters) formed with tartaric acid were used to study the effects of crystallinity and chirality on dielectric constant for this new class of polymers. It was noted that the D and L forms of tartaric acid gave amorphous polymers due to the hydroxyl groups' steric interactions while a mixture of the two produced a more crystalline polymer. Also, copolymers with glutaric acid using a 50:50 feed ratio were synthesized to tailor the crystallinity and ultimately the dielectric constant. The homopolymer of p(DMT D-Tar) showed the highest dielectric constant at 6.18, while pellets of DL tartaric acid were unable to be tested. The copolymers showed that the D and L tartaric systems had higher dielectric constants of 5.31 and 5.55 compared to the DL-Tar copolymer with 4.97. For additional support, computations were also performed on all these different systems- Minima Hopping revealed the same kind of α, β, and γ-motifs for each system, and the DFT computed dielectric constants for the most stable structure in each case has been shown in Figure 15. Computationally, the polymer p(DMT 2,5-TDC) was seen to have the highest dielectric constant, followed by the pyridine and benzene based polymers. The experimental trends and the computational trends do not quite match up, which comes from the calculations being performed on purely crystalline systems and experimental measurements being at ambient temperatures.

6.5 Computational and theoretical methods

The computational workhorse used in this study is density functional theory (DFT) as implemented in the Vienna Ab Initio Simulation Package (VASP).[11-13] The total energies

EDFT of the examined structural models were calculated with the Perdew-Burke-Ernzerhof (PBE) exchange-correlation (XC) functional.[31] For tin, carbon, oxygen and hydrogen, the $4d^{10}$ $5s^2$ $5p^2$, $2s^2$ $2p^2$, $2s^2$ $2p^4$ and $1s^1$ states were treated as the valence states. Monkhorst-Pack k-point meshes with spacing of 0.1 $Å^{-1}$ are used for integrations over the Brillouin zones of the models.[32] A plane wave kinetic energy cutoff is chosen to be 500 eV while atomic and cell variables were simultaneously relaxed until the residual forces were smaller than 10^{-2} $eVÅ^{-1}$.

All diacids and m-cresol were procured from Acros Organics. Succinic acid was purchased as the disodium salt form and oxalic acid was the dihydrate form from Acros Organics. Sodium hydroxide (NaOH) and triethylamine (TEA) were purchased from Fisher Scientfic. All monomers were used as received. Tetrahydrofuran (HPLC grade) was purchased from J.T. Baker. 1,1,1,3,3,3-hexafluoroisopropanol (HFIP) was procured from Synquest Laboratories and chloroform was purchased from BrandNu. Deionized water was obtained using a Millipore purification system. Stainless steel shim stocks (diameter = 2 in., thickness = 0.01 in., and ASTM A666 stainless steel) were acquired from McMaster Carr. Quartz glass slides (3 in. × 1 in. × 1 mm) were procured from Ted Pella, Inc. In general, Scheme 1; a molar excess of the diacid was added to a round bottomed flask and dissolved in 20 mL of water. To the diacid solution was added 2.1 equiv, with respect to the diacid, of sodium hydroxide. To the rapidly stirred aqueous solution was added 20 mL of a dimethyltin dichloride solution in tetrahydrofuran. The precipitate is filtered and washed with 50 mL portions of tetrahydrofuran and water and dried *in vacuo* at 115 °C for 20 h to remove any residual solvent.

Reference

1. G. Pilania, C. C. Wang, K. Wu, N. Sukumar, C. Breneman, G. Sotzing, and R. Ramprasad, *J. Chem. Inf. Model.,* 2013, **53 (4)**, 879.
2. A. Mannodi-Kanakkithodi, C. C. Wang and R. Ramprasad, *J. Mater. Sci.* 2015, **50**, 801.
3. C. C. Wang and R. Ramprasad, *International Journal of High Speed Electronics and Systems* 2014, 23, 1420002.
4. Aaron F. Baldwin (2014). Synthesis of Next Generation Dielectric Materials through Rational Exploration of Chemical Space (University of Connecticut, Doctoral Dissertation)
5. C. E. Carraher Jr. and R. L. Dammeier, *J. Polym. Sci. Part A,* 1972, **10**, 413-417.
6. C. E. Carraher Jr., *Organotin Polymers in Macromolecules Containing Metal and Metal-like Elements*, Zeldin M., Eds.; Wiley-Interscience: Hoboken, New Jersey, 2005, 264-310.
7. A. F. Baldwin, R. Ma, A. Mannodi-Kanakkithodi., T. D. Huan, C. Wang, M. Tefferi, J. E. Marszalek, M. Cakmak, Y. Cao, R. Ramprasad, G. A. Sotzing, *Advanced Materials*, 2015, **27**, 346.
8. A. F. Baldwin, T. Huan, R. Ma, A. Mannodi-Kanakkithodi, M. Tefferi, N. Katz, Y. Cao, R. Ramprasad, G. A. Sotzing, *Macromolecules*, DOI: 10.1021/ma502424r.
9. A. F. Baldwin, R. Ma, T. Huan, Y. Cao, R. Ramprasad and G. A. Sotzing, *Macromolecular communication*, 2014, **35**, 2082–2088.
10. G. Kresse and J. Furthmüller, *Comput. Mater. Sci.*, 1996, **6**, 15-50.
11. G. Kresse, Ph. D. Thesis, Technische Universität Wien (Vienna), December, 1993.

12. G. Kresse and J. Furthmüller, *Phys. Rev. B*, 1996, **54**, 11169.

13. Q. Zhu, V. Sharma, A. R. Oganov and R. Ramprasad, *J. Chem. Phys.*, 2014, **141,** 154102/1.

14. C. R. Bealing and R. Ramprasad, *J. Chem. Phys*., 2013, **139**, 174904.

15. G. Pilania, C. C.Wang, K. Wu, N. Sukumar, C. Breneman, G. A. Sotzing and R. Ramprasad, *J. Chem. Inf. Model.*, 2013, **53**, 879.

16. G. Pilania, C. C.Wang, X. Jiang, S. Rajasekaran and R. Ramprasad, *Sci. Rep.*, 2013, **3**, 2810.

17. C. C. Wang, G. Pilania, S. A. Boggs, S. Kumar, C. Breneman and R. Ramprasad, *Polymer*, 2014, **55**, 979.

18. U. Gedde and A.Mattozzi, *Long Term Properties of Polyolefins*, Springer, Berlin 2004, vol. 169, pp. 29-74.

19. T. Furukawa, H. Sato, Y. Kita, K. Matsukawa, H. Yamaguchi, S. Ochiai, H. W. Siesler and Y. Ozaki, *Polym. J.*, 2006, **38**, 1127.

20. S. Goedecker, *J. Chem. Phys.*, 2004, **120**, 9911.

21. S. Goedecker, *Modern Methods of Crystal Structure Prediction, (Ed: A. R. Oganov)*, Wiley-VCH, Weinheim, Germany 2011, Ch. 7, pp. 147-180.

22. M. Amsler, S. Goedecker, *J. Chem. Phys.*, 2010, **133,** 224104.

23. C. E. Carraher, *Macromolecules Containing Metal and Metal-Like Elements: Group IVA Polymers,* Vol. 4 (Eds: A.S. Abd-El-Aziz, C. E. Carraher, C. U. Pittman, M. Zeldin), Wiley, Hoboken, NJ, USA 2005, Ch. 10.

24. L. Q. Xie, Z. Q. Yang, Z. X. Zhang and D. K. Zhang, *Appl. Organomet. Chem.* 1992, **6**, 193.

25. Q. Xie, Z. Yang, L. Jiang, *Main Group Met. Chem.* 1996, **19**, 509.

26. H. D. Yin, C. H. Wang, Y. Wang, C. L. Ma, J. X. Shao, J. H. Zhang, *Acta Chim. Sinica.* 2002, **60**, 143.

27. H. D. Yin, C. L. Ma, Y. Wang, H. X. Fang, J. X. Sao, *Acta Chim. Sinica.* 2002, **60**, 897.

28. M. Gielen, E. Joosen, T. Mancilla, K. Jurkschat, R. Willem, C. Roobol, J. Bernheim, G. Atassi, F. Huber, E. Hoffmann, H. Preut and B. Mahieu, *Main Group Met. Chem.* 1995, **18**, 27.

29. L. A. Dissado, J. C. Fothergill, *Electrical Degradation and Breakdown in Polymers*, IET, London 2006.

30. J. P. Perdew, K. Burke and M. Ernzerhof, *Phys. Rev. Lett.,* 1996, **77**, 3865.

31. H. J. Monkhorst and J. D. Pack, *Phys. Rev. B*, 1976, **13**, 5188.

Chapter 7

Exploration of Zinc and Cadmium Organometallic Polymers

7.1 Transition metal based organometallic polymers

The enhancement in dielectric constant of when incorporating tin within the polymer backbone is due to the increase in dipolar and ionic polarization as the result of the larger difference in electronegativity of tin-oxygen versus carbon-oxygen. Increasing dipolar orientation can be further exploited by replacing tin with other transition metals that are more electron-positive. A series of polymers were synthesized containing calcium, titanium, cadmium, zinc and tungsten through a modified interfacial technique. And here, we focused on the ones containing cadmium and zinc.

As discussed in Chapter 6, metal oxide nanocomposite has widely attracted attention as the additive for polymer electronic materials, and zinc oxide is one of them. ZnO is a wide-bandgap semiconductor of the II-VI semiconductor group. This semiconductor has several favorable properties, including good transparency, high electron mobility, wide bandgap, and strong room-temperature luminescence. Those properties are used in emerging applications for transparent electrodes in liquid crystal displays, in energy-saving or heat-protecting windows, and in electronics as thin-film transistors and light-emitting diodes. One example of this area is the nanocomposite for organic field-effect transistor (OFET), which has been reported in the fabrication of active-matrix displays and integrated circuits for logic and memory chips. It has been reported that the electrical properties of solution processed polymer/ZnO nanocomposited devices showed enhanced

p-type mobility up to three orders of magnitude higher than pure polymer.[1] One example of the polymer nanocomposite for dielectric application is the PVDF-ZnO composite thin films.[2] People found that by incorporating ZnO in the mass ratio of 1-6% into PVDF, the permittivity of the nanocomposites increases with increasing the ZnO content. The dielectric loss at higher frequency and higher temperature decreased. Similar effect was also observed in ZnO/Polyaryletherketone (PAEK) composite system.[3] Other studies reported ZnO/polymer composite such as polyethylene and polyurethane systems, in which the dielectric constant increases with increasing the mixing ratio, however the dielectric loss increases as well.[4,5] However, the effect of incorporating zinc, or other transition metals into the polymer system on dielectric properties is not well understood. As discussed in Chapter 6, by covalently adding metal element in the polymer backbone circumvents the disadvantages of poor mixing and interface. Therefore, we studied organozinc and cadmium polyesters in parallel with organotin polyesters here.

Coordination polymer networks have drawn extensive attention because they provided an approach to truly rationally design and control the molecular structure through changes in chemistry. And it is also referred as crystal engineering. Like the systems we are studying here, coordination polymers[6] are infinite systems build up with metal ions and organic ligands as main elementary units linked via coordination bonds and other weak chemical bonds. Incorporating metal ions in supramolecular networks allows us to control metal atom positions in the final material, and alters properties of the materials through different binding motifs. The process of building a coordination polymer is principally directed by the coordination bond. Coordination bonds are the donation of a lone electron pair of the ligand (Lewis base) to the metal cation (Lewis acid)

and electrostatic attractions between the positively charged metal ion and a negatively polarized or charged donor atom of the ligand. Coordination polymers are promising material with tunable functions for applications in gas storage, anion exchange (due to the porosity and zeolitic-like behavior), catalysis, conductivity, luminescence, chirality, magnetism, spin transition behaviour, nonlinear optics (NLO) or deposition of thin films. For example, Yaghi and co-workers report also other coordination polymers based on bis- and tris-bidentate carboxylate linkers copolymerized with Zn (II). In these compounds, the rigid metal carboxylate structure allows the stability of the porous materials, which affords efficient and robust materials for gas storage or liquid separation.[7-9] Evans and Lin outlined strategies to build noncentrosymmetric metal-organic frameworks for the application in NLO.[10] They used *p*- or *m*-pyridinecarboxylate linear, rigid and non-symmetric organic ligands as linkers between Zn^{2+} and Cd^{2+}. The building blocks lead to the construction of three dimensional diamondoid networks or two-dimensional frameworks. Even with weak electron donor/acceptor combinations, it is possible to obtain efficiently NLO properties, as the well-chosen complexation can allow a good alignment and cooperation between the molecules.

Different from constructing coordination polymers, we chose to build the polymer in a conventional way to ensure the molecular weight as well as the high thermal durability. The coordination of carboxylate group to the metal atom works as a secondary effect to form the three dimensional network. Compared to the organotin polyester in chapter 6, the interesting about transition metal is that they have the ability to ligate water, forming layers of tightly bound and free water held close by van der Waals forces. People have studied the change of geometry by altering the bonded small molecules.[11] A series of [Zn

(bdc)] coordination polymers was reported with solid state transformation by removal or replacement of strongly hydrogen-bonded molecules, including DMF, methanol, ethanol or water. This drives the change of geometry of the metal complex. In our study, the water content can be studied by TGA, and its effect on dielectric properties will be reflected by the dielectric spectrum at different temperature.

7.2 Synthesis of Zinc and Cadmium Organometallic Polymers

Similar to what we have for organotin polyesters, we studied cadmium and zinc polymers with different length of aliphatic organic chain segments, as shown in Scheme 7.1 below. The synthesis is similar as that for organotin polyesters, in which two compounds were mixed together followed by the precipitation of white powder which is the polymer formed. The compounds were then filtered out of the reaction system, followed by washing with water and THF, and then dried under vacuum.

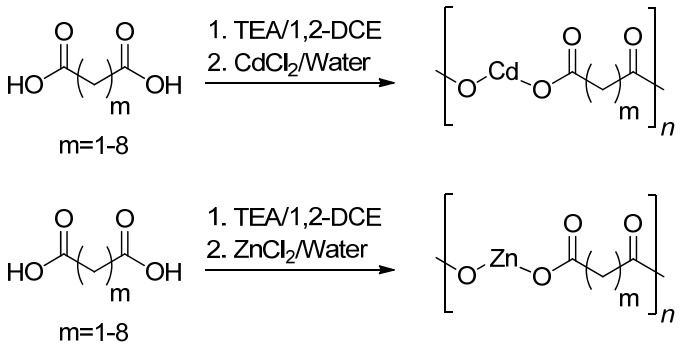

Scheme 7.1 Synthesis of Cd and Zn polymers

A variation of precipitation time was observed which appears to be an increase of reaction rate when the number of CH_2 unit increases. Table 7.1 and 7.2 are showing the variation for different monomers and the yield for the final products. As we increase the

number of the CH_2 unit, the yield also increases. It can be contribute to the decreased solubility of polymers with longer aliphatic chain segment.

Table 7.1 Reaction time and yield of organocadmium polyesters

Cadmium	**Reaction Time**	**Yield**
Malonic (1 CH_2)	Overnight	55%
Succinic (2 CH_2)	1-2 hour (in the form of sodium salt)	72%
Glutaric (3 CH_2)	Overnight	58%
Adipic (4 CH_2)	1-2 hour	82%
Pimelic (5 CH_2)	1-2 hour	85%
Suberic (6 CH_2)	Less than ½ hour	84%
Azelaic (7 CH_2)	Less than ½ hour	87%
Sebacate (8 CH_2)	Less than ½ hour	79%

Table 7.2 Reaction time and yield of organozinc polyesters

Zinc	**Reaction Time**	**Yield**
Malonic (1 CH_2)	Overnight	53%
Succinic (2 CH_2)	Less than ½ hour (in the form of sodium salt)	74%
Glutaric (3 CH_2)	1-2 hour	83%
Adipic (4 CH_2)	1-2 hour	86%
Pimelic (5 CH_2)	Less than ½ hour	89%
Suberic (6 CH_2)	Less than ½ hour	90%
Azelaic (7 CH_2)	Less than ½ hour	90%
Sebacate (8 CH_2)	Less than ½ hour	91%

7.3 Structure Characterizations of Zinc and Cadmium Organometallic Polymers

The formation of Sn-ester bond is confirmed by FTIR and the coordination structure was also started based on the peaks of carboxylate group. Like the organotin polyesters described in **Chapter 6**, the metal polymers form coordination complexes with the carbonyl oxygen atoms. The carboxylate group is able to coordinate to metal ions by

three different modes, as discussed in Chapter 6. Scheme 7.2 described the possible coordination modes for the carboxylate group,[12] in which Type 1 refers to unidentate mode, and Type 2 and 3 are bidentate mode. The difference of Type 2 and 3 is whether the two oxygen bind to the same metal atom or different ones. It results in what we call intra-chain and inter-chain motif for Type 2 and 3 respectively in Chapter 6. The coordination modes can be classified based on the difference between the wavenumbers of the asymmetric and symmetric carboxylate stretching bands, $\Delta\nu$ (cm^{-1}) = $\nu_{as}COO^-$ (cm^{-1}) - ν_sCOO^- (cm^{-1}).

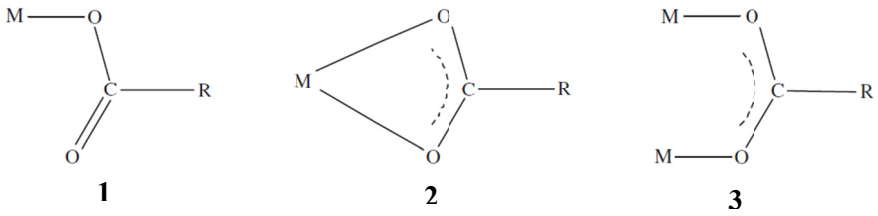

Scheme 7.2 Possible coordination features for the carboxylate group

Table 7.3 and 7.4 below are listed values of asymmetric and symmetric carboxylate stretching bands and their difference for each cadmium and zinc polymers. According to the reported values for the carboxylate binding to Zn and Cd,[12] the coordination type was determined.

The $\Delta\nu$ (cm^{-1}) values of Cd polymers are above 200 cm^{-1}, which can be determined to be in Type 3 according to the literature. [12] Except for succinic acid as the monomer, the $\Delta\nu$ value actually indicates a unidentate binding mode. For adipic acid system, although the binding mode is determined as Type 3, there are two different structures found. As discussed for organotin polyesters in Chapter 6, this particular system can be classified as the hybrid mode, where the intra- and inter-chain motifs coexist. The coordination of zinc with carbonyl group was found to be a combination of Type 2 and 3 as well when the

number of CH_2 is larger than two (not including two). As we increase the number of CH_2, a three dimensional network is favored, due to the increased chain flexibility of the polymer. For suberic acid system, three different binding modes were observed. As mentioned in Chapter 6, the carboxylate oxygen can bind with the zinc on the other chain that is already in either inter-chain mode or intra chain mode, the IRs are showing multiple peaks for the symmetric stretching, and they correspond to different hybrid binding modes.

Table 7.3 IR determined binding mode for Cadmium polymers

Cadmium	$\nu_{as}COO^-$ **(cm^{-1})**	ν_sCOO^- **(cm^{-1})**	$\Delta\nu$ **(cm^{-1})**	**Type**
Malonic (1 CH_2)	1540	1350	200	3
Succinic (2 CH_2)	1560	1300	260	1
Glutaric (3 CH_2)	1530	1340	210	3
Adipic (4 CH_2)	1530	1330, 1300	200, 230	2,3
Pimelic (5 CH_2)	1530	1300	230	3
Suberic (6 CH_2)	1540	1350	190	3
Azelaic (7 CH_2)	1530	1330	200	3
Sebacate (8 CH_2)	1540	1320	220	3

Table 7.4 IR determined binding mode for Zinc polymers

Zinc	$\nu_{as}COO^-$ **(cm^{-1})**	ν_sCOO^- **(cm^{-1})**	$\Delta\nu$ **(cm^{-1})**	**Type**
Malonic (1 CH_2)	1550	1360	190	3
Succinic (2 CH_2)	1540	1390, 1310	180, 230	3
Glutaric (3 CH_2)	1530	1400, 1360	130, 170	2, 3
Adipic (4 CH_2)	1530	1400, 1340	130, 190	2, 3
Pimelic (5 CH_2)	1530	1400, 1320	130, 210	2, 3
Suberic (6 CH_2)	1540	1400, 1370, 1300	140, 170, 240	2, 3
Azelaic (7 CH_2)	1530	1400, 1350	130, 180	2, 3
Sebacate (8 CH_2)	1530	1400, 1340	130, 190	2, 3

The structure of Cd and Zn polymers were also analyzed using X-ray diffraction. Figure 7.1 shows the XRD patterns of each polymer with different length of aliphatic segment. For Cd polymers, the powder started to be amorphous from 1 CH_2 to 3 CH_2, and then became crystalline afterwards. It is clear that the size of the unit cell increases as we increase the length of aliphatic chain segment, which is indicated by the switching of the first peak. All the Zn polymers were found to be crystalline according to the XRD patterns, and similar trend was also observed.

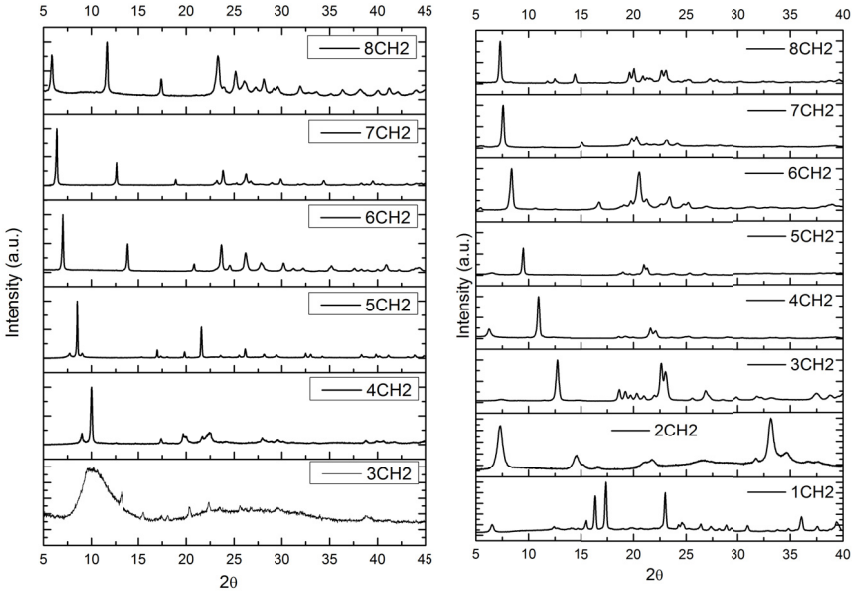

Figure 7.1 X-ray diffraction patterns from Cd (Left) and Zn (right) powder materials

7.4 Dielectric Properties and the Effect of Water Content on Zinc and Cadmium Organometallic Polymers

The polymers were tested for dielectric constant and loss through frequency domain spectroscopy, in comparison with the computational predicted values, shown in Figure 7.2. Two examples of the spectra are shown in Figure 7.3. For Cd polymers, in general, as the number of CH_2 increases, the dielectric constant decreases. Similar to what we

discovered in organotin polyester systems, as number of CH_2 increases, the dielectric constant follows the even-odd trend as observed for physical properties of alkanes. The experimental value showed a peak at the point of 4 CH_2, whereas the computational results have a slight peak at 5 CH_2. If we refer to the binding mode determination by FTIR, the hybrid mode was observed at the point of 4 CH_2. The resulting dielectric constant is higher for this hybrid system which is out of the trend, indicating the intra-chain motif compared to inter-chain could be beneficial for Cd polymers.

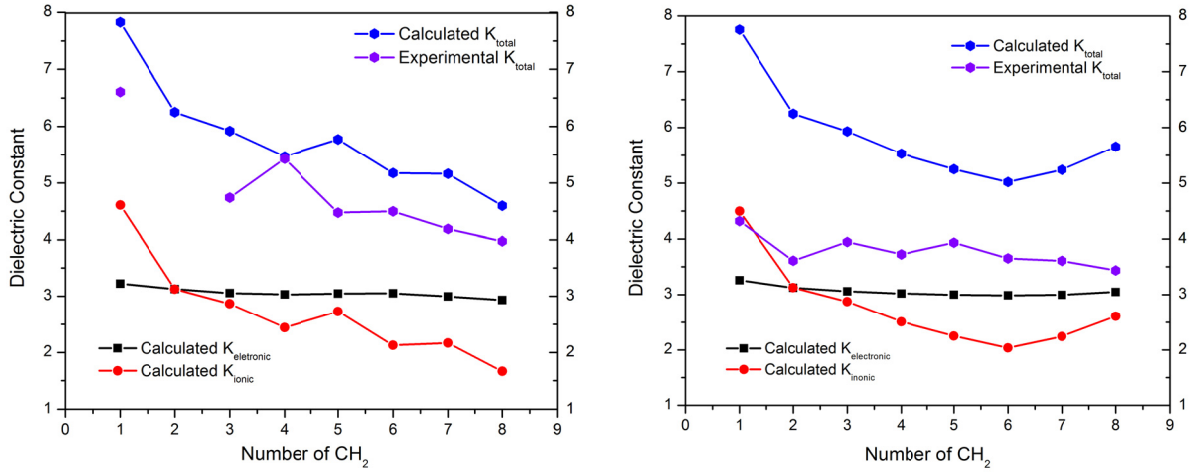

Figure 7.2 Dielectric Constant Experimental vs. Computational (Left: Cd, Right: Zn)

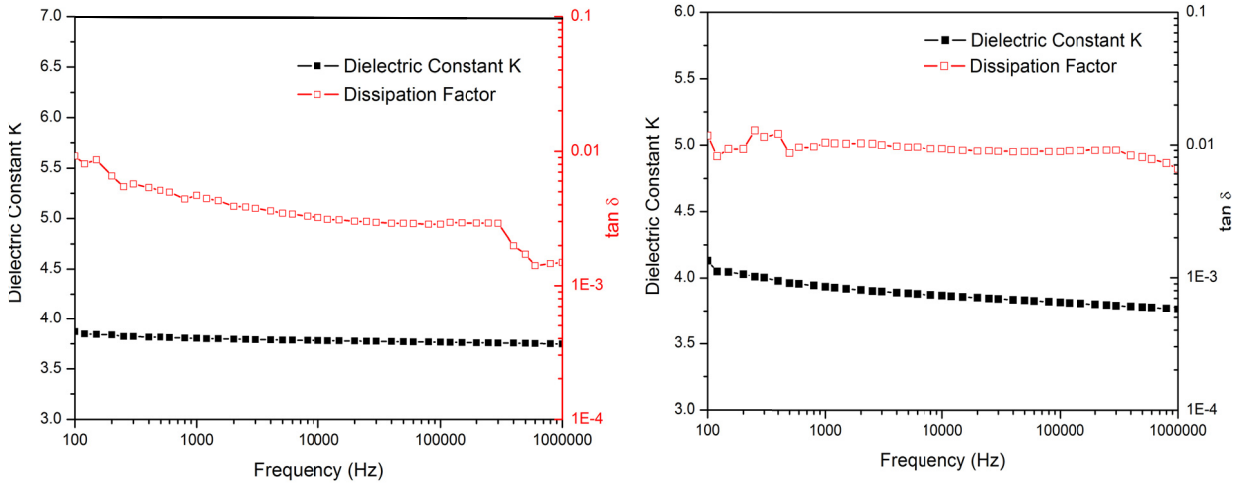

Figure 7.3 Dielectric Spectra (Left: Cd-Sub-6CH_2, Right: Zn-Pim-5CH_2)

For Zn polymers, the predicted total dielectric constants are significantly higher than measured value, and the experimental values are actually pretty close as the number of CH_2 changes. We also observe an even-odd trend of the dielectric properties. Figure 7.3 is showing a pretty stable dielectric constant over a range of frequency as well as a loss tangent stays below 1%.

Comparing the calculation results of Cd and Zn system, they showed pretty similar electronic part of the dielectric constant (all around three). The main contribution to the difference, both the trend as we increase the number of CH_2 and the actual value is the ionic part of the dielectric constant. It is clear that for both of the system, the ionic part of the dielectric constant and the total dielectric constant follow the exact same trend. Further computational work will be conducted to search for more stable structures in attempt to explain the gap between the experimental and predicted values.

As mentioned above, the effect of the water in the polymer may affect dielectric constant. Cd-Seb ($8CH_2$) is shown here as an example. In the TGA figure, the left one showed clear weight loss when isothermal at 100^{o}C (Figure 7.4, left), followed by cooling and another heating to high temperature above degradation. No obvious weight loss was observed below 250 ^{o}C in the second heating (Figure 7.4, right). This means there are water compound that were removed during the first heating, and not able to be desorbed back to the polymer. However, there was still free water in the polymer after cooled down.

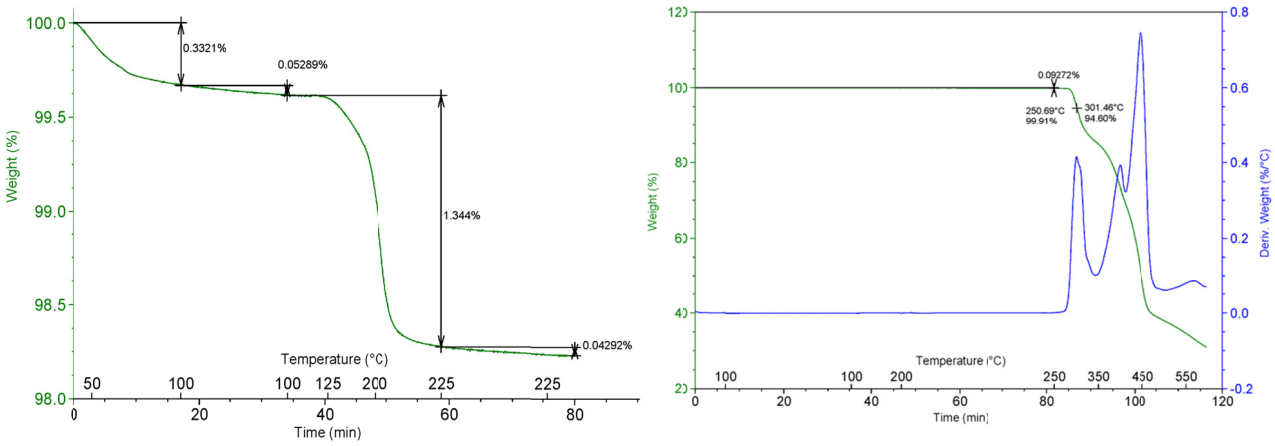

Figure 7.4 TGA of Cd-Seb ($8CH_2$)

Therefore, the dielectric measurements were conducted following similar heating procedure to study the effect of the water loss on dielectric behavior. The samples were first tested at room temperature and then held at several elevated temperature (50 ^{o}C, 75 ^{o}C and 100 ^{o}C) in an air circulated oven for half an hour before measurement. Then the samples were cooled down to room temperature to repeat this sequence for any possible changes. The results are showing in Figure 7.5. In the first heating cycle up to 100 ^{o}C, the dielectric constant increases at each step, especially the curve at 100 ^{o}C. The large value at lower frequency can be contributed to the conduction loss generated in the sample, which indicates the existence of bond water or lose water. However, after heating up to 100 ^{o}C and hold for 30min, the dielectric constants for the second heating cycle significantly reduced. This means the compound in the polymer pellets which was causing the high conduction loss could not be reabsorbed when cooled down to room temperature. The results, along with TGA indicate the presence of bond water in the system, which increases the dielectric constants.

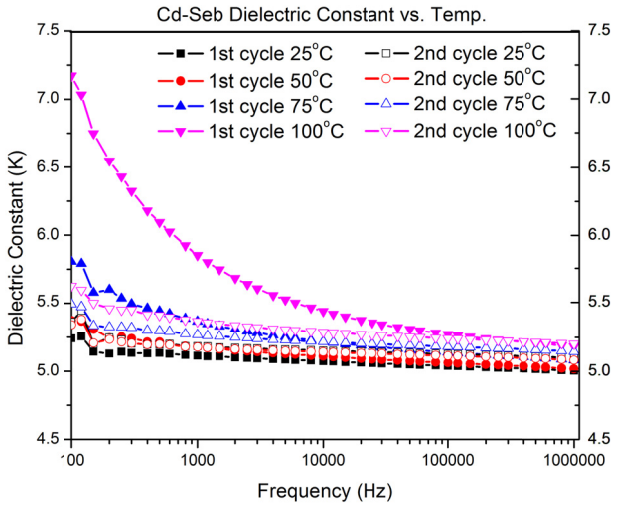

Figure 7.5 Dielectric Spectra of Cd-Seb ($8CH_2$)

After thorough drying on the pressed pellets, the dielectric loss can be reduced by the removal of bonded small molecules. The TGA and the dielectric spectra of two Zn polymers are shown in Figure 7.6 as an example. Based on the TGA results, no obvious loss of bonded water was observed after isothermal treatment. And the dielectric measurements after that showed much lower dielectric loss compared to our polar system discussed in Chapter 4-6. Over the testing frequency range, the dielectric loss stayed relatively stable without indication of conduction loss. As testing temperature increases, the dielectric constant and loss both dropped slightly before increase again. The Zinc-Glu, which has shorter aliphatic chain segment, gives higher dielectric constant, as mentioned above.

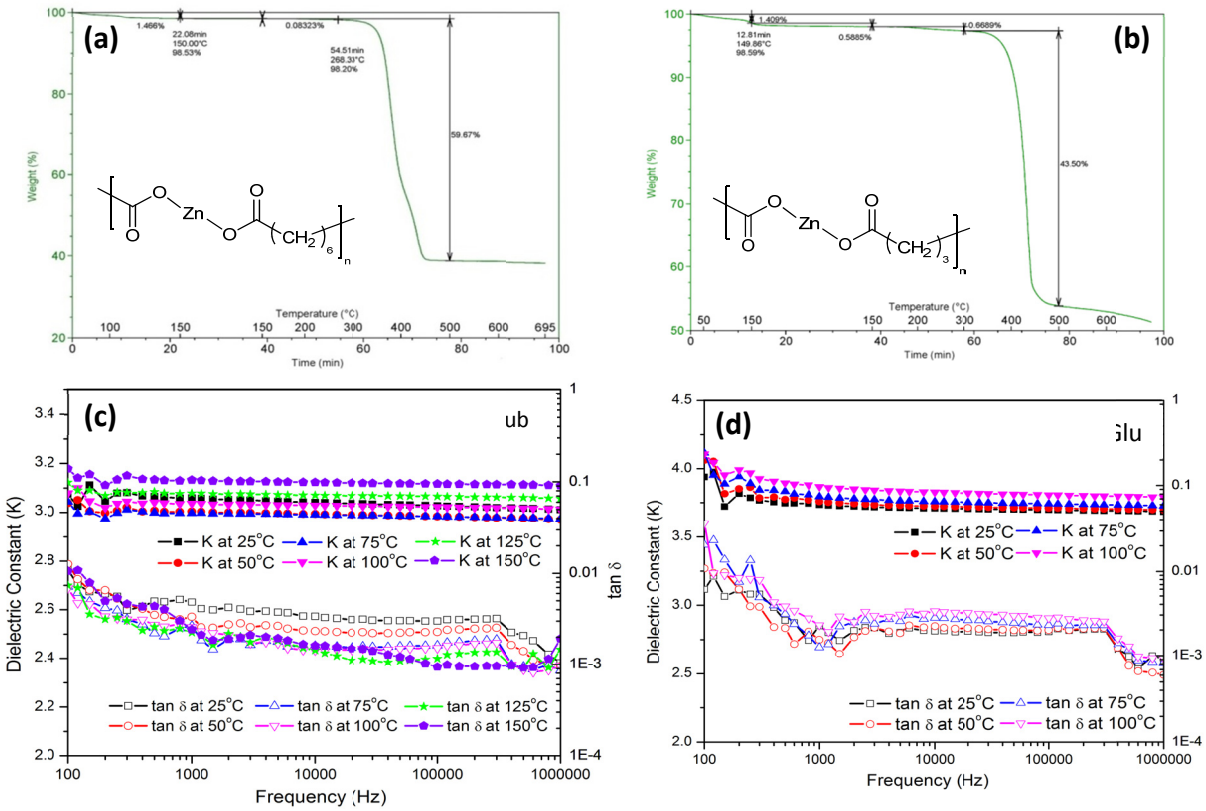

Figure 7.6 TGA (a and b) and Dielectric Spectra (c and d) of Zn-Sub ($6CH_2$) and Zinc-Glu ($3CH_2$)

7.5 Conclusion and Future Work

In parallel with the study on organotin polyesters, we incorporated transition metals Cadmium and Zinc into the similar polymer system and investigated the dielectric properties. Similar to the first system for tin, we studied aliphatic diacids with different number of CH_2 unit. Experimentally, an even-odd trend was observed for both of the system and a peak value at the point of $4CH_2$ indicates a hybrid motif could be beneficial in increasing dielectric constant for Cd polymers. The predicted value of dielectric constants are much higher and further optimization of calculation is still being conducted.

The effect of water content in the polymer system was investigated and proved to cause great change on dielectric constant and loss. The bonded water formed during the synthesis cannot be recovered after a heating treatment which will cause decrease of dielectric constant and loss. The problem remains how to control the bonded water content and utilize to contribute to improving dielectric performance, for example, in increasing dielectric constant and maintaining a low dielectric loss.

After the initial study on aliphatic chains, we could expand synthetic space for cadmium and zinc polymers assisted by DFT calculations. Compared to organotin polyesters, the addition of polarizable groups in the aliphatic chain and aromatic or heteroatom groups can have an effect on increased dielectric constant. These groups could also be helpful to improve the solubility and processability of these polymers.

It is now well known that there is a benefit to the dielectric properties by coordinating the metal atoms in polymers containing electronegative oxygen atoms through carboxylate bonds. There are very few metal organic systems are reported including transition metals in literature. This synthetic space has great potential to explore unique structure and properties, including alkali metals, alkaline earth metals, inner transition series and others. More studies needs to be conducted on calcium (Ca), magnesium (Mg), which are alkaline earth metals. Some preliminary results in the group suggest that reactivity of Ca with dicarboxylate acids seems much higher in similar conditions in a two phase condensation reaction, which could leads to higher molecular weight and better processability. As discussed in Chapter 6 and here in Chapter 7, we are comparing the covalently incorporated metal system into the polymer with polymer nanocomposites. Figure 7.7 showed the dielectric constants of several metal dioxides and it is clear that the

systems we studied are at the lower end of dielectric constant. There are certainly more space that are worth exploring especially TiO_2, which has a dielectric constant of 86-173 depending the crystal structure. Barium titanate, which has a dielectric constant over a thousand, is a commonly used nanoparticle for preparing polymer nanodielectric material, as discussed in Chapter 1. Therefore, it is worth exploring different metal element systems for synthesizing polymer dielectrics as well as their special dielectric properties.

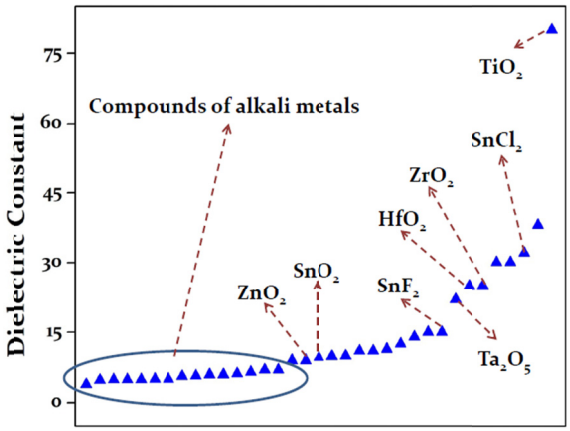

Figure 7.7 Dielectric constants of common Metal Oxide and Halides

7.6 Computational and theoretical methods

The computational workhorse used in this study is density functional theory (DFT) as implemented in the Vienna Ab Initio Simulation Package (VASP). The total energies EDFT of the examined structural models were calculated with the Perdew-Burke-Ernzerhof (PBE) exchange-correlation (XC) functional. Monkhorst-Pack k-point meshes with spacing of 0.1 $Å^{-1}$ are used for integrations over the Brillouin zones of the models. A plane wave kinetic energy cutoff is chosen to be 500 eV while atomic and cell

variables were simultaneously relaxed until the residual forces were smaller than 10^{-2} $eVÅ^{-1}$.

All diacids, m-cresol, cadimuim dichloride, zinc dichloride were procured from Acros Organics. Succinic acid was purchased as the disodium salt form and oxalic acid was the dihydrate form from Acros Organics. Sodium hydroxide (NaOH) and triethylamine (TEA) were purchased from Fisher Scientfic. All monomers were used as received. Tetrahydrofuran (HPLC grade) was purchased from J.T. Baker. Deionized water was obtained using a Millipore purification system. Stainless steel shim stocks (diameter = 2 in., thickness = 0.01 in., and ASTM A666 stainless steel) were acquired from McMaster Carr. Quartz glass slides (3 in. × 1 in. × 1 mm) were procured from Ted Pella, Inc. In general, Scheme 1; a molar excess of the diacid was added to a round bottomed flask and dissolved in 20 mL of water. To the diacid solution was added 2.1 equiv, with respect to the diacid, of sodium hydroxide. To the rapidly stirred aqueous solution was added 20 mL of a dimethyltin dichloride solution in tetrahydrofuran. The precipitate is filtered and washed with 50 mL portions of tetrahydrofuran and water and dried *in vacuo* at 80 °C for 20 h to remove any residual solvent.

Reference

1. Z.-X. Xu, V. A. L. Roy, P. Stallinga, M. Muccini, S. Toffanin, H.-F. Xiang and C.-M. Che, *Appl. Phys. Lett.* 2007, **90**, 223509.
2. M. S. Gaur, A. P. Indolia, *J Therm Anal Calorim*, 2011, **103**, 977.

3. D. Vaishnav and R. K. Goyal, *IOP Conf. Series: Materials Science and Engineering* 2014, **64**, 012016.
4. Z.-M. Dang, L.-Z. Fan, S.-J. Zhao, C.-W. Nan, *Materials Science and Engineering* 2003, **B99**, 386.
5. T. S. Velayutham, W. H. Abd Majid, W. C. Gan, A. Khorsand Zak, and S. N. Gan, *Journal of Applied Physics* 2012, **112**, 054106.
6. J.C. Bailar Jr., *Prep. Inorg. React.* 1964, **1**, 1.
7. M. Eddaoudi, H. Li and O.M. Yaghi, *J. Am. Chem. Soc.* 2000, **122**, 1391.
8. N. L. Rosi, J. Kim, M. Eddaoudi, B. Chen, M. O'Keeffe and O.M. Yaghi, *J. Am. Chem. Soc.* 2005, 127, 1504.
9. H. K. Chae, D. Y. Siberio-Perez, J. Kim, Y.B. Go, M. Eddaoudi, A. J. Matzger, M. O'Keeffe and O.M. Yaghi, *Nature* 2004, **427**, 523.
10. O.R. Evans and W. Lin, *Acc. Chem. Res.* 2002, **35**, 511.
11. M. Edgar, R. Mitchell, A. M. Z. Slawin, P. Lightfoot and P.A. Wright, *Chem. Eur. J.* 2001, **7**, 5168.
12. M. S. Refat, D. N. Kumar and R. F. De Farias, *Journal of Coordination Chemistry* 2006, **59(16)**, 1857.

Chapter 8

Summary and Relational Database

In this dissertation work, a complete design strategy loop for polymer dielectric material is presented, with a synergetic combination of 1) first principles computation work using Density Functional Theory, molecular dynamic on polymer structure, dielectric constant and band gap, intrinsic breakdown strength, etc.; 2) systematic synthesis based on computational guidance in determination of promising polymer systems, and an experimental screening based on thorough characterization of new polymer systems' dielectric behavior; 3) an exploration and optimization of large scale synthesis and processing conditions; and in the end, which will be discussed here 4) a summarization of experimental and computational data for relational database.

The work discussed in this dissertation, especially on specific polymer types is based on two approach of material design: 1) systematic study of organic polymer systems in order to establish structure-dielectric property relationship, modification of common organic polymer systems, and improvement of processing conditions; 2) explore a wide chemical space on the periodic table, discover unique hybrid system (organometallic polymers), and systematic experimental study. Both parts of the work are combined with computational insights in designing material as well as validation of computational method and newly developed models.

Since the launch of the Materials Genome Initiative (MGI) in 2011, there has been an increased focus on developing a "materials innovation infrastructure" containing computational tools, experimental tools, digital databases and collaborative networks.

The idea is to significantly accelerate the discovery and manufacturing of advanced materials; computations play an extremely important role here in assisting experiments. With the advent of high-performance computing, it is possible to obtain a lot more computational data on the same kinds and number of material systems than corresponding experimental results. This is the power of modern computations, but what is also crucial is complementarity with experiments. Any computation has to be realistic, meaningful and of direct value to scientists involved in synthesis and testing. This kind of synergy is what makes rational co-design the future of materials innovation.

Besides a hierarchical design strategy based on high-throughput modeling combined with experiment validation, a data-driven model discovery can also be applied as a more efficient approach to access a larger amount of data (shown in Figure 8.1), as discussed in Chapter 3.

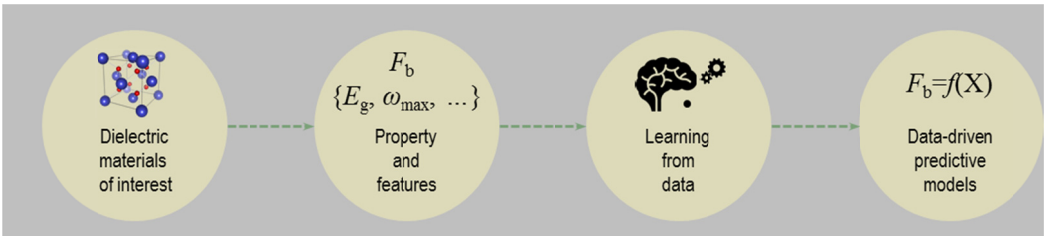

Figure 8.1 A data-driven model discovery

The first two sets of data obtained from the computational work are plotted below (Figure 8.2) in terms of electronic, ionic contribution and the total dielectric constant. The structures of each set of polymers were described in Chapter 4 and 6. For the electronic dielectric constant, it is clear that organic polymer systems possess higher electronic contribution to polarization than the hybrid system, which means electrons have higher mobility in the organic systems. As discussed in Chapter 3, enhancement of delocalization of electrons will sacrifice the band gap. For the systems with the same

electronic dielectric constant, hybrid system has higher band gap. However, if we examine the total dielectric constant values, at the same band gap value, hybrid system has higher total dielectric constant then organic system. Then it is obvious that for hybrid system, ionic contribution (atomic polarization and dipolar polarization) plays important role in the high dielectric constant. Particularly, this system allows the increase of dielectric constant through enhancing atomic polarization besides dipolar polarization. The close examination of the two systems answered the question we proposed in Chapter 2: what is the upper limit of electronic dielectric constant at certain band gap? And how much can we improve? Based on the computational data, we set band gap of 3 as our screening limit (Chapter 4), as most of the semiconductor materials have a band gap below 3. At this point, we can achieve electronic dielectric constant of ~5.

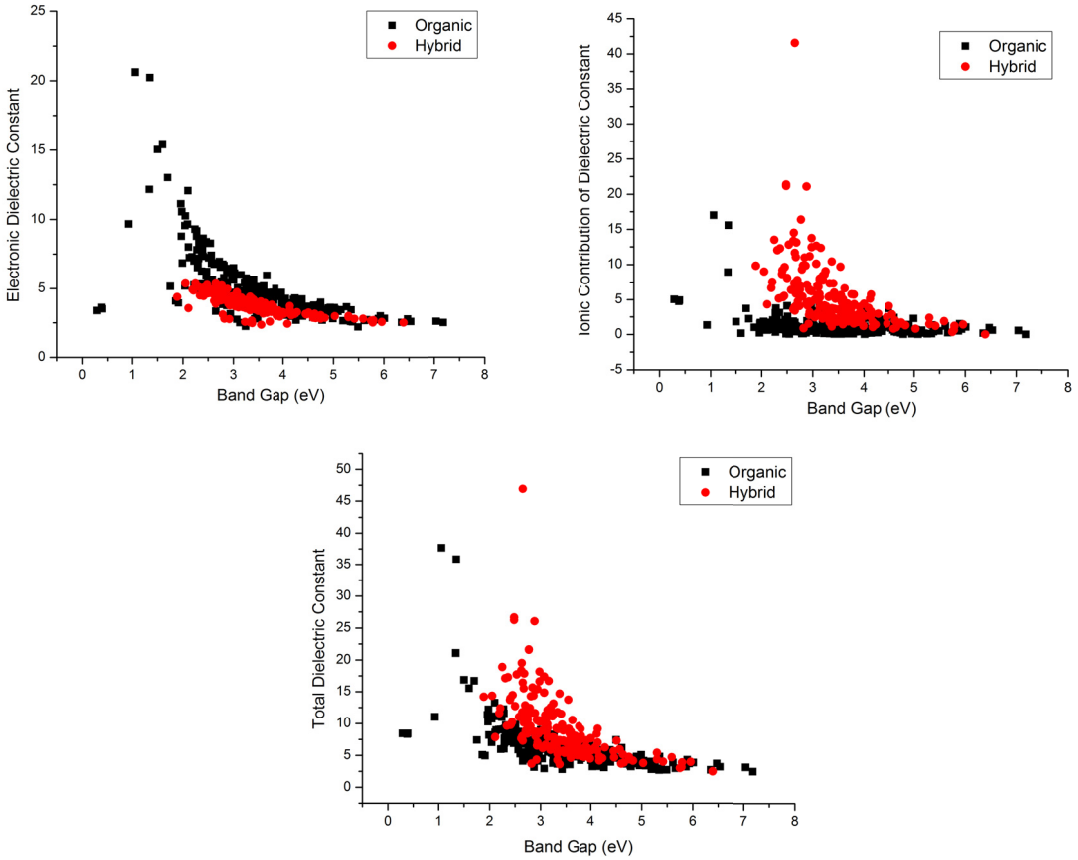

Figure 8.2 Calculation dataset using high throughput DFT

However, most of the improvement is realized by other contributions, especially dipolar polarization. As stated in the former chapters, how to select the dipoles and place them in an environment that will create the highest mobility is extremely important. As we discovered in the organic systems, dipole moments scattered in an amorphous system or a domain small enough to minimize the inter-domain interactions is preferred, not only for the purpose of increase dielectric constant, but also helps to improve intrinsic breakdown strength through additional electron-dipole scattering (Chapter 5).

In addition to a large quantity of computational data, we also achieved a rather considerable experimental database. We plotted each polymer in terms of several main design criteria discussed in Chapter 2: dielectric constant and loss, band gap, glass transition temperature and breakdown strength, as shown in Figure 8.3. Due to processing issues mentioned in Chapter 6 and 7, the breakdown strength data are mainly on organic polymer systems. It is clear that organometallic systems are achieving both higher dielectric constant and band gap at the same time. Some systems have lower dielectric loss as well. Organic polymers have higher dielectric loss, however, with the optimization of processing to prepare high quality film samples, they can achieve high energy density. Several rules are transferrable between each type of systems. First of all, by incorporating polar groups and utilizing dipolar polarization, we can achieve higher dielectric constant without sacrificing band gap too much. In addition, the increase of the mobility of dipoles not only enhances polarization, but also minimizes the loss at certain frequency range. Aromatic system generally decreases the band gap of the system, however, the engineering breakdown strength was found to be highly dependent on morphology, which can be controlled by altering chemical structure.

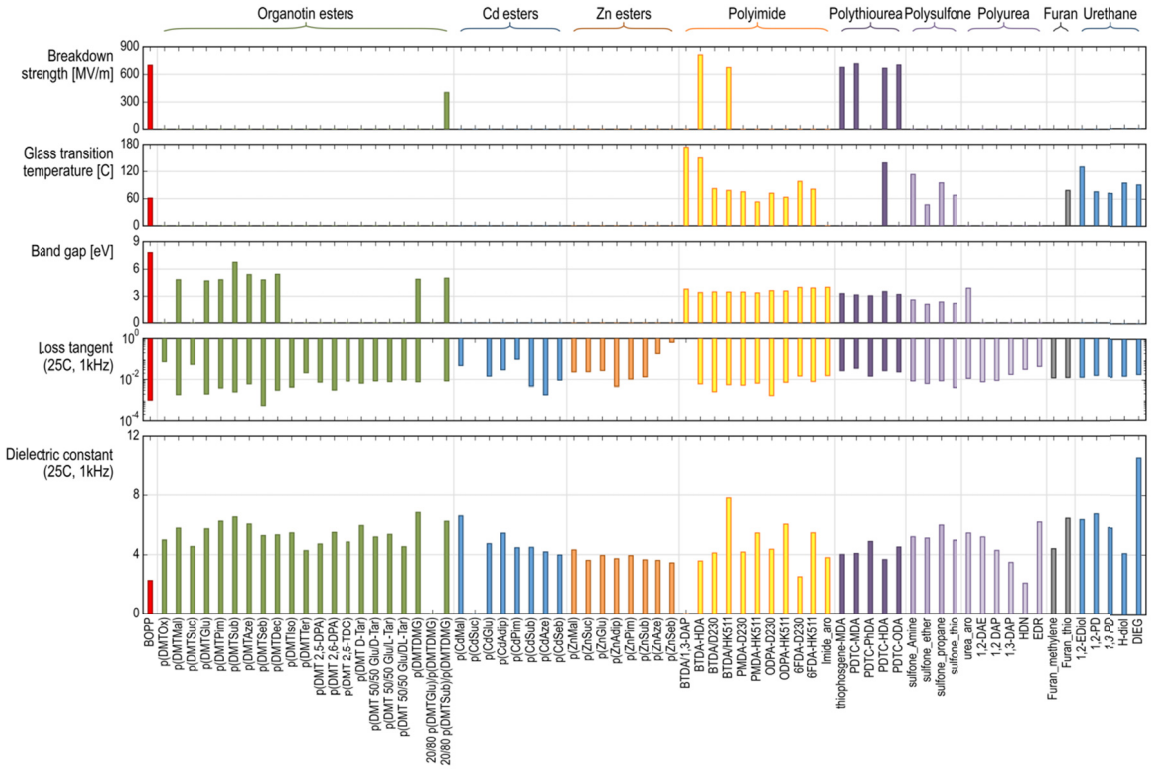

Figure 8.3 Experimental data for each polymer

In order to compare with the calculation results, the experimental data were plotted in the similar way (Figure 8.4). It is clear that for the same band gap value, the dielectric constants for the organometallic systems (hybrid system) are higher than the organic system. The size of the experimental dataset is not comparable with the computational dataset, however, we still observe a clear inverse relationship of dielectric constant versus band gap, as in Figure 8.2. The organometallic system pushed to the preferred range in the spectrum: higher dielectric constant and higher band gap. The dissipation factors were plotted against the total dielectric constant as well. There are no obvious correlations between the two and both system are mapping the whole area.

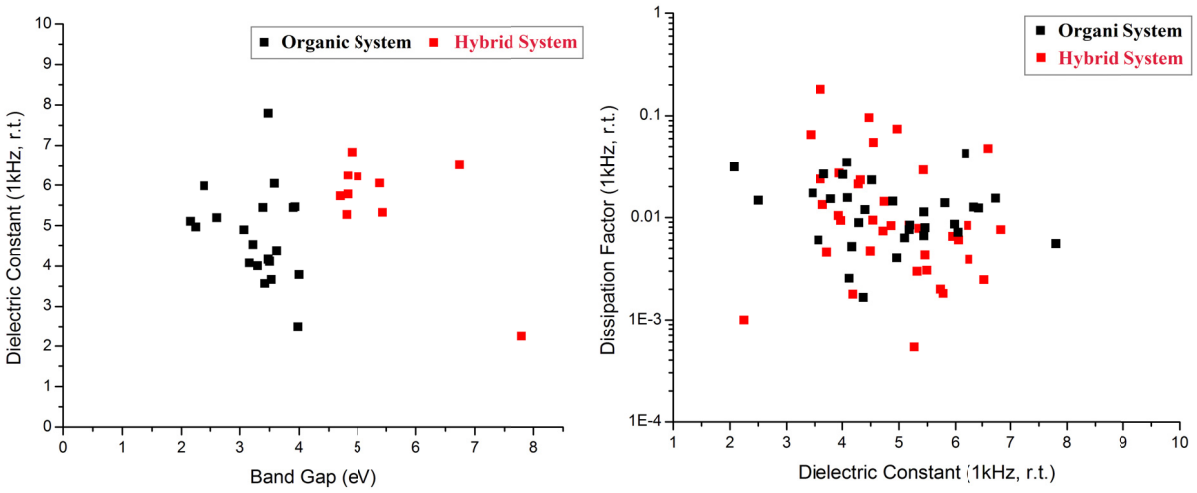

Figure 8.4 Experimental dataset

In summary, we investigated a wide range of polymer materials for capacitor energy storage applications and established dielectric material design strategy with a combination of computation and experiments. With the dataset we created in many approach, we are building a database which allows estimation of dielectric properties for proposed new polymer structures. The big data exploitation was proposed by our colleagues in accelerating the discovery process (Figure 8.5).

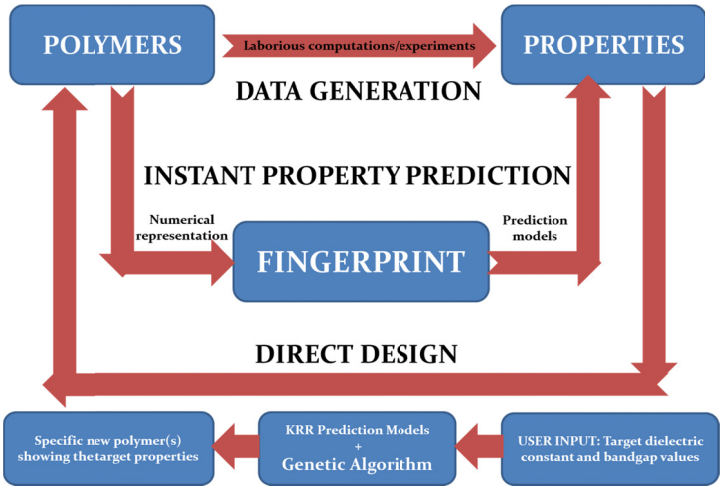

Figure 8.5 big data exploitation towards accelerated discovery of organic dielectric polymers